CARL VON OSSIETZKY universität OLDENBURG

Fakultät II – Informatik, Wirtschafts- und Rechtswissenschaften
Department für Informatik

Automation Capabilities in the Nanorobotic Handling of Nanomaterials

This dissertation is submitted for the degree of
Dissertation zur Erlangung des Grades eines
Doktor der Ingenieurwissenschaften
vorgelegt von
Malte Bartenwerfer

30. November 2018

Zusammenfassung

Die konventionelle Miniaturisierung von Elektronik, Sensoren und Mikrobauteilen stößt mittlerweile an inhärente technologische Grenzen. Nanoskalige Objekte hingegen bieten –verursacht durch quantenmechanische Effekte oder durch das enorme Oberflächen-Volumen-Verhältnis– einzigartige physikalische Eigenschaften, welche Nanomaterialien und Nanoobjekte zu vielversprechenden Kandidaten für neue Sensoren, Aktoren, Logikeinheiten und Energiewandler macht. Nanomaterialien und Nanoobjekte dienen somit als ultrakleine Bausteine in größeren und komplexeren System.

Eine reibungslose Integration dieser Bausteine ist eine universelle Voraussetzung für viele neuartige Anwendungen und Konzepte, welche Nanomaterialien einsetzten und ist somit unerlässlich für die Realisierung von neuen Bauteilen. Das volle Potenzial von Nanomaterialien und -objekten kann allerdings nur ausgeschöpft werden, wenn diese als individuelle und funktionale Objekte in ein Bauteil integriert werden. Diese Art der Integration stellt jedoch große Herausforderungen an die Handhabungsmethoden solcher Objekte.

Ein allgemeines Verständnis der auf der Nanoskala herrschenden Kräfte ist vorhanden. Ein direkter Transfer hin zu allgemein anwendbaren Handhabungsstrategien ist allerdings kaum möglich, da diese Kräfte kaum beherrschbar oder messbar sind. Einerseits existieren mehrere erfolgreiche Ansätze, welche nanoskalige Effekte nutzen, zur Handhabung und Manipulation von Nanoobjekten mit dem Ziel einer reibungslosen Integration. Andererseits sind die meisten Ansätze nur für ein sehr spezielles Handhabungsscenario gut geeignet, da sie auf dieses spezifische Problem ausgerichtet sind und die spezifischen Umgebungsbedingungen benötigen. Darüber hinaus sind praktische Aspekte, wie z.B. die Wirtschaftlichkeit einer Integrationsmethode, von großer Bedeutung, um für industrielle Anwendungen brauchbar zu sein. Der Durchsatz und vor allem die Automatisierbarkeit einer Nanohandhabungsmethode

sind daher ebenso entscheidend wie die Genauigkeit. Bislang wurden jedoch noch nicht alle dieser Aspekte der Nanohandhabung ausreichend untersucht.

Aufgrund der Anforderungen an die Integration wird typischerweise das Rasterelektronenmikroskop (REM) als Arbeitsumgebung verwendet, da es Geschwindigkeit und Genauigkeit der Bildakquise sinnvoll kombiniert. Allerdings ist der Einsatz des REMs auch mit störenden Nebenwirkungen verbunden, die durch Ladungseffekte auf der Nanoskala hervorgerufen werden.

In dieser Arbeit werden zwei Hauptthemen behandelt, die sich mit den oben genannten Anforderungen und den Herausforderungen der Integration von nanoskaligen Bausteinen befassen: i) die Entwicklung anwendbarer Handhabungsstrategien und ii) die Entwicklung der Automatisierung für die Nanomontage.

Zunächst werden nanorobotische Strategien zum Einsatz innerhalb des REMs entwickelt, um präzise Bewegungen, Handhabung und Montage von Objekten mit Abmessungen bis in den Nanometerbereich zu ermöglichen.

Mechanische Mikrostrukurierung wird zur Entwicklung von Werkzeugen eingesetzt, welche präzise Manipulationen ermöglichen und die Integration von Nanoobjekten mit einer Positioniergenauigkeit im Nanometern Bereich und einer Ausrichtungsgenauigkeit von wenigen Grad ermöglichen.

Mit dem Ziel, Automatisierbarkeit zu erreichen, werden Methoden entwickelt und bewertet, welche das Potenzial des REMs nutzen, aber dessen störende Ladungseffekte als zusätzliche Informationsquellen nutzen, um den Status einer laufenden Bearbeitungssequenz zu messen. Die entwickelten Techniken werden durch die Integration von Nanodrähten in bereits existierende Elektrodenstrukturen und MEMS Komponenten demonstriert.

Zum Anderen werden unter Einbeziehung der neuen Messmethoden weitere Automatisierungsstrategien entwickelt und somit eine vollständig automatisierte Montage ohne Benutzerinteraktion realisiert. Diese Automatisierung wird in einer vollautomatischen Nanomontagesequenz von mikroskaligen Bausteinen umfassend demonstriert.

Zusammenfassend zeigen die Ergebnisse dieser Arbeit die Möglichkeiten der nanorobotischen Montage und dass deren Entwicklung neue Perspektiven für Nanomaterialien öffnen kann. Die Ergebnisse der entwickelten Automatisierung zeigen, dass Durchsatzzahlen von etwa einem Stück pro Minute erreichbar sind und demonstrieren weiterhin das Potenzial, welches durch Automatisierung besteht.

Abstract

The conventional downscaling of electronics, sensors and building blocks is facing inherent technological limits. Nanoscale objects, on the other hand, offer unique physical properties, caused by quantum-mechanical effects or by the enormous surface-to-volume-ratio that makes nanomaterials and nanoobjects promising candidates for new sensors, actuators, computing units and energy converters. Nanomaterials and nanoobjects in devices act as building blocks with ultra-small dimensions within a larger and more complex system.

Hence, a smooth integration of these building blocks is a common requirement for many novel applications and concepts that use nanomaterials and is essential for the construction of real devices. The full potential of nanomaterials and -objects can be exploited only if they are fully integrated into devices as individual and functional objects. However, this kind of integration presents major challenges to the handling capabilities of such objects.

A general understanding of the forces ruling on the nanoscale is existent, but the direct transfer to the development of handling strategies is lacking, since these forces are hardly controllable or measurable. Hence, on the one hand, there are several considerable approaches to handling and manipulating nanoobjects for a smooth integration, which take advantage of effects specific to the nanoscale. On the other hand, most approaches are well-suited for one particular handling scenario only, since they are developed focusing on this specific problem and need the specific environment. Furthermore, practicality aspects, such as the economy of an integration method, are of major importance in order to be applicable to industry-relevant applications. Hence, the throughput and especially the automation capabilities of a nanohandling method are as crucially important as accuracy. So far, nanohandling strategies which sufficiently include all aspects have not been developed.

Due to these demands on the integration, the scanning electron microscope (SEM) is typically used as a working environment, since it reasonably combines image acquisition speed and accuracy. However, the SEM is also associated with disruptive side-effects caused by the charging effect on the nanoscale.

In this thesis, two major topics are addressed, tackling the demands mentioned above and the challenges of the integration of nanoscale building blocks: i) the development of applicable handling strategies and ii) the development of automation for nanoassembly.

Firstly, nanorobotic strategies inside the SEM have been developed in order to provide precise movements, handling, and assembly of objects with dimensions as small as the nanometer scale. The structural design on the nanoscale is used for handling tools that enable precise manipulations and allow the integration of nanoobjects with a positioning accuracy of few nanometers and an alignment accuracy of few degrees. Aiming to achieve automation capabilities, methods are proposed and evaluated that use the potential of the SEM but exploit its disruptive charging effects as useful sources of information on the status of an ongoing handling sequence. The developed techniques are demonstrated in the integration of nanowires into pre-existing electrode structures and micro-electromechanical system (MEMS) devices.

Secondly, automation strategies have been developed incorporating the new information sources in order to gather sufficient information for an automated assembly without user interaction. This automation has been extensively demonstrated in a fully automated nanoassembly sequence of microscale building blocks.

In summary, the results of the thesis demonstrate the abilities of nanorobotic assembly and show that their developments open new perspectives for nanomaterials. The achieved automation reveals that throughput figures of about one piece per minute are achievable and demonstrates the potential and improvements achievable through automation.

Table of contents

List of figures

List of tables

List of acronyms

AFM atomic force microscope
BLOB binary large object
CAD computer-aided design
DOF degree of freedom
EBID electron beam induced deposition
FEM finite element method
FIB focused ion beam
GIS gas injection system
MEMS micro-electromechanical system
OAF *OFFIS automation framework*
ROI region of interest
SE secondary electron
SEM scanning electron microscope
TEM transmission electron microscope

1 Introduction

The size of a tool or device has been a crucial figure of merit in almost all applications since the early establishment of mechanical systems in a pre-industrial society. Today objects and devices that appear inconsiderably, are important pieces of our daily lives. Many of these devices would be non-existing without the development of general miniaturization during the most recent history.

The most prominent and intuitive example of this miniaturization, applied to mechanical systems only, is clocks: immobile clocks became portable pocket watches and finally light wrist watches. The development of miniaturization in electronic devices, however, is even more distinct, since they evolved on a much smaller time-scale: first commercial transistors —e.g. the Raytheon CK703 released in 1948 [80]— had the size of about 2 cm by 6 mm. In comparison, today an average transistor as small individual electronic component[1] has the size of about 0.4 mm by 0.2 mm [151]. Today's minimum feature size of transistors, which are embedded in *integrated circuits*, is in the range of tens of nanometers [6].

The combination of mechanics and electronics, as found in micro-electromechanical systems (MEMS), have experienced an even stronger development: Miniaturization led to an entirely novel kind of sensors; the most prominent, because the most successful, example is the acceleration sensor, which can be found thousandfold in devices of all fields. By this device, MEMS technology has already shown how powerful and life-changing the combination of different physical domains can be: Conventional and very expensive inertial measurement units based on ring laser gyros have already been replaced by small and cost efficient MEMS-based inertial measurement units. This affected high-quality systems, in which conventional devices were substituted by MEMS-based devices; even in highly demanding applications such as aviation [100]. But the most tremendous change happened

[1] in surface-mount technology

to low-power and small-footprint devices: MEMS-accelerometers and gyroscopes are now available with a footprint of about $2 \times 2\,mm^2$. They are part of automotive safety systems, consumer electronics, and metrology devices. Bosch alone has sold more than 2 billion MEMS sensors since 1998 [103].

The most important MEMS sensors, that had an accumulate market value of about US$12 billion, are (in descending order or their market share): Pressure sensors, inertial combos, projection systems, accelerometers, microfluidics for in vitro diagnostics, gyroscopes and ink-jet heads [167].

These and and all other kinds of MEMS-sensors are based on miniaturization and contribute in an important but very concealed way to our daily lives. Last but not least, the miniaturization of energy storage systems, which can store large amounts of energy in a small volume, contributed to the development of portable devices with high computing capacities and sensing abilities. The most apparent example for a device, which benefits from this technological development in MEMS, is the smart-phone. However, beside consumer articles, particularly medical devices, such as pacemakers and hearing aids, have improved tremendously due to miniaturization.

For electronics and especially integrated circuits, upcoming developments will be very different from developments in the past. In the 1960s, Gordon Moore described the development of compact digital integrated circuits by doubling the transistors per area every two years [54]. Referred to as *Moore's Law*, this prediction became a major paradigm in the semiconductor device industry. But this paradigm is based on the assumption that conventional down-scaling of transistors can be pursued without borders. Instead, this technology has reached inherent limitations and the physical limits in these systems are already pervasive in the semiconductor device industry. Hence, new technologies have to be developed in order to increase the capabilities of these systems.

Two different descriptions of technology step changes are given by the Semiconductor Industry Association (cf. Fig. 1.1):

More Moore refers generally to all developments based on the CMOS technology and it includes nearly exclusively digital components. In order to be compliant to Moore's Law, a continuous down-scaling of all CMOS devices was pursued. Since this down-scaling has reached its limits, current developments focus on the parallelization of several digital devices, without changing the design of the single device significantly: computational power is increased by more parallel cores instead of cores with more transistors. *Beyond CMOS* is possibly the most long-term perspective amongst all other

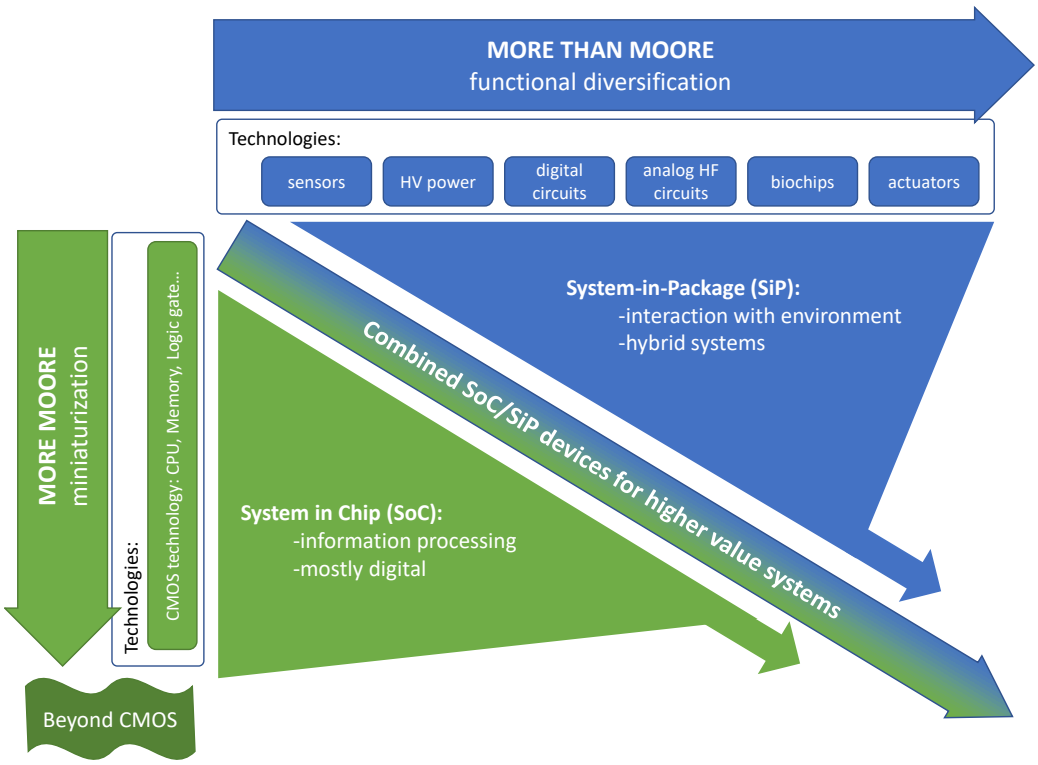

Fig. 1.1 Distinction between two major development trends: *More Moore* refers to the continuous development of CMOS technology towards more miniaturization as well as incorporation of non-CMOS based technologies. In contrary, *More than Moore* refers to the development of diversification beside pure electronics. (according to [6]).

More Moore-developments, since it focus on the application of novel materials in order to substitute the conventional CMOS material silicon. Carbon based materials such as graphene or carbon nanotubes, molecular electronics in general, as well as spintronics and memristors, have become the most common candidates for alternative materials.

More than Moore refers to technological approaches which enable non-digital micro- and nanoelectronic systems. The main objective is a diversification of these devices. Hence, they are intended to process more than just electrical information: mechanical, thermal, chemical, and optical information are to be processed and converted into each other. With this understanding, the fundamentals of micro/- and nanotechnology are predestined for *More than Moore*-developments.

Beside these two major development trends, there is a large variety of approaches, which go far beyond the fundamental principles of semi-conduction. All have in common the goal to extend the abilities of current devices in order to increase the impact of their applications.

1.1 The Micro-/nanoscale

1.1.1 What is the Micro-/nanoscale?

In 1816, Hegel already published the idea that qualitative changes can be achieved by changing quantitative figures sufficiently [102]. Today, micro- and nanotechnology are promising enabling technologies for future devices, applications and entire domains, but the first fundamentals are already ancient. Furthermore, the first idea of exploiting the smallest possible scale of matter is half a century old.

In 1959, Richard P. Feynman had given an inspiring talk with pioneering concepts and visions about the nanoscale - without using the term *nano* at all [82]. Anyhow, the content of this lecture was the first documented modern thought experiment about technology exploiting the potentials of the small scale. Hence, Richard Feynman is considered to be the "Father of nanotechnology".

Years later in 1986, Eric Drexler used the term *nanotechnology*[2] is his article *Engines of Creation: The Coming Era of Nanotechnology* [72] and since then, this term has been established and is now extensively used in several fields of research and technology.

Today, the term nanotechnology addresses an interdisciplinary field of research, which can refer to all technologies at the nanoscale. *Nanoscale*, concerning the spatial dimension, considers the range from 1 to 100 nm. Hence, the term *nanomaterials* refers to all matter that is spatially limited to 100 nm in at least one dimension[3]. In extrapolation of this definition, also the term *nanoobjects* becomes meaningful, describing all objects with limited spatial size in at least one dimension.

Overall, a definition of nanotechnology is reasonable, in order to distinguish between simple miniaturization of common technologies and the novelty, uniqueness, and potential of nanotechnology:

Nanotechnology pertains to the processing of materials in which a structure in the dimension of less than 100 nm is essential to obtain the required functional performance [62].

This definition includes the novel functionality and performance that emerge on the nanoscale. Appropriately, it is applied in the official standards ISO/TC 229 [138] and

[2]The actual term *nano* is derived from the Greek word $\nu\alpha\nu o\varsigma$, which means dwarf, and is the name for the unit prefix representing the factor 10^{-9}.

[3]The fact that all matter is built of sub-nanometer sized atoms is not sufficient to call it nanomaterial.

DIN CEN ISO/TS 80004-1 [8]. By this definition, there currently are almost 1.5 million publications referring to *nano*-topics[4].

1.1.2 Benefits of the Micro-/nanoscale

The micro-/nanoscale is of high importance for current and future developments in technology. The appearance and behavior of almost any material change compared to its bulk properties, if the spacial dimension is in the nanometer regime. In this way, nanomaterials and nanoobjects possess unique physical properties, which are caused solely by their small size or by the special atomic configuration:

- The small size alone can be very beneficial, since the surface-to-volume ratio increases. This ratio is an important figure of merit, especially for sensors' transducers that depend on the interaction with their environment: The neutral signal of a transducer depends mostly on its volume, while the information signal depends on the interaction surface. If a wire with the diameter r is a transducer, the information signal strength scales with $1/r$.
- Working on the nanoscale also means, that the environment is not governed by classical physics, but quantum mechanics. Quantum mechanics has eminent effects different from classical physics, which can be exploited particularly on the nanoscale: Special microscopes, such as the scanning tunneling microscope, allow the characterization of surfaces with sub-nanometer resolution. Part of their working principle is the measurement of a quantum tunneling of electrons between two objects that are separated by less than a nanometer [46].
- The special atomic configuration of some materials are accompanied by unique physical properties, which is also a direct result of quantum mechanical effects. Carbon nanotubes and graphene, for example, are so called *ballistic conductors* without electron scattering and therefore, negligible electric resistivity.

Hence, nanomaterials and nanoobjects are promising candidates for any kind of novel active or passive transducers, such as sensors, actuators, computing units, et cetera. Nonetheless, not every nanoobject or nanomaterial necessarily uses quantum mechanical behavior or exploits fundamental different physical effects on its own. In some cases, the functionality arises from the integration into a system or the combination of several objects to a system. In this perspective, nanoobjects and nanomaterials can be considered as micro-/nanoscale building blocks resulting in a consentaneous definition:

[4] Source: Web of Science, Result from 11.07.2018

Nanoscale building block pertains to nanoobjects that a) can be or have to be integrated to or into systems, and b) obtain or provide the required functional performance by a spatial dimension or a compulsory integrational precision in at least one dimension of less than 100 nm.

In conclusion, nanoscale building blocks can be claimed to be crucial and fundamental components for research as well as future innovations technology.

1.1.3 Challenges and Opportunities

The great potential of nanoscale building blocks is beyond controversy. Their integration can improve existing technologies and allows further innovations. Anyhow, in today's applications of nanomaterials, they are very often rather a kind of mass-additive to other components and cannot contribute their full potential. According to the definitions above, the unique properties can be exploited only, if these objects are integrated as individual and functional objects into devices. But this integration requirement remains as a major challenge for the handling abilities of these objects.

Challenges

The major obstacle for the integration of nanoscale building blocks is the lack of sufficient handling abilities. A variety of reliable techniques have been developed to fabricate nanomaterials and -objects. However, their products are still subject to variations and their properties need to be validated before they can be integrated into a system. In any case, techniques are needed to transfer nanomaterials- and objects from a production substrate to the intended place of their final functionality. A few approaches and techniques exist to pick and place nanoobjects, and some approaches have been developed to produce nanoobjects in their destination. The feasibility to integrate nanoobjects with high precision at a predetermined place, is still highly required.

The challenges of handling capabilities on the small scale arise from physical differences of that micro-/nanoscale in contrast to the macroscale in the same way as the benefits of micro- and nanoscale building blocks arise (cf. Section 1.1.2). The small size alone has negative consequences for the handling, as depicted in two fundamental problems, which were described by R. Smalley [177] as follows:

Fat finger problem Refers to a situation of nanoscopic positioning were an object is not independent of all other objects in its vicinity. Smalley claims that this problem can

not be tackled by additional control of freedom on the nanoscale. Hence, controlling all degrees of freedom is impossible.

Sticky finger problem Refers to the situation where a minuscule building block it to be released from a manipulating hand. According to Smalley, this is impossible on the atomic scale, since already connected atoms tend to adhere to each other.

These principle assertions are hypothetical, are based on certain assumptions, and they consider especially chemical reactions. But in essence, they address the fundamental challenges of the nanoscale: Since gravity and inertia scale with the volume and adhesion scales with the surface, all objects on the micro-/nanoscale tend to cling together. Simple handling tasks, such as dropping or separating objects can become impossible on this scale. In addition, another crucial obstacle of the micro-/nanoscale is the limited ability to visualize the scenery. Regular optical systems for visual light offer fast, accurate and reliable image acquisition on the macroscale. However, the resolution capabilities of systems that work with visible light are subject to the physical diffraction limit: In ambient conditions, two objects in an image are indistinguishable. if they are closer together than roughly 200 nm. For this reason, vision based feedback is more complex on the nanoscale and demands a more complex microscopy system.

In summary, the small scale is not only reason for opportunities but also reason for severe obstacles for the integration of nanoscale building block. However, most of these obstacles can be tackled, overcome or circumvented.

Solutions

Despite the challenges mentioned above, the micro-/nanoscale can be exploited and used in order to reach new levels in technology and to advance towards novel knowledge. The “fat finger” problem prevents manipulations mostly in the perspective of chemical reactions. If external and especially mechanical constrains are applied, the hardly controllable chemistry is not the only factor anymore influencing the manipulation. Furthermore, additional reactants or other reaction-changing influences can be applied to solve the “sticky finger” problem. Hence, a steerable mechanical constraints and the application of external forces allow controlled processes spatially on an atomic level. This is the reason for the application of robotics. A robot that can control mechanisms on the nanoscale does not even have to be that small itself. In this understanding, a definition which is independent of the robots size is reasonable:

A nanorobot is a device that can operate with respect to a spatial resolution of less than 100 nm, allowing the manipulation of nanoscale building blocks.

Robotic handling is a effective way to facilitate and improve manipulations on the nanoscale. The accuracy and precision of positioning of existing nanorobotic systems are already in the sub-nanometer range and the limited mass on that scale makes handling sequences stable for high acceleration and jerk. This allows movements with large velocities and accelerations. Nanorobots are flexible concerning their working environment: Environmental conditions as well as specially controlled or encapsulated environments are possible. Especially vacuum conditions are of special interest, since they reduce the interaction with surrounding atoms and molecules to a minimum, with is another approach to reduce the "sticky finger" problem. Furthermore, nanorobotic systems can serve in serveral different ways: They can be used for different manipulations, diverse characterizations or act as combined systems for visualization. As mentioned above, visualizing is quite challenging on the nanoscale and hence, combining capabilities and tasks within few robotic systems is advantageous.

Different physical interactions can be measured by robots on the nanoscale, and allow an extensive and comprehensive analysis. The ability of a nanorobot to control spacial positions precisely, offers the possibility to perform mappings of all these different physical dimensions. Thus, by means of robotics, a variety of quantities can be used for standard imaging or even hyper-spectral imaging. Finally, robotic processing is always accompanied by a serial processing structure. This might be slower than parallel processing, but entails intrinsic advantages: Due to the serial nature, every processed object can be treated individually. This lead to the possibility of a tailored production - either in respect to the individual object or in respect to a certain external demand. Hence, the incredible demands on highly reproducible processing technologies can be lowered. The final status of any object can be measured and it can be individually determined before, after or even during processing.

Possibilities

A well-directed control of the building block on the micro-/nanoscale will facilitate an exploitation of the benefits of the small scale by the means of novel devices. As introduced in Section 1.1.2, the micro-/nanoscale is an extraordinary source for useful physical behavior. If a technology is sufficiently mature to control nanoscale building blocks with a decent accuracy, novel functional devices will be possible.

The opportunities depend on future developments, just as their chance of realization. However, their potential outcome can be a great improvement and can address different fundamental improvements for industry, researchers and society. The following examples are all motivated by the potential of the micro-/nanoscale: they are theoretically possible, but they still suffer from immature assembly technologies on the micro-/nanoscale:

Size Many future devices need tiny energy sources if they want to work untethered and autonomously. This is important for consumer electronics, autonomous robots, energy saving, as well as for medical in-vivo devices. All these future devices are intended to operate with an increasing range and lifetime: Small-sized consumer electronics (e.g. smartphones) offer increasing operational power which involves increasing energy requirements [78]. Autonomous robots, especially in harsh environments, need a long term power supply to stay active, but have limited payload. Medical implantes, which are much smaller than pacemakers, need electrical power sources that cannot be exchanged frequently [197]. All these applications are extremely useful but need tiny energy sources.

Sensitivity The micro-/nanoscale allows the increase of the sensitivity of sensors up to levels, since they can be built as portable sensors that do not exist so far. For instance, mercury detection is tremendously important for the safety of workers in the oil and gas industry. However, there is no personal exposure monitoring device for mercury. Additionally, due to the application field in oil and gas industries, such a device has to fulfill all requirements of intrinsic explosion protection (in this particular example the intrinsic safety class *Ex ia* according to the international standard IEC 60079-11 [2]. Hence, limited current and voltages are mandatory [5]. These conditions cannot be fulfilled by state-of-the-art devices [9]. In contrast, sensors on the micro-/nanoscale could work with very limited current, voltage, and power consumption. They offer fast response times and a high resolution. However, even if the fundamental electrical structures are easy to build, the integration of the actual nanoscale transducer remains a challenge.

Energy density As mentioned above, downsizing batteries is a motivating goal for technologies on the micro-/nanoscale. Besides shrinking the overall size, the energy density and power density are other figures of merit which have to be increased, which is already tackled by means of nanomaterials. Storing and releasing much energy in a short time is important for energy recovery, renewable energies, and entire decentralized energy supplies such as smart grids. Nanomaterials, such as Graphene, Nickel hydroxide flakes or Tungsten-trioxide nanowires, and various nanostructured materials were

[5] less than 1.5 V and 100 mA are common

already discussed as promising candidates to build energy storage devices with large power and energy density [211]. A fundamental issue in this field is the combination of different materials and strict requirements for their assembly [187]. Furthermore, during their operation many energy storing systems based on nanomaterials change their morphology which results in a major challenge for their integration into devices [208]. All these requirements result in high demands on the assembly of all involved components.

Novel devices Completely novel devices are a strong motivator micro-/nanointegration due to their high impact. The combination of different optical components allow the realization of optically sensing and computing devices. Future computing devices could be much faster using optical instead of electrical signals. To achieve this, conventional transistors and NAND-gates have to be substituted by optical equivalents.

Future realizations of quantum computing are even more exciting: Quantum computing needs an implementation of *qubits*, a quantum mechanical two-state system. Electrons in quantum dots are promising candidates for this application. In combination with photons for quantum communications, these systems could be a tremendous impact for scientific computing.

Both visions, optical as well as quantum computing, come along with very complex integration challenges on the micro-/nanoscale.

In conclusion, a variety of future applications will offer the extension of different capabilities and the improvement life, but manufacturing on the small scale is a substantial prerequisite. Firstly, the manufacturing and integration abilities of nanoscale building blocks will benefit researchers and developers: Existing products will become more efficient on an industrial level. Additionally, investigations that are impracticable today will become possible for researchers for the first time. Even more importantly, controlling the micro-/nanoscale will lead to novel domains and disciplines that have the potential to change life in a long term perspective.

1.1.4 Working the Micro-/nanoscale

Particular techniques are necessary when working on the micro-/nanoscale. Even though all matter contains nanostructures, the actual functionality has to be on the small scale - according to the definitions above. Most manufacturing approaches on the micro-/nanoscale can be categorized in two major groups:

Top-Down Top-down approaches are mostly further developments and miniaturizations of classical machining techniques and also cover all techniques from semiconductor device fabrication to MEMS technology [96]. The common working principle is to externally create or structure small devices by means of larger instrumentation. This is done with additive techniques such as coating and implanting, as well as subtractive techniques such as chip-forming machining, etching, and erosion. Assembly and packaging is done by handling (robotic or manual), also combined with transfer agents. Many top-down techniques are related to physics and engineering sciences.

Bottom-Up Bottom-up techniques are mostly developed from chemistry and biology. The common working principle is the self-assembling of molecular units such as molecules, proteins or bacteria. The components are typically much smaller than in top-down fabrication, but the assembly design is much more complex. Due to its nature, the only approach to bottom-up assembly are additive techniques, which can be biological or chemical synthesis. Hence, self-assembly as the only form of assembly limits the process, which is why packaging is more challenging than in top-down techniques.

Certainly, this classification into two categories does not comprise all existing approaches and technologies. Furthermore, the aforementioned potential of the micro-/nanoscale can hardly be exploited by the means of one single technology alone. In nearly any case, different materials and components have to be combined in order to build functional devices. As mentioned in Section 1.1.3, this demands technologies, which are capable for integrating of nanomaterials and nanoscale building blocks into particular surrounding devices, which are produced in a different process. This micro-/nanointegration constitutes a key enabling technology and is of tremendous importance for the exploitation of the potential of nanomaterials. Hence, it can be defined by:

Micro-/nanointegration refers to technology, which constitutes an interface between the macro-/microscale and the nanoscale allowing the exploitation of effects on the nanoscale as the fundamental functionality of functional macro- or microstructures.

Micro-/nanointegration is a bridge between the two approaches bottom-up and top-down, but also utilizes techniques from both. Building this bridge, micro-nano-integration allows the construction of complex systems, which is the key to connecting the nanoworld to the macroworld and harness its potential. Therefore, scientific findings and successes can be to transferred to novel technologies. While, a general understanding of the forces ruling the micro-/nanoscale exists, direct transfer to the development of handling strategies is still lacking, since these forces are hardly controllable and measurable – despite the fact that some of them are deterministic.

1.2 Objectives

Existing techniques for micro-/nanointegration are still lacking to address individual nanoscale building blocks. The objective of this work is the accurate definition of strategies for micro-nano-assembly of individual nanoscale building blocks as well as the development and evaluation of novel strategies to enable efficient micro-nano-integration for research and industrially relevant applications. These two different applications have common as well as diverse demands on the three figures of merit of each process:

Accuracy and Precision - in all directions and orientations - are the most important and common demands for all micro-nano-assembly tasks. Researching investigations as well as industrial exploitation of the micro-/nanoscale need an accuracy which is at least in the same order of magnitude as the involved nanoscale components. Furthermore, precision is important for industrial applications in order to perform processes with high repeatability.

Speed and success rate of an assembly process are mainly important for industrial applications, where throughput is a key factor for the economy of a process. Speed and success rate are both direct factors which influence the *effective throughput* of a process.

Cost-efficiency acts as an abstract measure if a process is actually able to perform a precise integration task with appropriate effort, personal and instrumental costs. This figure is mostly important for industrial exploitations but can also be an obstacle for researchers.

Automation capability has a direct impact on the throughput and the cost-efficiency of a process. Moreover, on the micro-/nanoscale, automation can be a key technology to make some integration steps feasible in the first place.

In order to achieve the objective and to meet the particular demands, several handling and automation strategies are defined, implemented and assessed. Existing boundaries for micro-nano-assembly are pushed by novel techniques and further developments of existing ones. Finally, the developed techniques and strategies are applied to two case studies - one for research and one for industrial applications. The common core task in both case studies is micro-nano-assembly and both demonstrate use-cases of the novel strategies and the automation capabilities, which further the scientific results towards an applicable technology.

1.3 Outline and Author's Contribution

The author contributes to advancements of micro-nano-assembly with novel nanorobotic handling strategies and the application of automation capabilities on that scale. In this context micro- and nano-assembly refer to the manipulation of objects with functional dimensions and precision on the micro-/nanoscale, by means of macroscopic but precise robots.

The thesis is structured in seven chapters:

Chapter 2 gives a comprehensive overview of existing nanohandling approaches and systems, which have been developed for manipulation and assembly on the micro-/nanoscale. Furthermore, existing automation techniques and supporting software approaches are examined.

The following chapter 3 presents the fundamental tools and principles as well as the developed working environment for this contribution. The working principle of handling and assembly on the micro-/nanoscale are introduced, and prerequisites, limits and their abolition strategies are discussed. All instrumental components of hard- and software, such as the electron microscope, the robotic stages, and the software interface, are presented.

The strategies developed as part of the authors contribution are presented in chapter 4. Several different nanorobotic handling strategies are discussed and engaged according to their specific purposes and (dis)advantages. Precisely structured metal tips, adhesive-bond handling, and micro-grippers are used to pick, transfer and assemble nanoscale building blocks. The structural design of handling tips and samples is used to increase the spatial accuracy and in some cases the entire feasibility of assembly tasks. This is of high importance on the micro-/nanoscale, since handling robots and stages hardly offer more than simple translational movements. The structural design enables the determination of rotational degrees of freedom, allowing control over the orientation of handled objects.

Furthermore, fundamental characteristics of the scanning electron microscope (SEM) are exploited to increase the amount of information during an assembly process, in order to improve the automation capabilities of the developed strategies. Deriving three-dimensional information is a fundamental challenge in scanning electron microscopy, which is a major obstacle for assembly processes. The mentioned fundamental characteristics can be used to derive direct or indirect information on spacial conditions of different objects during an assembly process. So called *electron shadowing* and *electron beam charging effects* can be measured by the SEM and offer useful information of the automation.

Chapters 5 and 6 present two different case studies as applications of the developed strategies: Chapter 5 deals with the handling of nanowires with diameters in the regime of 100 nm. The research interest is an electro-mechanical characterization combined with simultaneous morphological investigations. This kind of measurement has to be performed inside a transmission electron microscope by means of a specially developed MEMS-based testbench. During observation by the transmission electron microscope and simultaneous electrical measurements, the nanowire is subjected to tensile stress. The particular challenge for this research project is the actual integration of the nanowire onto this MEMS-workbench. This assembly task has three major conditions that have to be fulfilled:

1. The nanowire has to have a precise position on the workbench as well as a precise alignment with the operational direction of the workbench.
2. The nanowire has to be fixated to the workbench in a mechanically stable way in order to endure the mechanical stress.
3. The nanowire's fixation has to be electrically conductive.

The assembly sequence of this case study demonstrates the accuracy and capabilities of the developed strategies.

The second case study is presented in Chapter 6. The NanoBits-project aims to build specialized tips for atomic force microscopy probes. These probes have exchangeable tips made of silicon with flake-like dimensions: few by few micrometers by about one hundred nanometers. These so called NanoBits are produced with electron beam lithography, but need to be assembled into a micro-cartridge system. This includes several typical nanohandling steps, such as picking and transfer, but also some very challenging steps: Each NanoBit has to be rotated for example, which presents a very difficult operation on the micro-/nanoscale. Furthermore, a predetermined breaking point has to be broken in order to release each NanoBit from its production substrate. The final assembly into the cartridge is an uncertainty-intolerant process step, since protruded parts of the NanoBit are most sensitive. The overall assembly demands for precisions higher than 50 nm. In this case study, nanogrippers are used as handling tools, and electron-shadowing effects and discharging is used as status information. A fully automated assembly sequence of a NanoBit is realized.

The final chapter 7 summarizes and concludes all results about the developed handling for nanomaterials and the automation capabilities. A final assessment according to the defined figures of merit acts as a basis for general recommendations for future applications of automated nanohandling. A closing outlook offers a perspective for future extensions of this contribution.

2 State of the Art

Micro-/nanointegration is a topic that is addressed by many researchers. However, automated handling on the small scale is a rather niche topic due to technological challenges. Actuators and sensors are limited and it is difficult to gain control. Hence, only little research and development is completed in this field. While robot assembly and automation are very large fields of research, each change of topic towards the small scale reduces the research community to onyl few contributors. In the last decade, 5642 publications were released on the topic combination *assembly* and *robotic*. In comparison and in the same time, 54 publications were written on the topic combination *assembly*, *scanning electron microscope (SEM)*, and *robotic*. If *automation* is added as an item, the publications are further reduced to 16 [1].

This chapter introduces the SEM (Section 2.1), which is the fundamental visualization tool on the micro-/nanoscale if high update rates are necessary. Furthermore, fundamental handling methods on the micro-/nanoscale are introduced (Section 2.2) and existing automated nanoassembly approaches are presented (Section 2.3). Section 2.4.1 finalizes this chapter with an overview of other contributions that had goals comparable to those in this contribution.

2.1 Scanning Electron Microscopy

The lower end of the microscale and all of the nanoscale are too small to be visualized with conventional microscopes and, hence, electron microscopes are essential. A microscope's

[1] All surveys conducted for the particular keywords as topic on August, 14^{th}, 2018 at *Web of Science*, Clarivate Analytics, including the years 1998-2018.

ability to visualize objects depends on the wavelength of the light used or the electromagnetic radiation. Optical microscopes use visible light that has wavelengths between 380 nm and 780 nm. The resolution power in this order is not sufficient for tasks in micro-/nanointegration, since it is limited by the so-called *diffraction limited* quantified by the *Rayleigh-Criterion*

$$d_0 = \frac{0.61\lambda}{nsin(\alpha)}, \tag{2.1}$$

where α is the maximal angle between the optical axis and the incident light, λ is the wavelength of the light used, and n the index of refraction in the environment [160]. As a result , d_0 gives the minimal distance of two details, that can be distinguished by this optical system. Considering all improving possibilities[2], the theoretical resolution limit of an optical microscope is 155 nm. Electron microscopy offers an alternative with better resolution. According to de Broglie, each waving particle has a corresponding *matter wave* of the wavelength

$$\lambda = \frac{h}{m_0 v}, \tag{2.2}$$

that depends on the particles rest mass m_0 and the particle's velocity v, with h as the Planck's constant. For example, electrons that are accelerated in an electric field of 30 kV have a de Broglie wavelength of 0.039 nm. Hence, the *diffraction limited* is orders of magnitudes smaller than in light optical microscopes.

The scanning electron microscope is the most prominent electron microscope. Besides the fact that electrons are used for illumination instead of light, its most important property is that it is a *scanning* microscope. The electrons are focused to an electron-beam of few nanometer radius that scans the samples surface pixel-wise in order to reconstruct an image. All other components known from light microscopy, such as lenses, filters, and apertures, are also available for the electron beam, but they are operated electrically or electromagnetically. Moreover, even the same optical aberrations exist and have to be compensated, such as chromatic aberration, spherical aberration, and astigmatism [160].

The most important imaging parameters of a scanning electron microscope are also comparable to a light microscope:

Magnification The maginification is determined by the ratio of image size to object size. The image size is defined by the PC-screen while the object size is defined by the

[2] meaning i) an optical angle close to 90°, ii) the use of immersion oil with $n = 1.5$, and iii) using violet light with $\lambda = 380\,\text{nm}$

	light microscope	SEM	SPM
resolution (nm)	> 155	2 - 10	1
viewfield	mm - tens of µm requires lens changes	cm - few µm seamless	µm - nm
framerate (Hz)	>25	10 - 0.01	0.1 - 0.01
type of information	2D	2D	2½D
depth of field	0.5 µm - 100 µm	10 µm - mm	not applicable
sample interaction	weak light exposure	strong e-beam irradiation	strong contact to prober

Table 2.1 Comparison of different microscopy instruments.

region/viewfield that is scanned by the electron beam. Since the size of this viewfield is determined by the electron beam control units, an SEM has the capability to change the magnification seamlessly and at any time. The viewfield of the Tescan Lyra SEM used in this contribution can be adjusted between 10 cm and few micrometers - corresponding to magnifications between 1.5x and 1,000,000x.

Resolution Different definitions of resolution are applied in microscopy. The Rayleigh-criterion is well known but theoretical. Since the resolution of an SEM depends on many effects and disturbance, the more practical 90/10 criterion can be applied [111]. Depending on all imaging parameters and the sample, modern SEMs can reach resolutions below one nanometer. The used Tescan Lyra SEM has a theoretical resolution of 1.2 nm, while the 90/10 criterion results in about 7 nm.

Depth of Field The depth of field, meaning the spacial range along the optical axis around the focal plane resulting in a sharp image, is very large for SEMs. While optical microscopes have a depth of field between 100 µm and 500 nm, the depth of field of an SEM is typically 1-2 orders of magnitudes larger [160].

Visual Feedback for Robotics

Table 2.1 shows a comparison of the most common instruments that visualize the nanoscale. For micro-/nanointegration, it is most reasonable to use the SEM as the tool for visual feedback, since it has the best combination of advantages (compared to other microscopy instruments): It has a very high resolution in combination with a scalable viewfield, which cannot be achieved by light microscopes or scanning probe microscopes. The update rate is adjustable and reasonably high.

However, the use of the SEM also has some disadvantages. It is combined with a large instrumental effort for the visualization and preparation. The vacuum working environment

itself poses several requirements on all materials and only low out-gassing materials can be used, while the vacuum chamber itself prevents direct access to the setup and limits the spacial conditions of the setup. This also effects the electron illumination scenario, since the SEM cannot be rearranged. Therefore, the visual perspective and the direction of the perceived light source cannot be changed. This limits the ability to acquire 3D information and prevents setting optimal illumination conditions for the assembly. Hence, monocular vision and shadowing effects have to be accepted.

Furthermore, the electron beam can be the cause of further drawbacks. Due to the high energy, sensitive samples can be damaged by simple exposure. Additionally, the interaction of sample and electron beam can lead to contamination by residual carbon particles in the vacuum chamber. Finally, the electron beam induces charge on the sample, which can lead to considerable distortions of the electron beam and thus of the visualization system itself.

Using the SEM as visual feedback for robotic systems raises other more particular issues. On the one hand, the large degree of freedom (DOF) is advantageous for imaging, on the other hand no depth information can be derived from such an image. Hence, even though the SEM offers very good lateral resolution, one particular challenge in SEM-based handling is the acquisition of precise depth information along the optical axis by focusing.

Some of the mentioned characteristics of the SEM are advantageous for in-situ micro-/nanointegration tasks in robotics. On the other hand, other mentioned characteristics are rather obstructive. However, some of them can be exploited and used as a source of information for micro-/nanointegration and automation. The most prominent examples are stereo-vision, depth-from-focus, and depth-from-shadow methods. Chapter 4.2.1 introduces two additional methods to derive depth information from SEM-typical distortions.

FIB

Beside electron microscopy, ions can also be used for microscopy and even machining purposes. Typically, the ion beam, generated from a liquid metal ion source, can be in the range from sub-pA to tens of nanoampere. A focused ion beam microscope has the same working principles for charged particle beams as the electron microscopes and it scans the surface of the sample with ions. The resulting interaction of the ion beam with the sample also leads to the emission of "‘secondary"’ electrons which can be used for imaging [93]. Moreover, the kinetic energy of the FIB ions is high enough to sputter the samples’ material by elastic scattering. Depending on the ion current, the abrasions rate can be up to

$2x10^5$ m^3/min [203]. Thus, the FIB system can be used for imaging and machine processing, whereby both processes always run simultaneously.

GIS

The electron beam induced deposition (EBID) technique uses a gas injection system in addition to the vacuum chamber The GIS allows the fabrication of highly localized material depositions inside the SEM [191]. These GISs can offer several different precursor materials, which are all fed into the chamber in the gaseous state. The gas flux in the SEM chamber is highly localized due to the high vacuum conditions, which makes the distribution of the precursor molecules ballistic. For this reason, the precursor molecules have to be released in close vicinity to the processing area. All GISs possess a precursor-releasing nozzle, which is driven by a robotic system in order to reach the processing area. The precursor molecules can be decomposed by little energies and they decompose in a volatile and nonvolatile part. While the volatile parts diffuse in the vacuum chamber, the non-volatile parts deposit on the next surface they hit leading to a growing deposition on the substrate. The decomposition of the precursor occurs due to a bond dissociation of its molecules with dissociation energies in the range of few electronvolts. Hence, the primary electrons of the SEM electron beam have too much energy to crack the precursor molecules. However, the secondary electrons leaving the substrate have energies between 0 and 50 eV. This leads to a localized deposition process, since precursor molecules are only cracked in regions where secondary electrons exit the substrate. Depending on the material, typical deposition rates are in the range of few tens of $nm^3nA^-1min^-1$ [191]. For this reason, EBID depositions can be applied purposefully on specific spots of a sample by means of controlled electron beam exposure. This makes the EBID technique useful for in-situ manipulations on the micro-/nanoscale, since highly localized depositions can be used as a nanoscale adhesive bond technique.

2.2 Handling on the Micro-/nanoscale

Handling, which is to be understood as the basic ability to move an object in general, has limited techniques on the micro-/nanoscale. On the microscale, some end-effectors are available that have functionality; however, operational freedom is still very limited. Nevertheless, they are capable to be actuated with at least one degree of freedom or to measure at least a single datum. On the other hand, there are hardly any end-effectors with

controllable functionality on the nanoscale. Hence, handling techniques on this scale have to rely on additional effects and interactions.

Indirect handling techniques Indirect handling techniques do not need end-effectors and, therefore, are easy to transfer to the small scale. However, their requirements on the environment are obligatory.

Microhandling is mostly related to the manipulation of biological cells which is often performed in a liquid environment. When the liquid is in microfluidic channels or chips, contained cells or particles can be moved or sorted by controlling the liquids flow. This can be achieved by microfluidic chips with several ports and pumps in order to create a controllable flow-field [143].

Furthermore, microfluidics can be used as fluid carrier while other physical forces are used to manipulate cells without direct contact: Magnetic actuation [71], dielectrophoresis [179, 113], magnetophoresis [140], acoustic waves [70], and optical-tweezers [147] are all well-known techniques that control particles in liquid environments.

Direct handling techniques Direct handling techniques are mostly in physical contact with the manipulated object. End-effects for direct handling can be active by means of additional controllable components or passive.

Pipettes are the best-known instruments to fixate and manipulate cells and particles in liquid environments [126]. Pipettes can also have additional electrodes to investigate ion currents through cell walls [166].

Some *large scale transfer* methods for nanoobjects must also be considered as direct handling techniques, but they are not applicable to individual nanoscale building blocks [123].

Grippers Grippers are one of the most intuitive tools for operators. Even though they are known from the macroscale, their physical working principle is slightly different on the micro-/nanoscale (cf. Section 4.1.3). A variaty of microgrippers is available in industry and research (presented in decreasing size):

Femto-ST developed a large gripper that handles building blocks of hundreds of micrometers in dimension [53]. However, this gripper has several DOF for each gripper jaw that can be controlled independently. Hence, this gripper addresses a core topic in micro-/

nanointegration, since it is capable to rotate buidling blocks and manipulate them with four DOF.

Femtotools offers industrial grade electrostatic microgrippers for the manipulation of objects between 1 µm and 100 µm diameter [15]. The gripper opening is between 30 µm and 100 µm and the thickness of the gripper jaws is 50 µm [45]. Only one gripper jaw is actuated, while the other gripper jaw can be used as force sensitive counterpart [15].

The *University of Toronto* developed an active electrostatic gripper with two actuable jaws and an additional plunger in center position, which is used to overcome the adhesion. The gripper opening is about 17 µm and it is used to pick-and-place spheres with an accuracy of about 0.7 µm [59]. Additional decoration of the gripper's tips with 1 µm thick extensions allows to pick spheres of about 100 nm [60].

The *Technical University of Denmark* developed even smaller grippers based on the thermoelectrical expansion of silicon. The grippers are 5 µm thick and have an opening of few micrometers [33]. Depending on the dimensions of the grasped object, the grippers can apply forces of up to 10 µN. The application of these grippers is demonstrated in a case study presented in Section 6. It can already be noted that these grippers are the only ones that allow for sub-100-nm manipulations.

An outstanding example of grippers is presented by *Samsung Advanced Institute of Technology* [108]. Two multi-walled carbon nanotubes are perpendicularly mounted onto electrodes. By the application of a potential difference of 50 mV, the nanotubes are attracted to each other and act as gripper jaws. The gripper's opening is about 250 nm. However, in some cases, the gripper remains in the closed position due to van der Waals forces. Furthermore, this gripper is just a demonstrator and could not be used in any application.

The development of nanogrippers is challenging and the amount of applications is still limited. Hence, the research in the last eight years has mostly consited of reviews, theoretical investigations, descriptions, and smaller improvements of existing concepts [56, 60, 149, 200, 49, 92, 84, 97].

Passive Tips Only few examples for end-effectors with sizes <100 nm exist. Most of them are just passive elements that are used to touch a sample and prepare a subsequent processing step, which is typically a measurement or a manipulation task. The tips used for these tasks are either atomic force microscope (AFM) cantilevers or etched tungsten tips – known as STM-tips [145]: Cantilevers have been used for manipulations [85], electrical measurements [44], and mechanical measurements [214] of objects on the micro-/nanoscale.

Tips can be applied for electrical [127, 164] and mechanical [44, 127] characterizations as well.

Additionally, tips can be mounted on a vibration base, whose resonance frequency can be monitored, so, a force sensitive tip can be established even though the tip itself is not actuated [31]. This is also the fundamental working principle of the AFM.

In general, most scanning probe microscopes can also be used for nanhandling tasks if additional physical forces are applied. Several examples can be found for atomic force microscopes [34, 188, 61, 199, 114] and scanning tunneling microscopes [76, 101, 156].

2.2.1 Microhandling Stations

Several microhanding stations are commercially available. All operate based on light microscopy images and are, therefore, limited to the coarse sub-micrometer accuracy. The three most interesting and most mature systems are presented.

Percipio Robotics offers a tabletop robotic system called *Chronogrip* that is intended to perform teleoperated, as well as fully automated, microsassembly tasks [125]. The system uses one or two microscope cameras as a visual feedback system and can be controlled via keyboard, joystick, and gestures. The visual resolution is as small as 2.5 µm, the nominal positioning accuracy is 2 µm and the nominal precision is about 200 nm [14]. However, the effective accuracy and precision of an assembly result, as well as the rate, are not documented [125, 14].

SET Corporation SA offers a variety of flip-chip, bonding, and stacking machines [26]. Theses machines have two optical microscope cameras and at least four robotic DOF. The visual resolution is as small as 0.37 µm and laser leveling can be used to achieve high accuracies. The nominal positioning accuracy is 0.5 µm [137]. These systems are capable of performing predefined pick-and-place operations as well as an automated alignment of two components using optical markers. The throughput of these systems is mostly limited by the bonding technology and is in the range of several minutes [120].

Häcker Automation offers the most advanced assembly, soldering, and dispensing systems. In addition to the standard three translational DOF, they offer end-effectors with two-tiling axes and a tiltable sample carrier. Hence, they achieve an actual 3D assembly with an accuracy of 5 µm [18].

2.2.2 Nanohandling Stations

In contrast to a variety of systems that are specifically for microhandling tasks, there are only few nanohandling systems on the market. Most nanohandling setups and stations use commercial available platforms, but systems solely for nanohandling are rare. Rather the platforms on the market are for general purposes and used for probe microscopy, arbitrary alignment, positioning tasks, probing, and also for nanohandling.

Table 2.2 shows an overview of the most important systems on the market. System 1 is widely-known since it is the most used system for in-situ TEM lamella handling, which is the best-known microhandling task inside the SEM [134]. The systems 2-6 are modularly designed platforms. Most of them use modules with three robotic DOF that can be arranged to work cooperatively on the same working spot. Hence, complex handling setups with up to 24 robotic DOF can be achieved [3]. The systems 8 and 9 are hybrid SEM/SPM systems, that can also be used for nanomanipulation tasks.

Beside these commercially available systems, there are many self-developed nanopositioning stations in research and development departments worldwide. Most of them are assembled by several commercial nanopositioning axes and tailored for a specific purpose [109, 146, 115, 139, 156, 81, 31].

#	System	max range	finest resolution (open-loop)	DOF per unit max units	tech. spec.	applied in
1	Oxford Instruments OmniProbe 400	XYZ: 4 mm	N/A	4 1	[24]	[43]
2	Zyvex S200	XYZ: 12 mm	2 nm	3 8	[3]	[178]
3	Xidex NanoBot NX-2000	XYZ: 12 mm	1 nm	3	[4]	-
4	TNI LifeForce	XY: 10, Z: 5 mm	0.1 nm	3 4	[28]	[58]
5	Kleindiek MM3A	12 mm axial / 240°radial	N/A	1 translational 2 rotational	[21]	[121]
6	SmarAct SLC (here model1730)	XYZ: 21 mm	<1 nm	3 e.g. up to 4	[27]	[31]
7	Imina miBot BT-14	XY: mobile, Z-arm: 42°	1.5 nm	2 translational 2 rotational	[20]	[83]
8	NenoVision LiteScope	XYZ: 0.1 µm	0.2 nm	3	[23]	-
9	Getec AFSEM	XY: 7.5 mm, Z: 25 mm	N/A	3	[17]	[183]

Table 2.2 Overview of different nanohandling system on the market and their specifications.

2.3 Automation on the Micro-/nanoscale

In conventional macroscale handling, automation partly includes the simple re-execution of previously executed tasks, which are performed as open-loop tasks without verification and assessment of the environment. Two different programming and development approaches are used for such tasks. Online programming, which includes teach-in, playback, and master-slave programming, and offline programming, which can be textual or computer-aided design (CAD) model based [194]. In assembly scenarios, additional environmental sensors (such as cameras, distance and force sensors, lasers) are used to measure the environment and to adapt the planed operation. Since all movement operations can depend on the sensors' signals, this kind of automation has to be realized in closed-loop controlled sequences, which have to be programmed textually. Due to the small sizes of the involved objects and the comparably large information uncertainties, the online methods are not applicable to the automation of nanomanipulation as well. And the same applies to CAD model based programming - even though researchers have used CAD assisted teleoperation on the nanoscale [50]. Hence, automation on the nanoscale has to be closed-loop, which makes additional control software necessary.

2.3.1 Software Frameworks for Nanohandling and Automation

Most software frameworks for automation have several functions, which are depicted in Figure 2.1. The core task is to control the robotic hardware devices and to gather sensor information. Additionally, interaction with a human operator input/output might be necessary - especially for semi-automated or teleoperated tasks. In order to facilitate automation, scripting capabilities are fundamental. In combination with image and date processing and analysis, closed-loop and adaptive control becomes possible. Finally, data visualization and logging are fundamental for laboratory automation software.

Vendor-provided Software Nearly any company that offers robotic platforms, cameras, grippers, microscopes, etc. provides software kits to control their hardware. In the case of robotic platforms or controllers, these are typically tools to perform simple steps, store positions, or perform patterns [27, 25, 29, 10]. Microscope and camera suppliers also offer software kits to acquire and process images from their product directly [19, 12, 16]. However, these software kits are not able to control other devices and, hence, are not capable of acting as automation frameworks.

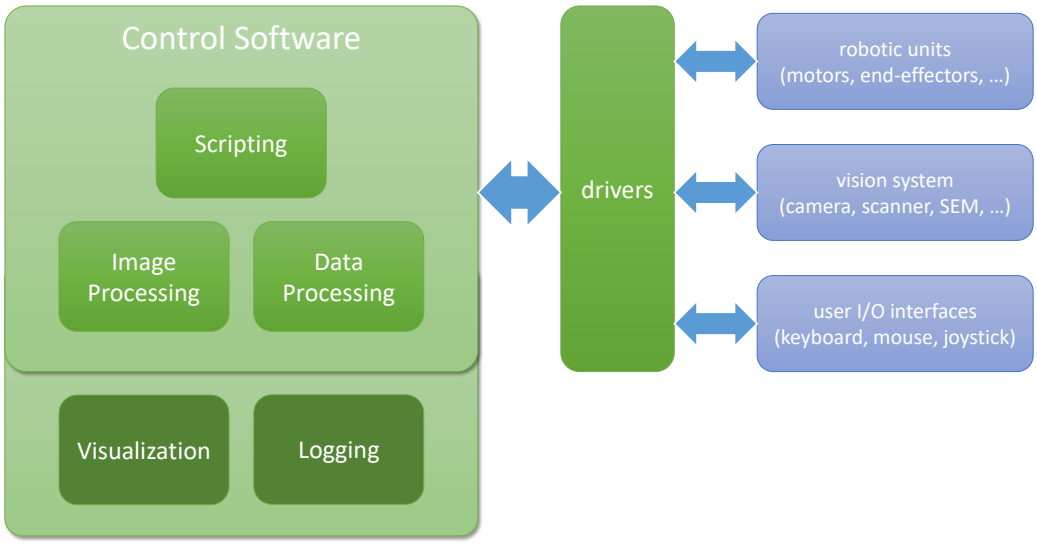

Fig. 2.1 Possible functions of an arbitrary software framework for automation. It exchanges data with the physical hardware via drivers, logs and represents data and has data/image/script processing units.

Software Frameworks Software frameworks that are used for robotic automation have either been developed explicitly for this purpose, or they are general purpose laboratory-automation frameworks.

The most popular example for specific developments is *ROS* [157]. *ROS* is an open-source linux-based operation system that also benefits from other open-source projects. i) Navigation system and simulation [90], ii) image processing [51], and iii) path-planing [67], for example, have been derived from other projects. A graphical user-interface is typically a component that is missing in *ROS*. Other dedicated robotic software frameworks are V-REP [161], Orca [55], Orocos [181], and Rock [112].

In-house developments are the last important branch of software frameworks that are used for automation on the nanoscale. *ViSP* is a software platform for visual servoing that can be used for real-time tracking of up to six DOF [128]. *APROS3* is a further development that uses ViSP and OpenCV [130]. APROS3 is tailored for tracking and visual servoing of objects inside the SEM. The *OFFIS automation framework* (OAF) is an open-source, PC-based software framework that was developed in order to facilitate automated robotic handling on the nanoscale (cf. Section 3.4). The OAF can be used to design image processing based on OpenCV by graphical processing chains [69]. The ccripting of automation tasks is done in Python and it offers a data logging system.

2.4 Automated Nanohandling

Nanohandling inside the SEM as a teleoperated task is time consuming, imprecise, and depends on the operators' skills. Mostly joysticks or positioning knobs are used as interfaces and the operator interprets the SEM's visual feedback with their experience. This method is still widely used among research institutes and industry if nanoscale samples have to be prepared in very small quantities. However, over the last decade progress has been achieved in the automation of in-situ nanohandling tasks. Table 2.3 summarized the most successful contributions of nanohandling and -manipulation inside the SEM. Most of them use the SEM as the image source and control the position of the robots in respect to the image information (cf. *visual servoing*, Section 3.3.3). Several noteworthy aspects can be derived from these contributions:

- Only little comprehensive data that includes all figures of merit are availabe.
- Achieving accuracies below 100 nm is challenging for actual handling tasks (referring to an operation where an object is moved from a source to a target spot).
- The same applies to throughputs below 1 minute.
- Control of all six DOF is not achieved so far.
- Automation of an assembly task is not achieved so far.

In conclusion, an automated assembly process with an accuracy in the sub-micrometer range has still not been achieved.

Table 2.3 Overview of the most successful nanohandling works in side the SEM and their parameters.

Type of operation	Autom. Level	Tools	Feedback	Object shape	Object Size	controlled DOF	Success rate	Throughput	Accuracy
Cell cutting [171]	full	nanoknife	SEM visual servoing mech. touch detection	cells	4 µm	3 trans.	not rep.	1-2 min	around 100 nm
Indentation [217]	full	AFM cantilever	self-sensitive AFM cantilevers	surface	-	3 trans.	100%	8.4 sec	< 200 nm
Probing [94] (w/o measurements)	full	STM tips	SEM visual servoing mech. touch detection	surface	-	3 trans.	not rep. (est. 100%)	7.7 sec just z-approach	150 nm (estimated)
Probing [164] (w measurements)	full	STM tips	SEM visual servoing mech. touch detection	surface	-	3 trans.	100%	not rep.	70 nm
Pick-up [172]	full	AFM cantilever EBiD	SEM visual servoing mech. touch detection	wires	50 nm / > 4 µm	3 trans.	80%	not rep.	not rep.
Pick-and-place [74]	partly	MEMS gripper / AFM cantilever EBiD	SEM visual servoing MEMS touch detection	wires	300 nm / 15 µm	3 trans.	not rep.	10 min	not rep. (est. z > 0.5 µm)
Pick-and-place [201]	full	STM tips	SEM visual servoing mech. touch detection	wires	> 70 nm / >13 µm	3 trans. 1 rot.	100%	10 min	not rep.
Pick-and-place [218]	full	structured AFM probes	SEM visual servoing self-sensitive AFM cantilevers	spheres	1160 - 237 nm	3 trans.	80 - 100%	112 sec	110 nm
Assembly [158]	-	MEMS gripper / AFM cantilever EBID	SEM visual servoing MEMS touch detection	complex	150 nm / >3 µm	3 trans.	not rep.	not rep.	not rep. (est. 1 µm)
Assembly [209]	-	MEMS gripper / AFM cantilever EBID / FIB	SEM visual servoing	wires	250 nm / 12 µm	3 trans. 2 rot.	not rep.	not rep.	not rep. (est. > 100 nm)

2.4.1 Case Study Related

The development of techniques for nanoscale assembly is usually closely tailored to the demands of the final application. Especially automated nanohandling is mostly done for specific tasks. This statement is also valid for the contributions mentioned in the previous chapter, but they are just the most successful examples for nanohandling inside the SEM. Considering this circumstance and the fact that comprehensive figures of merit are missing, a comparison of nanohandling techniques is only significant if similar tasks are compared. The case studies presented in the sections 5 and 6 are used as measure and demonstrate the capabilities of the techniques that are developed in addition to the state of the art. In order to assess the achievements of the case studies properly, contributions are presented that had goals comparable to those of this contribution.

Nanowire integration The handling and integration of nanowires is a common task that is needed to conduct fundamental research on nanowires. Most nanowires are produced with bottom-up methods and show statistically diverse properties that need to be measured in order to assess and identify the crucial process parameters. Furthermore, the often claimed potential of nanomaterials as nanoscale building blocks has to be investigated and proven through individual measurements. Hence, mcuh of the fundamental research questions can be answered only by working with individual nanoobjects. Moreover, in order to do the characterization, they often have to be attached to a microscale measuring device that acts as reference carrier for the nanoobject. Hence, the task to be accomplished is by definition micro-/nanointegration.

However, most experiments are performed on a very limited amount of samples. This is also the case for many research work that is performed on individual nanowires. Consequently, most research groups perform the nanowire integration task manually/teleoperated and do not report method and performance at all, since it is understood as preparation task only [153, 213]. Still, the groups that publish about the integration report, for instance that the integration of nanowires into an existing MEMS structure is *time-consuming and is of low throughput* and that it can take up to 40 minutes per nanowire [207]. The yield of such manual pick-and-place manipulations of nanowires can also be increased by up to 80% by the use of guiding structures, but information about accuracy and throughput are still not reported [206]. Figure 2.2 shows a MEMS-device that is a typical target for nanowire integration for further material investigations.

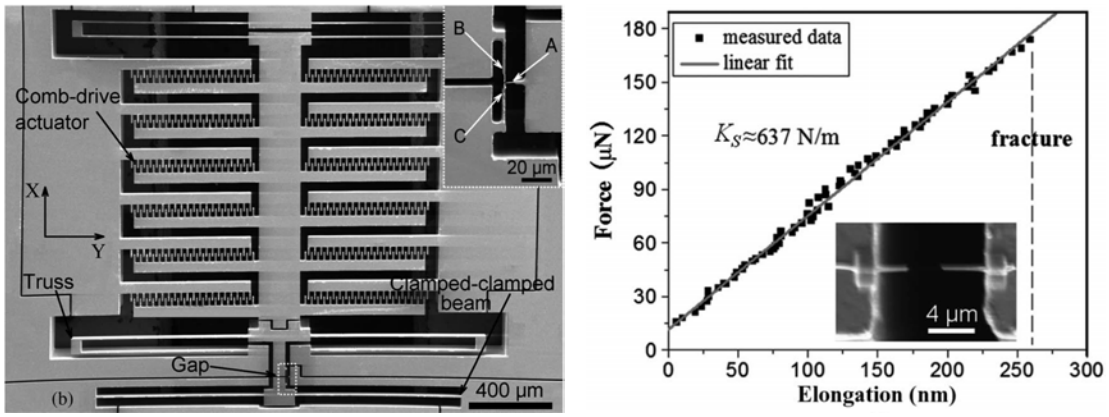

Fig. 2.2 Example of a nanowire integration into a MEMS-device (left) in order to perform fundamental mechanical tests on the wires (right). (Image from [207], ©2010 IEEE)

Exchange systems on the micro-/nanoscale In conventional robotics, tool changers are standard components that allow a robot to exchange its end-effector automatically [215]. In micro- or even nanorobotics, changing the end-effector is typically a task that has to be performed by a human operator. It interrupts the measurement and in most cases subsequent re-calibrations and re-initializations are necessary. If the end-effector is located in a sealed environment, such as the vacuum chamber of the SEM, the exchange can vitiate the entire measuring concept. Furthermore, on the nanoscale changing the end-effector typically means, that a bigger device carrying the end-effector has to be changed. Consequently, any alignment or reference coordinate system is lost.

The advantages of tool changers are evident and their existence would be beneficial for end-effectors on the micro-/nanoscale as well. Tool changers that work only mechanically would already be sufficient on the micro-/nanoscale, since most end-effectors have only limited functionality anyway. However, micro joining systems are rarely investigated - especially in combination with an automated exchange sequence.

A prominent and wide-spread microhandling task is the transfer of TEM lamellas [93]. The handling of TEM lamellas, which are thin slices of silicon wafer, is a standard operation in CMOS clean-room processes for quality inspection. It can be performed in-situ in the SEM as teleoperated operation [134] and needs the time-consuming *material enclose handling* (cf. Section 4.1.2) as transfer method. In order to simplify and accelerate this process, a mechanical joining technique based on a structurally designed end-effector was proposed, where a micro-clamp can pick up a TEM lamella and transfer it to a receiving substrate [95].

The AFM is a standard metrology tool on the nanoscale. It uses etched silicon chips of few millimeters size, that carry a cantilever (several hundred micrometers long) with a

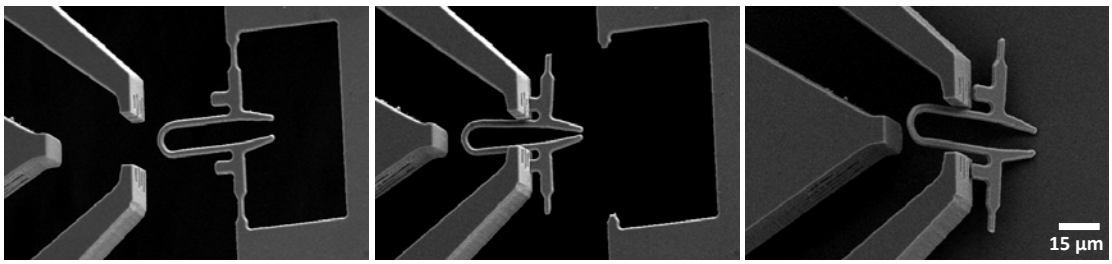

Fig. 2.3 Example of a microgripper with exchangeable tips, which can be collected from the production substrate. (Images from [58], ©2011 IEEE)

fine tip at its end (tip curvature of a few nanometers). This fine tip is in mechanical contact with the sample to be characterized and suffers notifiable wear during the measurement. However, changing the tip requires an exchange of the chip, which demands the opening of the instrument. Precious information about the current position is lost. The realization of exchangeable tool-tips for AFM cantilevers was the goal of the NanoBits project. This concept (cf. Section 6.1.2) is unique on the nanoscale, but has equivalents on the microscale. A concept for exchangeable AFM tips has been demonstrated by the Indian Institute of Science [142]. However, this concept aims to exchange entire parts of the cantilever and still only achieves positioning uncertainties in the micrometer range.

A comparable approach of an in-situ exchange of end-effectors has been demonstrated by the University of Toronto. They developed a microgripper with exchangeable gripping tips that is able to pick and place spheres with diameters as small as 100 nm diameter [58]. The manipulation is teleoperated inside the SEM and also the tip exchange can be teleoperated in-situ without breaking the vacuum conditions. However, figures of merit are not reported.

2.5 Conclusion

Today, no general automated handling technique exists that is suitable for assembly tasks on the nanoscale. While handling tasks and automation have generally become more feasible on the microscale, which has led to a development of microhandling stations, automated nanohandling is still in its infancy.

However, many researchers use nanomanipulation inside the SEM to prepare single samples for fundamental research. This effort is made in undocumented hours of manual, since teleoperated, work. Even the handling of TEM lamellas, which is a daily operation in the semiconductor device industry, is only partly automated and of all steps, the actual pick-and-place handling operations are still performed manually. At least it is evident results

of TEM lamella handling are sufficiently precise for further investigations (which implies only accuracies in the sub-millimeter range).

Nonetheless, little attention is paid to sound performance figures. Efficiency, accuracy, success, and economy of the results remain unknown in most contributions and a comprehensive description is mostly missing. Furthermore, most works focus on translational positioning only, while rotational control, which is needed for assembly tasks, was not performed. On the one hand, this is reasonable since many nanoscale objects already have a simple structure (spheres or wires), which makes controlling all six DOF unnecessary. On the other hand, these methods are missing and the assembly of more complex nanoscale building blocks is not considered as a possibility. Hence, the lack of controllable DOF is a major deficiency in micro-/nanointegration.

The defined objectives *accuracy*, *speed*, *success-rate*, and *automation capability* (cf. Section 1.2) can now be quantitatively expanded within the current limits. An envisaged assembly sequence that is

(i) accurate on the nanoscale in all degrees of freedom ($\leq$100 nm deviations),
(ii) fast (few minutes per piece),
(iii) successful (close to 100%),
(iv) and fully automated

is beyond the state of the art and needs to be developed. The development and demonstration of nanohandling methods that consider automation capabilities would increase the visibility of this technology and would make application driven developments easier in the long term.

3 Fundamentals and Tools in Nanorobotic Handling

Down-scaling to the micro-/nanoscale involves significant changes to all involved instruments. The fundamental principles, effects, and tools are introduced and their application is elucidated for the specific topic of automated handling on the micro-/nanoscale.

3.1 Fundamental Forces on the Small Scale

Even though the principles on the micro-/nanoscale adhere to the same naturals laws, down-scaling leads to a significant change in the dominance of all involved forces. Most forces are reduced models of a complex entity of fundamental physical interaction and they are dominant on a certain scale or under certain conditions. Furthermore, forces that scale with an objects volume and forces that scale with an objects surface can be distinguished. Thus, it is evident that the smaller the size of the objects, the more dominant the surface forces become (cf. Section 1.1.2). This changing relation is known as the *scaling effect* [176].

The following forces, dominant on the macro- or nanoscale, are responsible for the scaling effect and the understanding of handling principles on the small scale.

Body forces All body forces act on the body and hence the volume of an object. Therefore, for a spherical object they scale with r^3.

Gravity is a dominant attractive force on the macroscale and present since all objects have a gravitational mass. It is responsible for the fact that placing objects can be achieved by just opening and lifting the gripper.

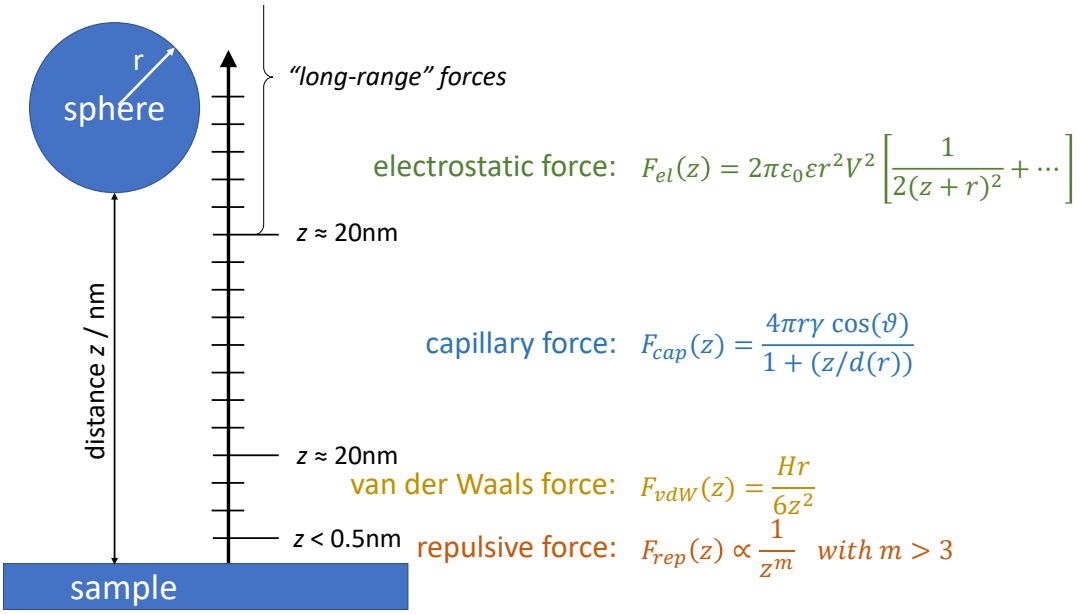

Fig. 3.1 Most dominant surface forces on the micro-/nanoscale estimated for a spherical object with diameter $r \gg 1$ nm in distance z to a flat surface: Electrostatic force F_{el}, capillary force F_{cap} with $d(r)$ the depth of wetting (not shown), van der Waals force F_{vdW}, and F_{rep} as general description for repulsive forces.

Inertia is dominant on the macroscale and also present, since all objects have inertial mass. Due to inertia, it is possible to shake off objects that adhere to other objects [219].

Electric forces caused by entirely charged objects can be attractive or repulsive and could be dominant on the macroscale. However, since most objects are in charge neutrality on the macroscale, this force is rarely present and hardly effects handling on that scale.

Surface forces In contrast to body forces, surface forces scale with the size of the surface which is relevant or influenced by a physical or chemical force. Depending on the particular force, they scale differently with the surface and distance from the next object.

Approximations The value of surface forces depends on the size of all involved forces. On the small scale, their calculation is complex; especially for distances that are smaller than the involved surfaces and approximations are necessary. The most prominent approximations are the *Derjagin-Muller-Toropovand* (DMT) approximation that focuses on long-range surface forces that act outside the contact area [66]. and the *Johnson-Kendall-Roberts* (JKR) approximation that focuses on short-range surface forces, which act within the contact area [110]. The most comprehensive approximation is the *Maugis* model that includes both

aforementioned approximations and can transit them into each other by parametrization [133].

Figure 3.1 illustrates selected forces that are dominant on the micro-/nanoscale. A spherical object's radius of r is assumed to be larger than several nanometers and the distance from a planar surface is z.

Electrostatic force On the micro-/nanoscale, local charging effects are more important than on the macroscale. A charge density distribution σ on a flat surface applies the force $F_{el}(z) = \frac{q\sigma}{2}$ to a particle charged with q. For non-idealized point charges, such as a sphere a radius of several nanometers, the calculation of this force becomes more complex. Using a potential difference of V, a result of this approximation is $F_{el}(z) = 2\pi\varepsilon_0\varepsilon r^2V^2\left[\left(2(z+r)^2\right)^{-1} + \mathcal{O}\right]$ [180, 88].

Capillary forces Due to the relative humidity, surfaces in ambient conditions are naturally wetted with a few layers of water [106], which are less than 1 nm thick [192]. Two objects in close vicinity to each other can form a common water film and hence are connected by a water meniscus. With respect to the liquids surface tension γ, the surface's contact angle θ, and the wetting depth d, the resulting capillary force $F_{cap}(z) = \frac{4\pi r\gamma cos(\theta)}{1+(z/d)}$ can be calculated [89].

Van der Waals forces The *van der Waals* forces are a summary of different electrodynamic forces acting between all atoms and molecules and the nomenclature slightly differs in literature. However, the different components can be distinguished [106]: *Keesom forces* are attractive or repulsive forces between permanent dipoles or multipoles. *Debye forces* are attractive forces between permanent and induced dipoles. *London forces* also known as *dispersion forces* is sometimes referred to be the only component of the van der Waals force [106]. London forces are attractive forces between polarizable molecules [144, 106]. The van der Waals force for the given sphere-surface example can be expressed as $F_{vdW}(z) = \frac{Hr}{6z^2}$ [88], with H as Hamaker constant [98].

Repulsive forces In vicinities below 0.5 nm, repulsive forces become prevailing. Different forces contribute to this repulsion: In distances between 1-10 nm, liquid media or films can build an electrostatic double layer with a repulsive force [106]. One to two orders of magnitudes below that (0.05 nm), *Pauli repulsion* dominates and generates a strong repulsive force [106]. In summary with other forces, this leads to so called *van der Waals packing radii* of atom and molecules, which is the minimal typical distance between individual items. Typical effective packing radii are 0.1 nm to 0.2 nm [106]. These forces are often described as repulsive and by $F_{rep}(z) \propto \frac{1}{z^m}$ with $8 \leq m \leq 15$ [106].

The best known total intermolecular potential approximating the sum of all attractive and repulsive surface forces is the *Lennard-Jones "6-12" potential* $U(z) = 4\varepsilon\left(\frac{\sigma^{12}}{r^{12}} - \frac{\sigma^{6}}{r^{6}}\right)$ [106] with the resulting force $F(z) = 48\varepsilon\left(\frac{\sigma^{12}}{r^{13}} - \frac{\sigma^{6}}{r^{7}}\right)$.

Contact mechanics The described surface forces already include attractive and repulsive forces as well as the origins of the normal forces. In classical mechanics, normal forces are contact forces that are perpendicular to the connected surfaces. The aforementioned DMT, JKR and Maugis approximation already consider repulsive forces and making a separate model for normal forces unnecessary.

However, for contact mechanics on the micro-/nanoscale it is noteworthy that non-classical dependencies have to be expected. Classical friction forces scale linear with the load between two surfaces, while on the micro-/nanoscale friction is controlled by roughness and adhesion. The dependency of the load becomes sublinear [141].

3.2 Conditions for Automation on the Micro- and Nanoscale

As described in [30], automation on the micro-/nanoscale requires special approaches that differ from those established in macrorobotics. In general, the approaches differ in particular with regard to the working principles used (direct driving instead of kinematic chains [119]) and the extensive use of sensors. The sensors available on the micro-/nanoscale are very limited and mainly:

- Optical systems (depending on the application and the size of the objects involved)
    1. Optical microscopes and cameras (mainly for micrometer-scale applications) [175, 174]
    2. Scanning electron microscopes (nanoscale) [195]
    3. Other imaging methods with sufficient resolution
- Atomic force microscopes, which are used for both imaging and measuring tasks.
- Internal position sensors for linear or rotatory positioning systems, e.g. integrated inside in robots (cf. Section 3.3.1).
- Microforce sensors such as the FT-S Microforce Sensing Probe from FemtoTools [45].
- Microscopic electrode probes, such as those from Capres, which can be used for the conductivity mapping of samples [152].

One of the main tasks of automation is to precisely position robots, tools and objects in relation to each other. This is the only way to reliably perform complex operations in the micro and nano range, such as pick and place. In addition, it is necessary to bring several robots and tools in the same work space to enable cooperative handling. The available internal position sensors of robots are not sufficient for positioning tasks for two reasons. First of all, a distance of several millimeters or even centimeters between the drive base and the tool center (TCP) is not uncommon and a great influence on mechanical changes. On the other hand, the sensor information is not reliable enough due to the always present effects on the small scale, such as thermal drift, electrostatic charge, or the positioning uncertainty of robots and tools [196, 68]. Therefore, the main sensor used on a small scale is an optical system.

Semi-automation is the most widely used for pre-processing and/or to support the user, e.g. in preparing the setup. Typical tasks are therefore: bringing robots and/or tools into a common working space, sample exchange via robot tables or point-and-click movements. Full automation, which is a rarity in the field of microrobotics, normally performs well-understood processes (especially in assembly or testing). The typical maturing of a process is usually: (1) manual assembly (using telecontrol technology), (2) optimization of the process for a possible automation , (3) semi-automation through all process steps and (4) a combination of all semi-automatic steps into a comprehensive sequence. The Section 2.4.1 we will highlight some recent work in this area to give an idea of what is possible.

3.3 Hardware/Robotic Components

3.3.1 Motors for the Micro-/nanoscale

Working on the micro-/nanoscale requires a specialized robotic system in order to reach the needed accuracy and precision. Especially precision is of high importance, while a lack of accuracy can be tolerated by the use of closed-loop systems (cf. *visual servoing* in Section 3.3.3). Conventional robotic drives using electromagnetic DC or stepper motors, preloaded gears, strain wave gears, or spindle drives, cannot achieve precisions in the µm range, since they suffer from mechanical uncertainties causing effects such as stiction or backlash [65]. Furthermore, several applications in micro-/nanointegration do not need high accuracy only, they also need traveling ranges of up to few centimeters. Hence, special driving systems have been developed that offer accuracies down to the nanometer range preserving

larger traveling ranges. This can be achieved by using the unique material properties of certain materials and different types of construction:

Piezo drives Piezoelectrically driven actuators are by far the most prominent principle on the micro-/nanoscale in today's robotics. The *piezoelectric effect* transforms the mechanical strain of material in a voltage potential by creating charge asymmetries in the crystal structure of the material. The *inverse piezoelectric effect* causes an electromechanical expansion of a crystal caused by the application of an external electrical potential difference [86]. This effect needs special polymers or crystals that already have an asymmetric charge distribution - the most prominent material that is used piezoelectrically is lead-zirconate-titanate (lat. plumbum zirconate titanate, short: PZT) [86]. The typical actuation voltages of PZT have several hundred volts and cause a mechanical expansion of the ceramics of about 0.1-0.2% [165]. Hence, by using high voltage generators, fine movements can be achieved. Most piezo materials have a very high stiffness and can be actuated rapidly, which allows to drive piezos in a wide bandwidth; from quasi-static movements up to ultrasonic vibrations [165].

Design of motors Depending on the design of the actuators and drives, diverse specifications can be realized. Different classifications can be applied for actuators in general. The most common classifications are [165]:

Motion type Two major motion types exist: linear and rotational. Both types of motion can be achieved with different drives. PZTs can be used to build linear, as well as rotational, actuators.

Input frequency High frequency driven actuators can be distinguished from quasi-static driven actuators. PZTs are used to realize both: static drives that are typically for very precise positioning (down to the sub nanometer scale), and frequency driven actuators that have long traveling ranges and fast movements (up to many cm and several cm/s). Some PZT based actuators can work in both modes: a quasi-static mode with high accuracy and a dynamic mode with fast/long movements.

Scale The scale of an actuator is an obvious measure but not less important, especially on the micro-/nanoscale.

Operation principle Different working principles can be realized for drivers and motors. All driving systems consist of a static part (stator) and a driven part (runner). Depending on the operational principle, they are either firmly attached to each other or movable in respect to each other.

The classification by operational mode is comprehensive and one can distinguish many different technical principles. The most prominent design principles for actuators on the micro-/nanoscale are [165]:

Quasi-static In quasi-static drives, the stator and runner are mechanically firmly connected to each other. In the simplest form, the runner-platform is directly attached to a piezo actuator that is again attached to stator-platform. Typically, parallel guides or solid state joints are used, which allow an optimized decoupling of the movement directions and also work as mechanical ratio or reduction. This kind of design is usually used for high precision platforms (below nanometers) with very limited stroke (around several micrometers).

Slip-Stick Slip-stick motors do not have a mechanically firm connection between runner and stator. Both are assembled with a common interfacing surface. The moving working principle has two phases: the stick phase and the slip phase. In the stick phase, an actuator (typically a PZT) moves the runner slowly – in the same way as it does in a static drive. Subsequently, in the slip phase the actuator moves so rapidly, that the runners inertia is large enough to allow a slipping of the interface between runner and stator. This cycle is a single step of the slip-stick actuator and these single steps are typically below 1 µm. However, if performed iteratively and quickly (typically up to 20 kHz), they add up to a traveling speed of several mm/s and working ranges that are only limited by the size of the stator [182]. Typically, the actuation of the slow and rapid movements of the PZT is generated by a voltage signal with a simple sawtooth shape. However, different optimizations have been investigated in order to optimize speed, force, and smoothness of the motor [73, 148]. Along with static actuators, slip-stick actuators are the most common in micro-/nanorobotics.

Inchworm Inchworm motors typically need three actuators but do not depend on inertia. One actuator is used for the slow stepping movement as in the slip-stick motor's stick phase. Instead of the slip phase, the inchworm motor used the two additional actuators to clamp stator and runner at two points that are at both ends of the stepping actuator. A sequence of releasing, stepping, and clamping allow the motor to move stepwise [182].

Ultrasonic In contrary to the aforementioned motors, ultrasonic motors use resonance frequencies in order to achieve large vibrations of the stator. The resulting surface waves of the stator are used as the driving motion for the runner. This working principle is not step-based but very fast. However, ultrasonic motors are not that common anymore in micro-/nanorobotics today.

Another important working principle for actuators and positioning stages on the micro-/nanoscale are devices based on micro-electromechanical system. They have several advantages when compared to conventional motors and motor-based stages [165]: MEMS-based devices have a very small footprint. Typically, an entire 3D-positioning stage has a size in the range of few mm^2 [124]. Due to the small size and the low mass, the positioning speed is very high. Furthermore, integrated sensors that feed the position signals back, can be implemented in the same design. This facilitates the integration of an on board closed-loop positioning of the stage [118]. However, MEMS-based positioning stages have some disadvantages as well. Typically, they apply to one particular application, since the are highly specialized and tailored. They are very sensitive and damage-prone during their development. And finally, due to their operational principle, their stroke is limited to few µm [186]. Hence, the are typically used only in highly specialized applications and they are custom-made for these purposes.

Challenges for Motors on the Micro-/nanoscale

Accuracy and precision are the most critical challenges for actuators on the micro-/nanoscale. Conventional physical effects are more dominant on the small scale due to the scaling effect. Additionally, certain effects arise on the micro-/nanoscale that are typical for the specific actuators. Furthermore, the scaling effect is important for entire robotic setups, since it also concerns the ratio of operational accuracy to the length of the kinematic chain (cf. Section 3.2).

Typical effects for actuators on the micro-/nanoscale are:

Drift effects are very common on the micro-/nanoscale. They are caused by small temperature fluctuations. In micro-/nanorobotics, the kinematic chain is typically very large in comparison to the needed accuracy. Hence, small temperature changes already cause significant mispositionings. This effect can be compensated only by a closed-loop control that monitors the end-effectors position in respect to the sample.

Hysteresis is a fundamental problem for piezo actuators. The position of the actuator depends on its past position and no clear dependency of the driving voltage and the actuator's position can be found. This effect is less important for step-based motors, but has a strong influence on the accuracy of static piezo drives. Hysteresis can be mitigated by a closed-loop positioning motor or by an iterative replication of the same control signals.

Creep is another typical problem for piezo actuators. Here, the position of the actuator is exponentially time-dependent and no clear dependency of driving voltage and actuators position can be found. The effect can be also mitigated by use of a closed-loop control.

Many inaccuracies and instabilities can be tackled by using a closed-loop control system. Internal sensors allow to measure the position of an actuator precisely and hysteresis and creep can be compensated based on this information. But every sensing system carries uncertainties that influence the accuracy of the final position of the actuator. Furthermore, internal sensors are capable of improving the accuracy of their particular axis in respect to the next mounting point. However, the effective accuracy between an end-effector and a sample cannot be improved by internal sensors (cf. Section 3.3.3).

3.3.2 End-effectors

The end-effector is the last component of a robotic manipulator, and interacts with the environment by means of any tool [5]. Only a very limited variety of end-effectors is available at the small scale (cf. Section 2.2).

Several tools are available if an accuracy of many micrometers is addressed: pipettes, microgrippers, and sensing devices can manipulate on this scale with sufficient accuracy. The accuracy limiting factor for those tools is their own size.

On the few micrometer scale only a few end-effectors are available that are still actuable, such as micro-grippers. However, all examples for microgrippers can be found only in academic applications and are specially tailored for specific purposes [33, 117]. Since the intrinsic positioning uncertainties of these end-effectors are already in the micrometer range, additional positioning units with higher accuracy need to be engaged if nanometer accuracies are demanded (cf. Section 3.3.3).

Finally, hardly any active end-effectors can be found on the nanoscale. Positioning and manipulating objects on this scale using end-effectors has to be done with simple nanoscopic tips. These tips are usually made from metallic wires and fabricated by wet-etching. Also atomic force microscope (AFM) tips are to be regraded as simple tips that can manipulate nanoobjects. However, the abilities of a simple tip are quite limited:

Mechanical forces The tip can apply mechanical forces to an object. This can be in a quasi-static or dynamical operational mode. The application of large forces can be used to push objects. Furthermore, the mechanical contact can be used to exploit adhesion forces in order to pull objects (cf. Section 3.1 on adhesion and Section 4.1.1 on tip

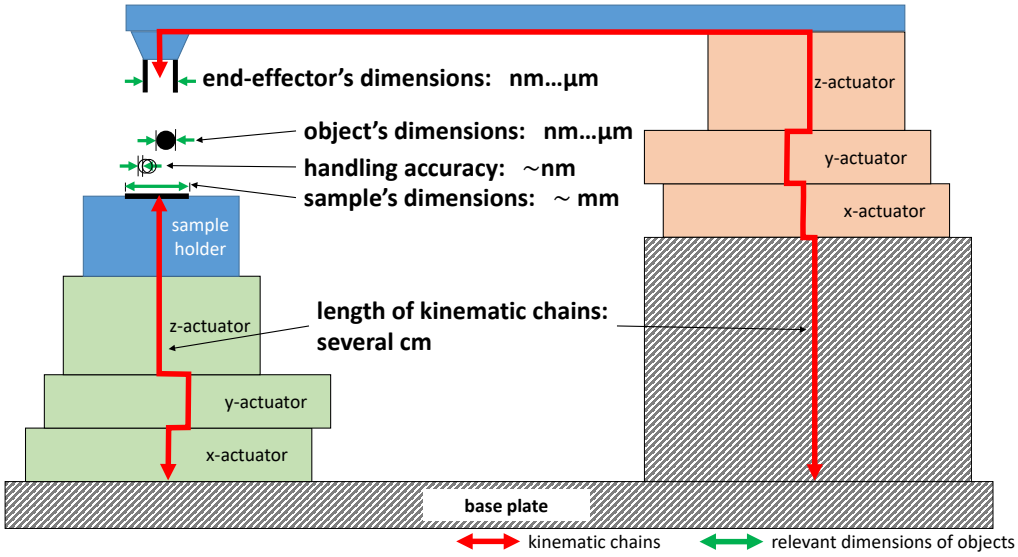

Fig. 3.2 Schematic sketch of a robotic nanohandling setup on the micro-/nanoscale. Two independant robotic drives (green and red) are used in order to combine the advantages of different systems. The typical sizes of all relevant objects and dimensions are indicated as i) the length of a kinematic chain is several centimeters, ii) the size of a sample is around few millimeters, iii) the sizes of end-effectors and objects to be handled are in the range of micro- or nanometers, and iv) handling accuracies are in the nanometer range.

handling strategies). The mechanical contact can be reinforced by the application of additional adhesives [129].

Dynamic contacts of tips and objects can be used for characterizations (as in the AFM) or for pushing objects rapidly [210].

Electrical contact The tip can also be used as an electrical contact in order to characterize an object or to detect a mechanical contact. Furthermore, the application of an electrical field can be used to manipulate objects by electromagnetic waves [57].

3.3.3 Setup Design for Nanohandling

A challenge for the setup design for nanohandling applications is the large variety of orders of magnitudes in size. This fundamental challenge is depicted in Figure 3.2. The setup has to manipulate objects with an accuracy that is typically few or even smalle than nanometers. The objects themselves and the used end-effector have the size of few nanometers (e.g. nanospheres and tips) or several micrometers (e.g. nanowires and grippers). The overall handling range can be several mm if, for instance, an object has to be picked from production substrate and placed to a target substrate, which is the core task in micro-/nanointegration.

Finally, the size of the entire setup is typically several centimeters due to the size of the used motors, which results in long kinematic chains. Hence, effects such as *thermal drift* cause major relative misalignment between sample and end-effector, regardless of whether the motors are equipped with accurate positioning sensors. For this reason, additional external sensors that can measure the relative positions of sample and end-effector at the same time are favorable. Most common systems for relative positioning are camera systems that observe the handling scene. On the micro-/nanoscale, the scanning electron microscope (SEM) works as such a camera system and the entire handling system has to be integrated into this microscope. The image of an observing camera or microscope can be used to identify objects and end-effector and to extract their positions relative to each other. Alignment tasks can be performed by using these image-based positions. This is called *visual servoing*.

A setup for nanohandling applications is generally of modular design and a combination of different motor principles. Due to the different requirements of accuracy and operational range, which cannot be met by a single motor system (cf. Section 3.3.1), a combination of different systems is used. The fundamental design principle for such setups is depicted in Figure 3.2. Two independent robotic system are used that have complementary advantages:

The coarse-positioning unit is used that can travel several centimeters. It can be used to move the sample holder or the end-effector and it allows for an easy sample exchange that is needed for micro-/nanointegration. Typically, the coarse-positioning unit consists of three linear slip-stick motors that are orthogonally arranged. The system can be used to approximate sample and end-effector quickly. The remaining distance can be covered by the fine-positioning system. In this way, the strongly vibrating coarse-positioning system does not damage samples and end-effector.

The fine-positioning unit is used to move either the sample or the end-effector precisely. Typically, quasi-static piezo actuators are used that offer a traveling range below 100 µm but positioning accuracies of about 1 nm. The fine-positioning unit is used for precise movement during a nano-integration task, since it exceeds only weak vibrations to the setup, which spare the sample and the end-effector. Furthermore, it allows for rapid movements as needed for scanning probe microscopy and is used as a scanning unit in the AFM.

The nanohandling setup that is used for this thesis is designed according to the mentioned principle: The *coarse-positioning unit* is a SmarAct slip-stick system with three linear orthogonal axes. It can also be equipped with a 360° rotatory axis. All axes are equipped with optical encoders enabling a closed-loop positioning accuracy of several nanometers and microdegrees, respectively. The full traveling range is $21 \times 21 \times 21$ mm^3. The *fine-positioning*

unit is a "Hera P-620" stage from Physikinstrumente (PI) with three linear orthogonal axes. They are equipped with capacitive sensors enabling a closed-loop positioning accuracy of about 1.6 nm. The working range is up to $100 \times 100 \times 50\,\mu m^3$. The system is closed-loop controlled by an analog "E-509" controller.

3.3.4 SEM based Manipulation

The apparent need for micro- and nanomanipulation can be particularly considered by the SEM (cf. Section 2.1). The SEM offers some clear advantages compared to other imaging and analysis tools:

Resolution The SEM offers resolutions of up to a few nanometers. At the same time, the field of view is infinitely scalable from a few centimeters to a resolution limit of about one nanometer.

Speed The image acquisition rate of the SEM is in the range of several Hz; it can be even higher using regions of interest (ROI). This is sufficient for handling, even in automated handling processes. However, the acquisition speed is inversely proportional to the noise level of the images. A fast image acquisition rate of a few Hertz involves already images with significant noise.

Space The working chamber of the SEM is spacious enough for the integration of several robotic stages, actuators and end-effectors. Normally at least a few hundred cubic centimeters are available.

However, using the SEM has also some disadvantages:

Complexity Overall, the use of SEM requires a great instrumental effort. The SEM itself requires many supporting devices and additional properties of the actual development instrument.

Compatibility Due to its working principle, the SEM is not suitable for all types of samples. All samples must be vacuum-compatible and, finally, slightly conductive in order to allow undisturbed image acquisition. Therefore, sample preparation is often necessary.

Invasiveness The interaction of sample and electron beam of the SEM can lead to changes in the sample. Very sensitive samples (e.g. graphene) can change their atomic configuration and thus their properties. All samples exposed to the electron beam can be contaminated with amorphous carbon by the residual gas in the vacuum chamber.

Image Distortions The same interaction of sample and electron beam can lead to low image distortions such as displacemnt or deformation. Hence, the SEM cannot necessarily be used as an absolute position sensor.

In conclusion, the SEM must be seen as a possibility of micro-nanohandling, among other things. Especially possible contaminations have to be considered in the treatment of nano-objects. But also some of the undesirable side effects can be transformed into powerful tools for SEM-based nanohandling, as described in this chapter.

This conversion of side-effects into useful auxiliaries, as well as the usage of the evident advantages of the SEM, are described for an exemplary use-case in Chapter 6.

But first of all, if one works with objects with nanometer size in two or even three dimensions, the SEM is the best compromise device. Especially, the need of automation of handling processes relies on fast and accurate position information.

The Scanning Electron Microscope as Fundamental Tool

The SEM is originally a powerful tool for taking high magnification images. Precise manipulations, however, require a kind of feedback to ensure that a manipulation task has been successfully completed. In combination of these two facts, nanomanipulation under SEM conditions seems theoretically an obvious approach.

The general operating principle of the SEM is to rasterize a sample with a well-focused electron beam. At each point where the beam hits the sample, an electron interaction with the surface leads to new emitted electrons. Thus a detector can observe a gray value for each point. A general requirement for the generation and propagation of the beam is a vacuum atmosphere.

In practice, several obstacles have to be overcome before work under SEM conditions becomes a possible technique for micro- and nanomanipulation:

Environment The vacuum environment of the SEM is already limited to all types of materials, which are involved. In general, all materials must be compatible with high vacuum, which excludes particularly living materials. However, special SEM approaches make it possible to work in a fine vacuum.

Insulation The most important restriction is the vacuum chamber of the SEM itself. Direct mechanical access to the observation area of the microscope is not possible, which is a big difference to all handling strategies in optical microscopy. There, fine manipulations can be carried out by simple but efficient mechanical linkage as a reduction.

However, these restrictions do not always apply and can be approached in different ways. In general, most materials and objects can be visualized with the SEM in high vacuum mode (10^{-6} mbar) without problems. This means that any handling strategy in which only compatible components are used can be implemented in SEM without restrictions. The use of other components or the processing of other materials leads to a higher instrumental expenditure. Outgassing materials, especially in form of living cells or cellulose fibers, cannot withstand the low pressure in high vacuum or are non-conductive, or even both. To overcome this disadvantage, some SEMs allow visualization at higher pressures (0.1 ... 30 mbar).

The unattainability of the working areas caused by the vacuum chamber has decreased in recent years as the robot platform is smaller, more cost-effective and more flexible. The integration of robot platforms with several degrees of freedom is today a task that can be easily solved with commercial or commercially adapted setups. The existence of control electronics, digital communication and programming interfaces for control PCs, is part of this development. This allows not only mechanical integration, but also control and monitoring, which is crucial for automation requirements.

The interaction of the SEM electron beam with the tested and manipulated samples is very important for handling and automation. On the one hand, the electron beam can cause unintentional damage and contamination as described in the Section 3.3.4. This is a major obstacle that must always be taken into account. On the other hand, the beam-sample interaction and its consequences can be used as a measuring or interactive probe. Local charge, emitted secondary electrons and their quantity can be used to derive more information as just a simple overview of the scenery.

3.3.5 The Local Surface Potential

In general, conductive and grounded samples are claimed to be most suitable for SEM applications. This fundamental statement is correct, but goes along with the general assertion that those samples would not charge. And this general assumption is only correct on a larger scale, but needs a differentiated consideration on the micro-/nanoscale.

A "perfect" grounding – meaning a resistance of $0\,\Omega$ – is already theoretically impossible and cannot be achieved in real-life conditions. Furthermore, is has to be taken into account, that the smaller an inspected sample is, the higher is the local density of the probe current. Looking at the nanoscale, these two facts cause a large local charge density on the sample's surface.

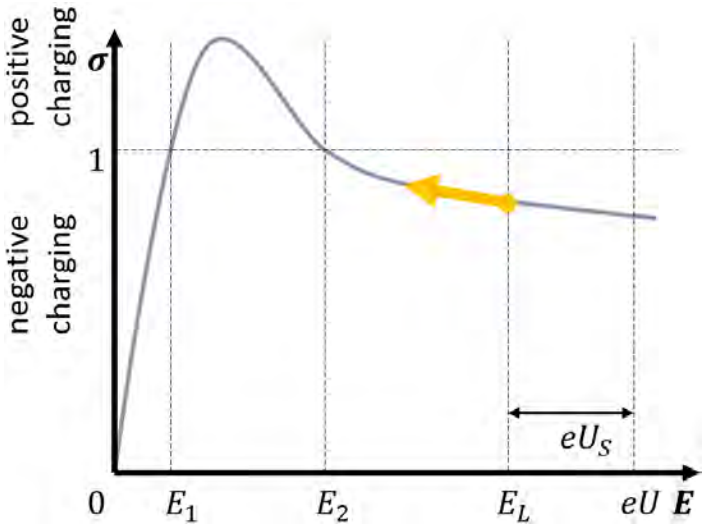

Fig. 3.3 Typical dependency of the total yield σ of the primary electron's energy. Positive charging occurs for $\sigma > 1$ and negative charging for $\sigma < 1$. Initially, the primary electrons hit the sample with an energy $E = eU$, which retards by time to the landing energy E_L due to the accumulating surface charge U_S until the $E_L = E_2$ (yellow spot).

The fundamental working principle of the SEM is based on incident and emergent electrons of a sample. In general, the amount of incoming and leaving electrodes is not equal and depends on several material properties as well as the beam energy. The ratio of incoming and exiting electrons is called total yield σ [160]. If the total yield is $\sigma = 1$ the same amount of electrons enter the sample as leave. Hence, there is no lack or surplus of electrons in the sample. If the total yield is $\sigma < 1$ ($\sigma > 1$), more (less) electrons enter the sample than leave.

For a given material, the total yield depends on the energy of the primary electrons. A typical dependency of the total is depicted in Figure 3.3. For two particular acceleration voltages U_1 and U_2 and their corresponding energies E_1 and E_2 the total yield becomes $\sigma = 1$. For all energies $E_1 < E < E_2$, the total yield is $\sigma > 1$.

Under initial conditions, the primary electrons hit the sample with the energy $E = eU$, with U as the accelerating voltage of the SEM. If this voltage U is higher than E_2/e, the sample charges negatively. The resulting negative surface potential U_S retards the landing energy of the incoming electrons to the level $E_L = U - eU_S$. This charging effect continues until the sample's potential is $U_S = U_2 - U$.

The induced surface potential U_S can be described as an accumulating charge Q. This accumulation reaches an equilibrium state in which the all currents can be described using

the equation

$$\dot{Q} = I_P - I_{SE} - I_G, \tag{3.1}$$

with I_P as the incident probe current, I_{SE} the amount of exiting secondary electrons (SEs) and I_G the current exiting the sample to ground. The latter is determined by the grounding resistance R. In this equilibrium state, the total electron emission yield σ changes due to the potential and is considered as effective yield σ_{eff}.

Furthermore, a charging sample can be treated as a capacitor and the fundamental relation $I_G = U_S/R_G$ and $Q = CU_S$ can be applied. Hence, the equation can be formulated as

$$\dot{Q} = I_P(1 - \sigma_{eff}) - U_S/R_G. \tag{3.2}$$

If only negative charges are considered for energies E with $E_2 < E$, the actual surface charging U_S can be determined by the particular integral of equation (3.2), or its equivalent

$$\frac{U_S}{R_G} = (1 - \sigma(E_L))\, I_P \tag{3.3}$$

Since the function $\sigma(E_L)$ is not defined, there is no general analytical solution of $U_S(E)$. Notwithstanding, in an equilibrium state with an constant value of E_L, it is noteworthy:

$$U_S \propto R_G \tag{3.4}$$

So far, all descriptions consider a stationary electron beam at the same spot of a sample at all times. However, the scanning movement of the electron beam distributes the bombardment of electrodes over a comparably large area, and hence the source of the local charging exists only for a limited time on each spot.

Local surface potential in scanning systems

Since the SEM beam scans the surface, the stationary solution has to be modified and becomes a time-description considering charging and discharging during the the scan movements. For each pixel, a on-to-off switching time t_P is assumed. The differential equation (3.2) is separated in a charging equation for the on-phase, and a discharging equation for the

off-phase:

$$\text{Charging: } U_S = U_{S0}\left[1 - e^{-t/\tau_0}\right] \tag{3.5}$$

$$\text{Discharging: } U_S = U_{S0}e^{-t/\tau_0} \tag{3.6}$$

in which the time charging/discharging time constant is determined by $\tau_0 = RC$ and $U_{S0} = \left(1 - \sigma_{eff}\right) I_P$, where $RC = \rho\varepsilon$ with ρ as the electrical resistivity and ε as permittivity with $\varepsilon = \varepsilon_0\varepsilon_r$.

The surface potential and all corresponding effects based on this charge can look quite different depending on the scan speed. Slow scans can be described using a full frame time T and N number of pixels resulting in a pixel time $t_P = T/N$. Fast scans are described with a full frame time T/n and a pixel time t_P/n, with $n \gg 1$. Hence, the surface potential after one or n scans can be described, respectively by

$$\text{Slow scans: } U_S = U_{S0}\left[1 - e^{-t_P/\tau_0}\right] \tag{3.7}$$

$$\text{Fast scans: } U_S = U_{S0}\sum_n \left[1 - e^{-t_P/n\tau_0}\right]\left[e^{-T(n-1)/n\tau_0}\right]. \tag{3.8}$$

This means that the surface potential U_S will be lower for fast scans than for slow scans, if $t_P < \tau_0 < T$. If $\tau_0 > T$, no significant change depends on the scan speed.

In summary, if surface charge effects are intended, scan speed, pixel size and scanned ROI must be limited. Consequently, going to the micro-/nanoscale, all previous conduction and assumptions are still valid. But since the size of the ROI and the pixel size are quite small, the charging effect has a heavier impact.

3.4 Software and Control Architecture

Working on the micro-/nanoscale is dependent on instruments with very high accuracy that are mostly PC-connected and controlled. This environment is shortly explained for completeness, but its development is not part of this contribution. Handling and manipulation is the core task of micro-/nanointegration and hence, robotic manipulation stages are needed. All robotic stages working in this range are already equipped with controllers, since they are physically driven by high voltages or high voltage signals that have to be generated. And nearly every standard commercial controller already offers an interface via which the

controller (and hence the stage) can be steered using an external device. Consequently, it is obvious that controlling all these devices with PC-based software is favored.

Furthermore, using a controlling software for manipulations on the micro-/nanoscale allows the realization of *closed-loop control* of processes that increase the accuracy and precision: Sensor information can be evaluated online and their feedback can be used to control the ongoing process [190]. Ths is how some tasks on the micro-/nanoscale become feasible in the first place (e.g. acquisition of AFM and STM images [46, 47]).

The automation capability is an intrinsic consequence-software based controlling and closed-loop setup: If all sensing information is passed through software, it can already be used to evaluate the current process status and control or decide the next process step. This automation makes processes on the micro-/nanoscale faster, reproducible and operator independent and the accompanying efficiency gain makes some processes on the micro-/nanoscale economical for the first time.

Software Demands The software used for automation processes has to be able to acquire all relevant parameters that change during a process and control all relevant parameters that have to be changed during the process. In automation for handling and integration on the small scale, this includes mostly the collection of microscopy images, force and voltage signals, and the control of robotic stages. In order to facilitate an easy development and prototyping of processes, simple user interactions must be applicable as direct telecontrol by devices such as keyboards, gamepads or joysticks. Furthermore, the actual automation has to be programmed in sequences, which requires a programming or scripting unit. And finally, some gathered sensor data have to be processed in order to derive useful information: microscopy images for example are processed so that spacial positions of objects are extracted. Hence, image and signal processing has to be part of the programming capabilities.

Software Framework for Automation The control and lab automation software used in this contribution is a specialized control and image-processing software dedicated to automation tasks on the micro-/nanoscale. The so called *OFFIS automation framework* (OAF) is an open-source [1], PC-based software framework that is developed in order to facilitate automated robotic handling on the small scale [69][2]. Figure 3.4 shows a scheme of the control software architecture and the interface to the hardware components. The control software consists of several units:

[1] https://github.com/OFFIS-Automation/Framework

[2] Detailed information can be found in [69], too.

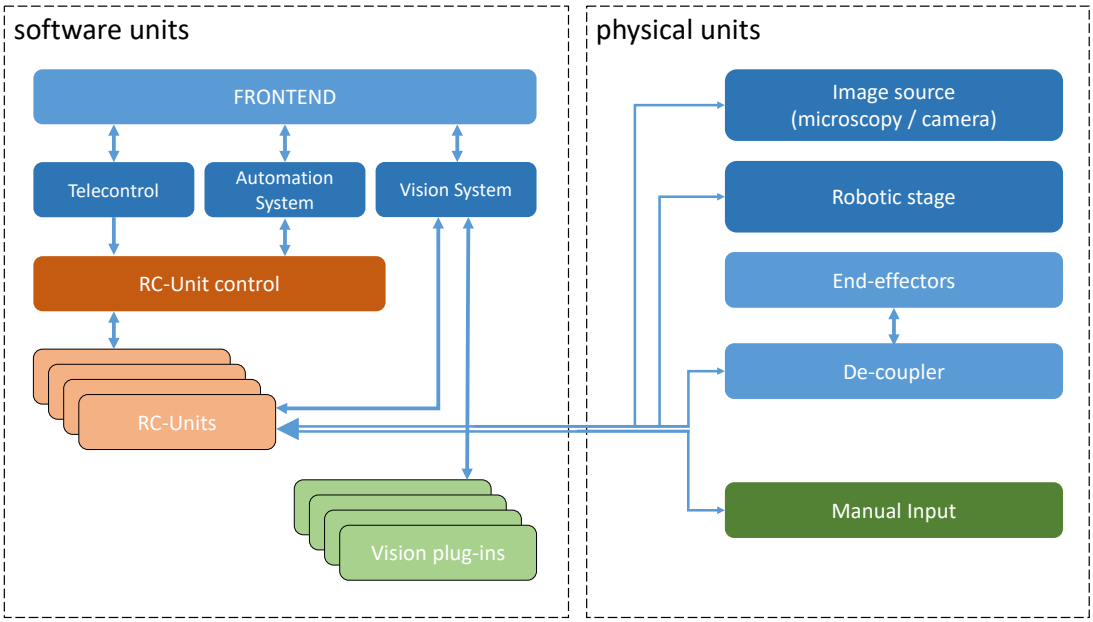

Fig. 3.4 Software control architecture of the setup. All physical units communicate with a software RC-unit, that interprets the communication to a high level control unit. Vision information, automation and telecontrol communicate to their RC-units and they are all implemented in an all-embracing frontend [69].

Frontend The frontend is a graphical representation of all user-relevant information and inputs.

Control Systems The frontend interacts with a telecontrol system, a scripting unit for the automation, and a vision system for image representation.

RC-Units All three control systems communicate with remote-controlled units (RC-unit) that consist of a hardware abstraction layer for all hardware components.

The RC-units themselves communicate with the hardware components, either via TCP communication, via an AD/DA interface by National Instruments, or via serial or USB communication (see below).

Based on this software architecture, especially the combination of robotical and visual systems, closed-loop control can be implemented by *visual-servoing*[104]. Hence, automation capabilities for handling processes on the micro-/nanoscale exist and can support manual operations or can constitute fully automated sequences.

Interfacing All hardware components are PC controlled by the OAF. However, different interfaces are used depending on the actual component.

SEM The scanning electron microscope *Tescan Lyra* is connected via TCP/IP using a proprietary C# interface provided by the supplier. This interface offers the options of controlling fundamental SEM parameters and reading image date. The controllable parameters are viewfield/magnification, scanspeed, region of interest size and position, resolution, and brightness/contrast. The image acquisition can be done either using full-frame updates or line-wise updates. All images are served according to the set parameters.

SmarAct systems All SmarAct systems act as coarse positioning units and are directly connected via USB to the PC. A self-developed driver allows access to all positioning and readout information as served by the supplier.

PI system The Physikinstrumente (PI) system is closed-loop controlled by an analog "E-509" controller, which holds the position of the stage according to a target value. This target value is served as an analog voltage signal between 0 V and 10 V. This signal is generated by a National Instruments PC plug-in card type *PCI-6229*.

Gripper Grippers need a current supply, for which any laboratory power supply can be used. The opening/closing is realized by an opto-isolator that controls the current to the gripper. The opto-isolator is controlled by an analog voltage of the National Instruments PC plug-in card.

3.4.1 Digital Image Processing

Closed-loop control is of major importance for automated processes, because they are able to achieve highly adaptive sequences that are capable of adjusting to uncertain handling conditions [48]. On the micro-/nanoscale, these relative uncertainties increase and closed-loop control becomes even more important. Camera systems, that offer fast 2D image streams, are widely used as online feedback systems to monitor robotic processes on the macroscale [91]. Several illumination and acquisition approaches exist, designed for special purposes in robotics, such as dark-field illumination, strobe lighting, and line projection [91]. Furthermore, a very large variety of the image processing algorithm is already developed and available, which can be used to process and optimize images as well as extract different kinds of data. The most important algorithms that are used in robot handling and position extraction from image information are available open source as part of the library OpenCV [155].

All image processing algorithms used in this contribution are derived from OpenCV and implemented into the OAF. The particular sequences are introduced in Chapter 4.3.

3.5 Conclusions

It can be concluded that the down-scaling effect leads to an extraordinary handling behavior of building blocks on the small scale. Adhesion effects outperform all usually dominant effects such as inertia and gravity and, hence, the simple down-scaling of macroscopic robotics is not practicable.

Furthermore, the conditions for nanohandling are difficult. Using the SEM as a high resolution imaging system implies several constraints to the setup, the setup's design, and the samples. However, the SEM acquires images quickly and with parameters that can be changed frame-wise. The application of charged particles to the scenery also has to be considered as extra influence during process development.

Nanopositioning units, on the other hand, are commercially available and meet all positioning accuracy requirements. They reach sub-nanometer, precise, and accurate positioning and even offer increased stability due to internal closed-loop control. However, even the combination of the best nanopositioning motors will create new uncertainties, since every combined system has larger spacial dimensions than the motors itself and thermal effects cannot be compensated on that level.

An apparent lack is the limited availability of functional end-effectors, since this limits the possibility i) to control as many degrees of freedom (DOF) as possible and ii) to involve automation, if the end-effector is not directly actuable. Furthermore, the limited amount of available sensors is a bottleneck for micro-/nanointegration-task in general and automation in particular.

Nevertheless, conventional software and control infrastructure is reasonably applicable in micro-/nanorobotics. Although there is no standard, the availability of hardware interfaces and control software is sufficient. Control tasks on the micro-/nanoscale are not particularly more demanding than high-speed tasks in conventional robotics. Image processing is, in fact, less demanding, since the SEM has a very low update rate anyway. Hence, image based closed-loop can be realized with few demands on information timing properties, such as latency, jitter, or real-time.

In summary, the main challenges in the development of an automated assembly sequence on the nanoscale will still be on the physical level.

4 Development of Automated Nanorobotic Assembly Strategies

Handling and manipulations on the micro-/nanoscale are widely implemented tasks. Scientists and developers in research and industry use micromanipulation in order to investigate, fabricate or manipulate small objects - as introduced in Section 2. However, complex assembly tasks or the integration of components of different scales are rare. Furthermore, automated procedures for these tasks are rather exceptional - even for a common and frequently conducted task such as TEM lamella handling [95, 7]. The two subjects - complex assembly and automation - are interdependent:

Complexity addresses the defined figures of merit accuracy, precision, and success. The feasibility of complex assembly tasks depends on automation, since they consist of several different steps and operations, such as investigation, handling, and validation. Complexity can already refer to tasks that are simple on the macroscale (such as pick and place operation in all three dimensions), since there are only few robotic degrees of freedom (DOF) available on the micro-/nanoscale. Developing such tasks without automation is nearly impossible, since crucial operational steps are not controllable for a human operator, because their perceptive capabilities are not trained for the nanoscale and they do not scale.

Vice versa, the feasibility of *automation*, depends on the complexity of the handling task, and addresses the defined figures of merit speed, cost-efficiency and automation capabilities in itself. Automation strictly depends on sufficient sensor information in order to work, because this information is needed for control loops, which are the core unit of every automation. This covers concrete control loops such as positioning tasks, as well as abstract tasks such as decision making [116]. Especially on the micro-/nanoscale, the amount of sensor information is a crucial bottleneck. Considering the amount of involved components, the maximal

working range and the addresses accuracy, only few sensors are available. Furthermore, most of them are hardly combinable, due to their complex working principles. As opposed to the macroscale, where additional sensors can easily be integrated when necessary, on the micro-/nanoscale is a strong mismatch of necessary information and available sensors. It can be concluded:

Automation and complexity are cross-dependent for assembly tasks on the the micro-/ nanoscale: Automation becomes more challenging with the increasing complexity of a task and the complexity can be increased only with automation. Additionally, automation depends on missing sensor information and complexity suffers from a lack of controllable degrees of freedom. Hence, automated assembly strategies can be realized by improving two factors: i) as much status information as possible must be acquired and ii) the task has to be reduced to as few degrees of freedom as possible in order to be controlled.

4.1 Robotic Handling Approaches

There are three fundamental gripping techniques that are applicable on the micro-/nanoscale: i) form locking gripping ii) force locking gripping and iii) material enclosure: These three fundamental techniques can also be applied to gripping approaches on the micro-/nanoscales: Form locking can be subdivided into under-grip approaches (as addressed in an Section 4.1.4) and actual form locking, referring to grippers with structured jaws. On the macroscale, force locking refers to a technique, where the static friction between gripper jaws and an object to be handled are larger than gravity. Even though this fact is still the same on the nanoscale, gravity is one the the smallest forces and the understanding of force locking has to be a different. Material enclosure is also directly applicable and to the nanoscale (cf. Section 4.1.2).

While all technique are used in the developed handling strategies, each has their specific advantages and disadvantages. They have been adapted and further developed to fit the particular demands of the intended automated handling task. Common to all handling techniques is that the adhesion force between the object and the object's carrier must be overcome. Figure 4.1 depicts the most dominant forces for pick-up and placement operations on the micro-/nanoscale and classifies them into categories:

Normal forces are the normal forces caused by mechanical counterparts. F_{n-Grp} is the force that is applied by the gripper to the particle and F_{n-Sub} is the force applied by the carrying substrate to the particle.

Adhesion forces are F_{ad-PS}, the adhesion between particle and substrate, and F_{ad-PG}, the adhesion between particle and gripper. The strength of the adhesion forces depends on the parameters described in Section 3.1.

Friction forces are $F_{fric-PG}$ and $F_{fric-PS}$ and occur as counter forces to the mechanical shear between two objects. Their depending is linear on the interaction surface between the two corresponding objects [141].

Due to their minor influence, the forces gravity and inertia are neglected in this model (cf. Sec 3.1). In this model electrostatic forces and capillary forces are treated the same but for different reasons: Electrostatic forces can be neglected since in grounded scanning electron microscope (SEM) conditions two objects are nearly on the same potential, equalize when in contact, and do no generate an electrostatic force. Capillary forces are minimized due to the vacuum conditions inside the SEM. Furthermore, even a minimal remaining water meniscus can be assumed as attractive part in the DMT approximation [132]. Based on these fundamental and most dominant forces, handling strategies in terms of picking and placing operations can be designed and evaluated: In order to pick up an object, the sum of the objects friction and adhesion to the gripper has to be larger than the adhesion to substrate: $\sum_i F_{i-PG} > F_{ad-PS}$. In order to place an object, the adhesion to the receiving substrate must be larger then all gripper related forces: $\sum_i F_{i-PG} < F_{ad-PS}$. In some cases the adhesion F_{ad-PS} cannot be overcome, but transverse forces F_{n-Grp} can be large enough to exceed the friction force $F_{fric-PS}$, resulting in an on-surface movement of the object. Although the later case is not pick-and-place handling, it can still be regarded as a 2D handling strategy. However, actual assembly of nanoscale building blocks demands an actual handling of objects, where at least all three translational degrees of freedom can be addressed.

Based on these most dominant forces and their interdependencies, a fundamental handling principle that is crucial on the micro-/nanoscale can be already deducted:

The surface hierarchy principle refers to the exploitation of adhesion for handling purposes on the micro-/nanoscale. Since the interfacial adhesion energy –whether it is dominated by van-der-Waals, double layer, or electrostaticaly forces– depends on the surface size that contributes to the interface, it can be assumed that larger surfaces result in a larger adhesion energy as long as all other parameters are comparable. Under this assumption, it can be concluded that interfacial binding with larger surfaces is stronger than binding with smaller interfacial surfaces, since all forces depend in the effective surface of interaction. This simple fact can be exploited in order to develop fundamental handling strategies based on *surface hierarchy*: Figure 4.2 depicts the principle of this strategy. Initially, a particle is attached

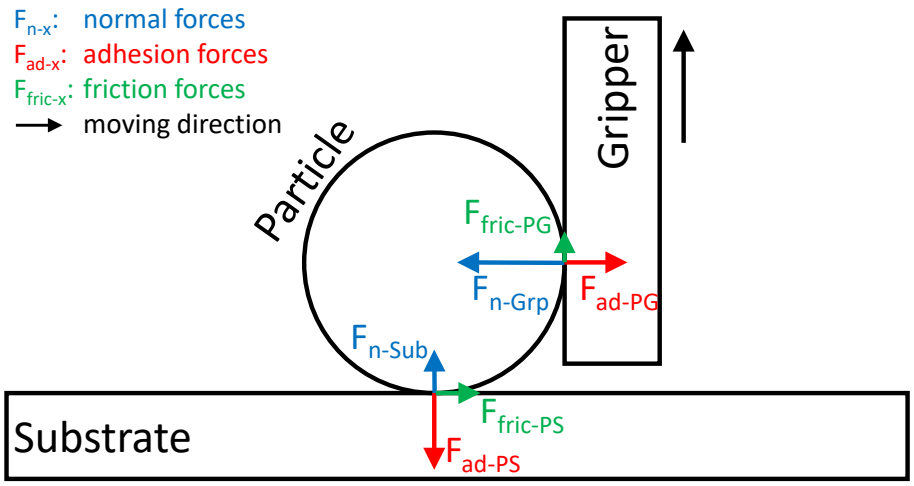

Fig. 4.1 Overview of the most dominant forces during pick-and-place handling situations on the micro-/nanoscale using a single end-effector.

to a carrying end-effector. After attaching a second end-effector is attached to the particle, the composition is pulled apart. The particle tends to remain on the end-effector with the larger common effective interfacial surface, which is the second end-effector. This step can be repeated with another end-effector with an even bigger surface. However, this principle is also subjected to uncertainties and works more reliably the bigger the differences of the two interfacial surfaces are. Hence, this principle can be used to perform only very few successive transfer steps.

4.1.1 Nanotip-Based Handling

Using simple tips as end-effectors is the easiest way to facilitate nanohandling. Depending on the application, a tip can be used for pushing objects on a surface [199], lifting them partly from a surface [199] or picking them up completely [139]. With respect to the application, single tip handling has to be seen either as form locking or force locking gripping. However, single tip handling is very limited in its applications: A tip that has a sufficient surface of interaction with an object to pick it up has in most cases too large surface of interaction to release the same object on a target, since $\sum_i F_{i-PG} > F_{ad-PS}$ at any time. Vice versa, a tip that has a very limited surface of interaction with an object can still apply sufficient normal force to overcome friction and adhesion, but the small surface cannot control the object for further handling. Hence, during single tip handling without additional supporting devices, handling objects either tend to stick to the tip or move uncontrollably as result of the picking.

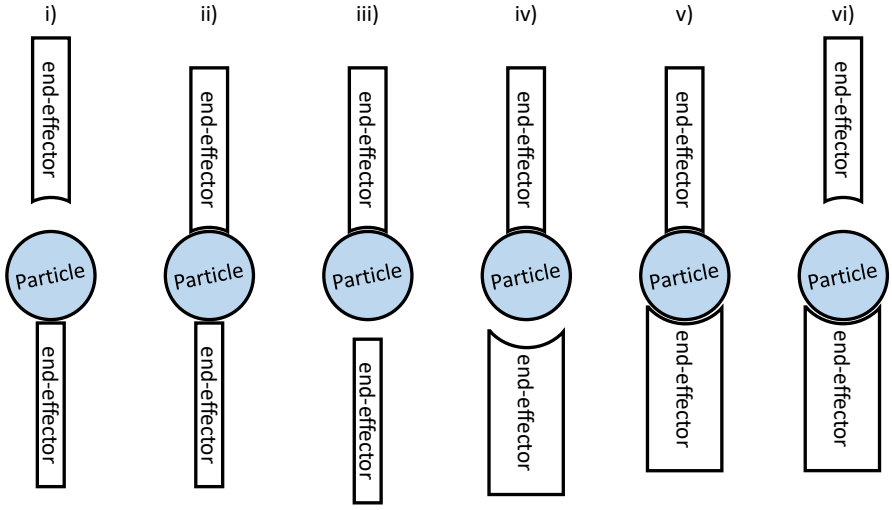

Fig. 4.2 Handling sequence according to the surface hierarchy principle: i) initially, a particle is attached to a carrying end-effector, ii) a second end-effector is attached to the particle, iii) when separated, the particle sticks to the end-effector with larger common surface of interaction, iv) - vi) a second transfer can be completed accordingly with a third end-effector.

For this reason, tip handling has to be combined with additional techniques in order to gain control over the all normal forces F_n and adhesion forces F_{ad}.

Dual Tip Handling

A dual end-effector technique allows to change the number of involved forces and their quantities, respectively [36]. One tip can be used as end-effector for pick up operations only, where the condition $\sum_i F_{i-PG} > F_{ad-PS}$ applies. The use of a second end-effector enables to apply additional normal force F_n, which can be used to assist either the normal forces to the substrate or the normal force to the first end-effector. Hence, dual end-effector handling is already an example for a handling setup with tunable forces. Furthermore, the second end-effector can be used to increase the friction force during the pick-up process due to the increased normal forces (cf. 4.1.3). The overall gripping force is the sum of all adhesion and friction forces with the same force vector orientation. Since the friction forces depend on the load, the overall gripping force can be tuned by additional normal forces [141]. This effect can be assumed even on the micro-/nanoscale, as long as significant surface roughness exists [141].

Figure 4.3 depicts a typical pick up and placing situation. In contrast to the single end-effector approach, the dual end-effector technique allows to apply the larger opposite normal forces F_{n-Grp1} and F_{n-Grp2}. Due to this force application, the corresponding friction forces

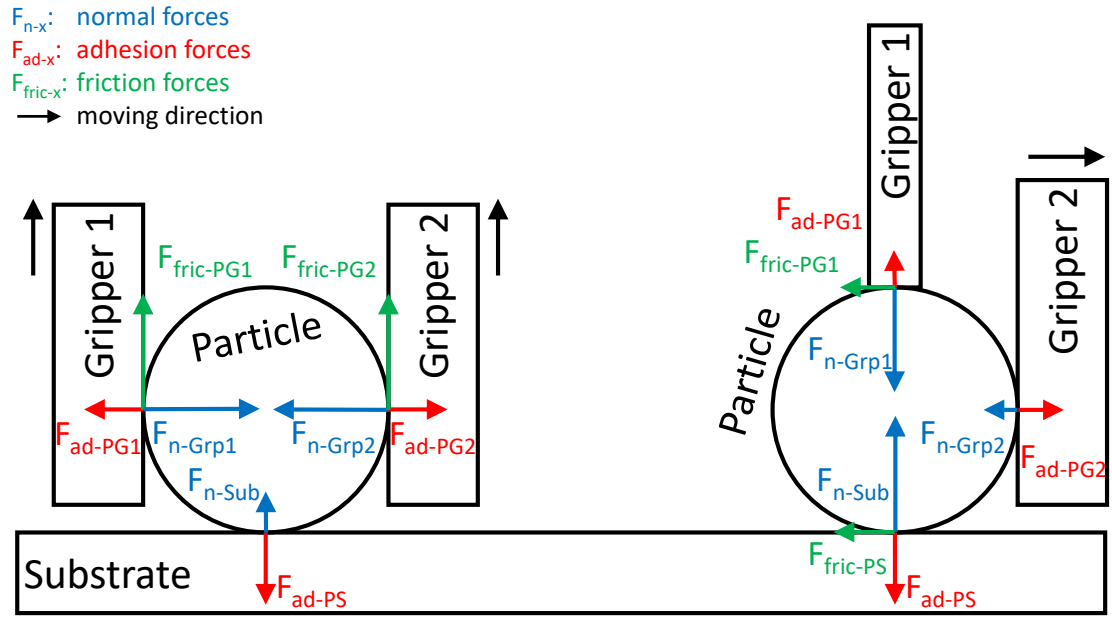

Fig. 4.3 Overview of the most dominant forces during pick (left) and place (right) handling situation on the micro-/nanoscale using two end-effector.

$F_{fric-PG1}$ and $F_{fric-PG2}$ increase as well. This is how the particle holding adhesion force F_{ad-PS} can be overcome in a controllable way. For a placing situation, a second end-effector can be placed in a different position in order to apply an additional normal force F_{n-Grp1}. Consequently, this force increases the particle holding friction $F_{fric-PS}$ and also results in an additional friction $F_{fric-PG1}$. This is how the first second end-effector can overcome the adhesion to the particle and can be retracted even without moving the particle.

In addition, if two completely independent end effectors are used, it is not only possible to control the pick-and-place forces, but also to determine the orientation of a micro-object. Figure 4.4 depicts such a handling situation: two end-effectors applying normale forces are able to control all six DOF of a gripped object. Since both end-effectors have three independent translational DOF x_i, y_i, z_i, they can control the three dimensional position x_O, y_O, z_O and three dimensional orientation ρ_O, θ_O, ϕ_O of the object. However, this approach is accompanied by a doubled instrumental effort concerning fine positioning.

All in all, tip-based handling is an easily implementable technique that only becomes powerful in combination with additional techniques, such as material enclosure handling or structural design.

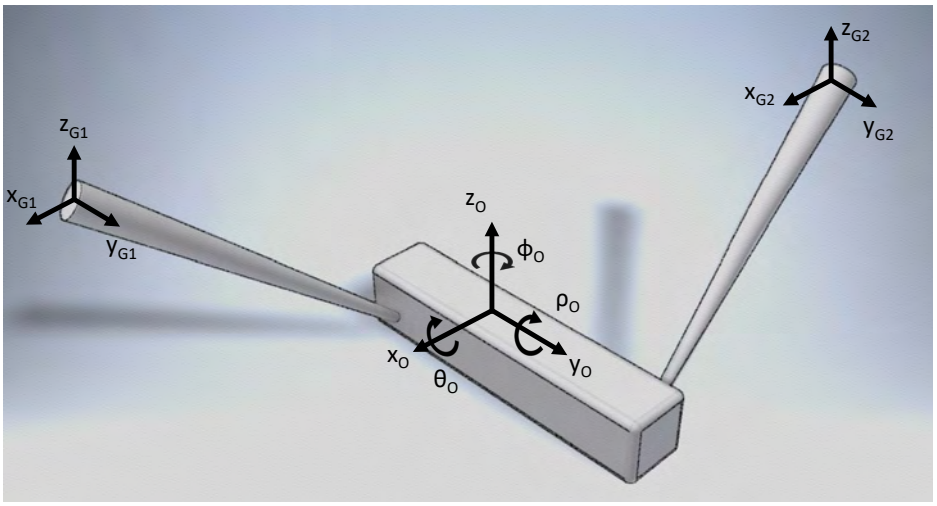

Fig. 4.4 Using two independently movable end-effectors allows to control all translational degrees of freedom x_O, y_O, z_O of an object as well as all rotational degrees of freedom ρ_O, θ_O, ϕ_O.

4.1.2 Material-Assisted Handling

Additional techniques are needed to increase the capabilities of tip based handling. Tips as only end-effectors can hardly control all DOF and a single tip alone does not have the capability to change interaction forces during a nanohandling sequence. Even a complex two tip approach has more control of the DOF, but it does not allow great forces to be exerted.

An additional technique to facilitate the pick-up process by increasing the adhesion between tip and the object to be handled is material enclose handling based on the electron beam induced deposition (EBID) technology (cf. Chapter 2.1). The working principle of EBID of localized material deposition allows to apply this technique as a joining method in handling sequences. An object to be handled can be joined to an end-effector for subsequent pick-up steps. The actual transport of the object does not need additional control of any parameters, since the material bond is permanent and stronger than all other involved forces. Another advantage of this technique is the electrical conductivity of the bond, which can allow for on-the-fly characterizations of handled and mounted samples. Disadvantages of this handling technique are the time-consuming deposition process, which is comparatively short on the nanoscale and possible additional contamination with bond material. Furthermore, with most precursors, EBID is just a joining technology. By using precursors containing fluorine, also etching the material can be realized. However, this process is kust as time consuming and etching rates depend highly on several material conditions making them hardly predictable. Overall, the EBID technique allows for an easy and reliable pick-up

process with mechanical and electrical bonding, but needs an additional subsequent separation technology.

The focused ion beam (FIB) technology offers the possibility to remove highly localized material and is therefore suitable as separation technology. Small material removements in the (sub)-micrometer range can be carried out and allow for the separation of different objects. Hence, an object to be handled that is joined with a handling end-effector can be separated by FIB treatment. In combination, gas injection system (GIS) and FIB offer complementary techniques to achieve common joining and separation technology. A disadvantage, additional to a slow process and precursor contamination, is the ion implantation. The FIB technique needs a few steps of ion imaging that expose the entire sample to a short ion irradiation. This leads to an almost negligible abrasion of all parts and to an implantation of ions, which can be an excluding factor for this technology anyway – depending on the specific purpose. Furthermore, this approach demands several specialized instruments, all in combination with an SEM: The GIS and FIB units are quire cost-intensive and especially the latter can hardly be added modularly. Figure 4.5 shows a conceptual handling sequence based on combined EBID and FIB technologies. The handled object is attached to an end-effector by EBID processing and detached from the source substrate by FIB-milling. On the target substrate, the object is attached by another EBID proces and detached from the handling end-effector by another FIB-cut.

In summary, a combined GIS and FIB technique offers a slow and invasive technology for handling on the micro-/nanoscale, but due to its working principle it is solid and reliable [81, 184]. Hence, this technology is one possible approach for nanohandling, but like other technologies it is also limited. Even though this technique has a potential for automation, the integration effort is large, due to the instrumental complexity. Furthermore, the processes are time consuming which makes automation even more complex.

4.1.3 Gripper-based Handling

Gripping as fundamental handling technology is well-known from the macroscale and even applicable to the micro-/nanoscale. Grippers can also work according to two different principles: form gripping as well as force gripping are both typical. In contrary to the macroscale, the involved forces and the different force hierarchy (cf. Section 3.1) require a different understanding of gripping principles: On the macroscale, a gripper's jaw clamps an object using a gripping force F_{n-Grp} in order to increase the friction with the object to be handled. As a result, the friction force $F_{fric-PG}$ is larger than gravity F_G and the object can

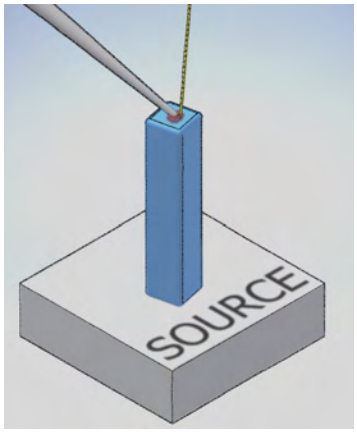

(a) An object (blue) is joined to an end-effector by a focused electron beam (yellow) induced deposition (red).

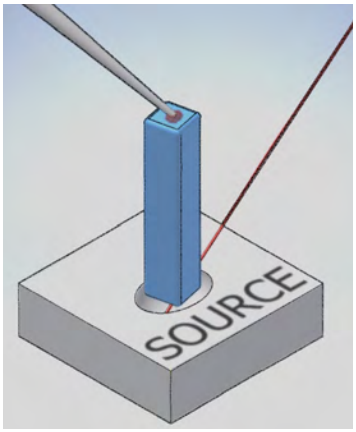

(b) The object is seperated from the carrying substrate by a focused ion beam (red line).

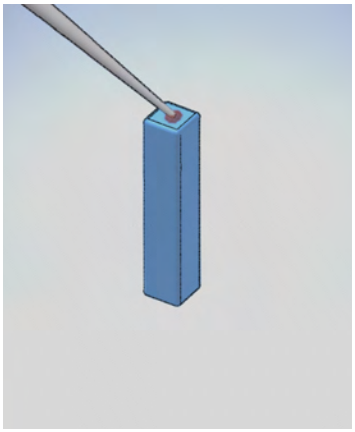

(c) The object is supported by the end-effector and can be carried to another substrate.

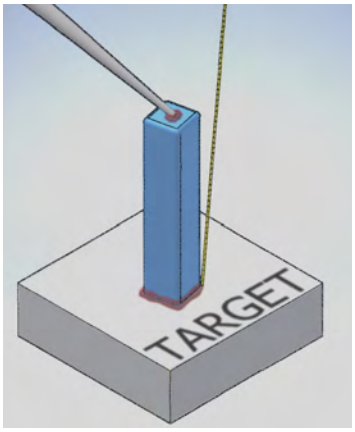

(d) EBID is used to join the object to the receiving substrate.

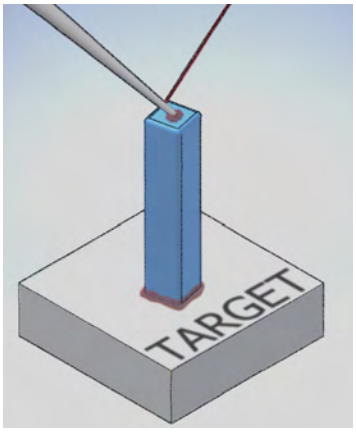

(e) FIB is used to cut the carrying end-effector in order to release the object.

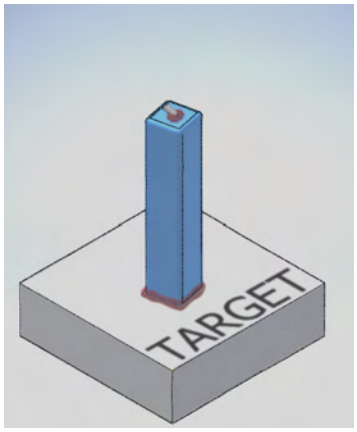

(f) The object is transferred and joined to the target substrate.

Fig. 4.5 Material-assisted handling based on focused ion beam and electron beam induced deposition. A building block (blue) can be attached to an end-effector and transferred to another substrate.

be held and lifted. On the micro-/nanoscale in contrary, adhesion forces are most prevailing and the object to be handled sticks to the surface with the largest area of interaction. As a consequence, a gripper can be opened, even when carrying an object, and will not lose the object, as long as no other surface is in contact. Furthermore, lifting an object from a surface using grippers is also just as consistent a technique as the exploitation of surface hierarchies. As a result, a gripper on the micro-/nanoscale is a rather simple end-effector that can double its interaction surface with the objects to be handled by the factor of two.

4.1.4 Structural Design Handling

Structural design is a fundamental approach to allow and improve other handling technologies, not being a self-contained handling technology itself. It is most likely comparable with *positive form locking* on the macroscale. Different principles can be realized or improved by structural design:

Geometrical Improvements Structural design allows to resolve geometrical constraints that are an obstacle for the handling task: Simple pick-up tasks can become an actual challenge on the micro-/nanoscale, due to the range of scales of all involved components. Figure 4.6a) shows a typical handling challenge in nanohandling. If an object to be picked up has smaller roughness or curvature than the handling end-effector, any kind of under-grip approach is impossible. This is a major obstacle when lifting objects laying on the surface. Even though gravity forces are negligible on the micro-/nanoscale, lifting the object is necessary to separate the object from the substrate by overcoming the adhesion forces between them. The structural design of object carrying samples allow to facilitate gripping approaches as depicted in Figure 4.6b).

The structural design and the resulting partial separation of object and sample also allows the application of other handling techniques, where the spatial proximity of object and substrate is an obstacle: Using the EBID technique to pick up objects for examples cannot be applied if object and substrate are in contact, since the resulting deposition would cover object, end-effector and substrate. In contrast, a structured object carrier allows to bring object and end-effector in contact and apply an EBID deposition without bonding the object to the substrate (cf. Figure 4.6a) and b)).

In general, the structural design of samples and end-effectors is a simple way to optimize geometrical conditions in order to facilitate and improve handling approaches.

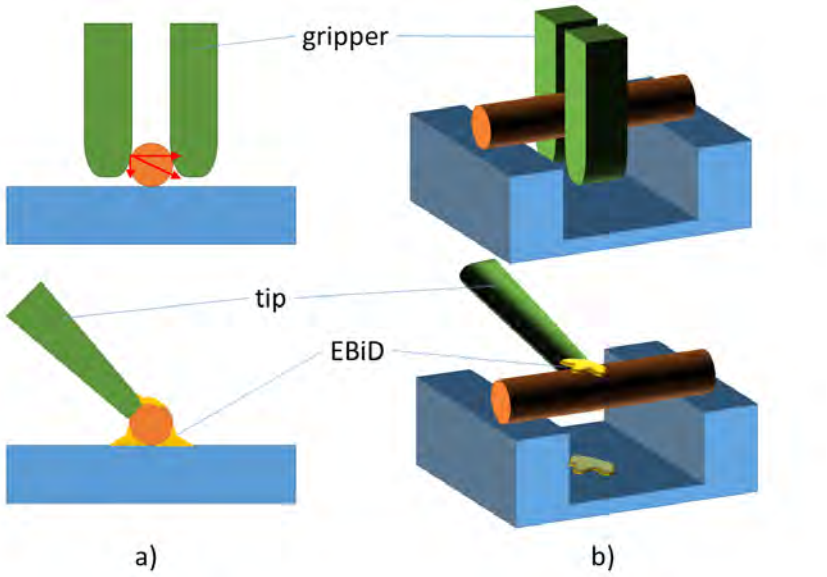

Fig. 4.6 Sketch of typical challenges in nanohandling tasks. a) The small object to be handled cannot be under-gripped or even freely grasp by the gripper. If the size of the object is smaller then the structures of the gripper, the gripping force (depicted for the left gripper jaw only) has components that push the object to the surface. In case of material-enclosure (e.g. EBID depicted in yellow), unintended enclosure of object and substrate is caused by their close vicinity. b) Structuring the substrate with grooves allows accessing the object with a gripper or end-effector without unintended side-effects.

Exploitation of Surface Hierarchy The structural design of end-effectors and substrates can be used in order to change the effective surface between an object to be handled and its counterpart. Therefore, handling sequences for object transport can be designed by gradually increasing the interaction surface. Figure 4.2 depicts the fundamental principle of this technique, were the involved corresponding interaction surface increases at each handling step. The only requirement for this approach is well-structured samples, end-effectors and substrates. Hence, structural design itself can facilitate the realization of a nanohandling step without any further assistance. However, most handling sequences can rely on this principle for few steps (typically one or two) only applying techniques [216].

Controlling DOF While structural design already helps to overcome limiting geometrical constraints, it can be used even more purposefully as a constraining structure in order to control geometrical degrees of freedom. This ability is strongly needed on the micro-/ nanoscale, since robotic degrees of freedom are quite limited and especially rotational degrees of freedom are hardly controllable. Structural design allows the determination of positions and orientations of objects by means of guiding structures and surfaces such as trenches, walls and end stops. If a handled object touches such a guiding structure, the increased surface pulls and keeps the object in the intended position, due to force hierarchy. The result is that unintended movements of objects to be handled can be reduced or even completely avoided. A nanowire placed on a surface keeps its position as long as all applied forces do not exceed the adhesion to the surface. If a force is applied that exceeds the adhesion, the nanowire loses its original position. This is a typical situation in nanohandling scenarios, where plain positioning is easily achieved by end-effectors and imaging systems; even with high positioning accuracy in two dimensions. But the actual assembly – placing or inserting an object in a predetermined position, controlling position and orientation – needs more robotic movements that just the initial contact. The fabricated guiding structure allows the nanowire to tolerate larger forces without losing its intended position compared to a simple unstructured surface.

The principle of controlling DOF by structural design also allows for the improved handling and positioning of general nanoscale building blocks. Specially designed target substrates facilitate a precise placement and guarantee to maintain the position. Consequently, even small deviations of the assembly sequence itself can be corrected or compensated.

Cartridge Systems

A consistent further development of this concept is a cartridge system for nanoscale building blocks, which is definied as *sorted storage device for components* [150]. For NanoBits, the cartridge systems allows for a precise arrangement by means of a pre-assembly [41, 42]. Figure 4.7 depicts the fundamental advantages of a cartridge concept that has the following key features:

Carrier First of all, a cartridge acts as carrier for smaller objects. This allows for easy handling, storing, and feeding several nanoscale building blocks at the same time. Logistical steps become parallel by means of using cartridges.

Defined infeed A cartridge system defines the environment of fed nanoscale building blocks exactly. Due to the well known geometrical conditions, the position of each component is defined and can even be expressed relative to a marker. This is how, each component can be found and addressed. Furthermore, the cartridge system guarantees sufficient clearance for all subsequent handling steps.

Controlled DOF A cartridge enables to control all three translational DOF as well as all three rotational DOF of a nanoscale building block. This allows to reduce the needed robotic DOF for handling, since all rotational alignments can be done already by the cartrige's design.

Protection A cartridge system allows to define particular parts where the cartridge itself as well as involved handling end-effectors are allowed to touch the stored

Overall, structural design allows to compensate the fundamental lack of robotic DOF in micro-/nanorobotics. Since rotational actuation is lacking, already approaching nanoscale building blocks can be challenging if the used end-effector and the objects to be handled are not well aligned. Structural design that offers geometrical constraints as guidance allows to compensate and enable translational and rotational alignment. This is how robotic uncertainties in micro-/nanointegration can be improved by means of structural design that constrains DOF purposefully.

4.1.5 Combined Handling Approaches

The combination of fundamental handling techniques is a crucial improvement for handling on the micro-/nanoscale Table 4.1 is an overview of the mentioned handling techniques including their specific advantages and disadvantages. Tip-based handling itself is very limited in its application, since controlled and reproducible handling is

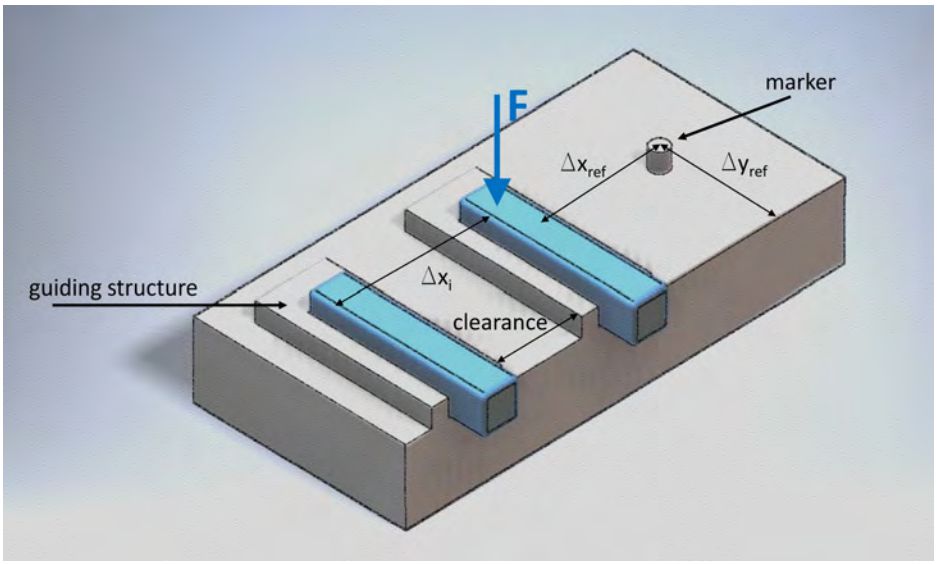

Fig. 4.7 Concept for a cartridge system that carries nanoscale building blocks. The structural design of the cartridge allow to guide the objects in well defined positions. The iterative distance Δx_i between objects, the clearance and the reference distances Δx_{ref} and Δy_{ref} to a possible marker are determined.

challenging in general. Material-assisted handling offers maximal joining reliability, but is accompanied by a large contamination of materials and is also lacking in control of orientation of a handled object. Gripper-based handling allows to switch interaction surfaces, but needs more development effort and is lacking in control of orientation as well. Structural design allows a better determination of orientations and enables an improved exploitation of handling based on surface hierarchy, even if it does not constitute a complete handling technology on its own. As a consequence, combinations of different handling techniques offer more advantages, as shown in Table 4.2. Especially the combination with structural design allows to gain orientation control, which is missing for most other handling techniques.

A combination of nanotip-based handling and material handling is one of the most reliable and prevalent techniques and can be found in many examples [93]. The additional combination with structural design allows to control final orientation of the objects to be handled and improve this technique. Guiding structures allow to align handled objects according to predefined conditions.

The combination of grippers and structural design is technologically challenging and effort-intensive, but is the best possible combination of advantages with minimal combinations of disadvantages for the final result. Firstly, a microgripper system is needed, which is already a demanding MEMS-device. Secondly, some of the involved components (gripper, handled objects, source substrate, and target substrate) have to be

structurally designed. This fabrication step has to be carried out for each affected part. This is already a combination of two crucial prerequisites for this handling technique. However, the combined advantages and avoided disadvantages are apparent: This handling technique is complete without any material-assistance and hence it has no contamination nor damage. The micro-gripper's capabilities allow to realize simple pick-up-sequences, since is has a switchable interaction surface (cf. Section 4.1.3). Furthermore, using enclosing grippers allows the exertion of large mechanical forces to the object to be handled. The structural design, on the other hand, facilitates high accuracies in position and orientation of the handled objects. Even more powerful, structurally designed grippers determine the position of handled nanoscale building blocks during their manipulation. Figure 4.8 shows a sketch of this working principle: A simple gripper can touch an object and increase its interaction surface by closing the gripper jaws. In this example, a structurally modified gripper also exerts a mechanical momentum to the handled objects. The consistent rotation of the grasped object is caused by the structural design only, but compensates the lack of rotational DOF.

Technique	Advantages	Disadvantages	Automation capabilities
Nanotip-based Handling	-easy to perform -no additional instrumental effort -easily prepared	-unreliable -little control of handling	-limited
Material-assisted Handling	-easy to perform -high repeatability	-large instrumental effort (FIB, GIS) -sample contamination -slow	-just partly -very high effort
Gripper-based Handling	-easy to perform -reliable actuation -fast	-complex production	-high
Structural Design	-control of orientation -no active parts -reliable	-preparation of each component required -not a complete handling technology	-inherent

Table 4.1 Overview of handling techniques and their advantages and disadvantages.

Technique	Advantages	Disadvantages	Automation capabilities
Nanotip-, material- and structural design based Handling	-easy to perform -highly repeatable -control of orientation	-large instrumental effort (FIB, GIS) -sample contamination -slow -praparation of each component	-possible -high effort
Gripper- and structural design based Handling	-easy to perform -reliable actuation -fast -control of orientation	-complex production -preparation of each component	-high

Table 4.2 Overview of combined handling techniques and their advantages and disadvantages.

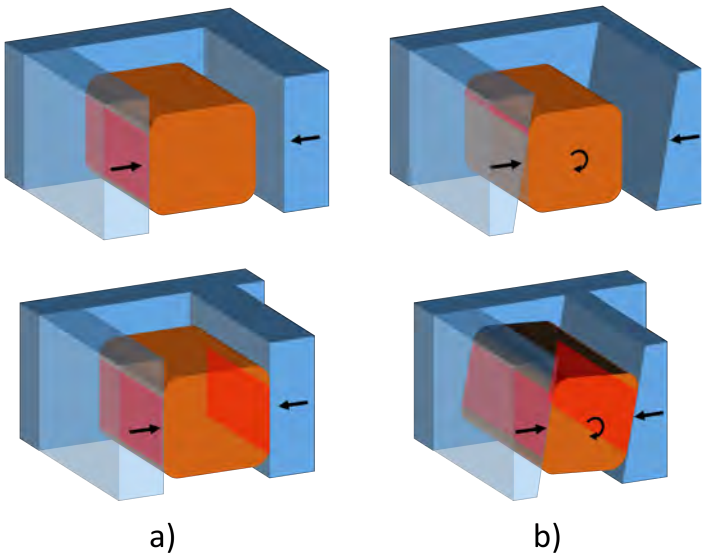

Fig. 4.8 Sketch of a gripper's working principle on the nanoscale. a) Closing the gripper's jaws, increases the surface of interaction (red square) by the factor of two. b) Structurally designed gripper jaws also apply an angular momentum to the handled object.

In summary, the developed combined handling techniques -especially all combinations with structural design- allow for improved handling on the micro-/nanoscale. Automated handling can be achieved only by tunable actuation forces and especially gripper based handling is predestined for that. Structural design, although it is not a self-contained handling technology, increases the controllable DOF, which supports handling and automation in general.

4.1.6 Evaluation of Handling Approaches

The evidence of the developed handling techniques is shown for structural design and combined handling techniques by a series of fundamental measurements. Extensive applications of these techniques are demonstrated in case studies (cf. Chapters 5 and 6).

Improved Handling by Structural Design

A simple nanohandling scenario that can be improved by structural design is depicted in Figure 4.9. A nanowire was picked from a production substrate by material-assisted handling. Firstly, the object was placed on a flat surface while a certain alignment of the nanowire needed to be achieved. Secondly, the nanowire was placed on the same substrate at a location that is equipped with a simple guiding structure giving the

nanowire a predefined orientation. In both scenarios, the originally stress-free aligned nanowire is moved by the end-effector after the placing sequence in the x-direction in order to apply force to the nanowire-substrate interface. The maximal applicable displacement was measured, before the adhesion to the surface was overcome by the mechanical stress of the nanowire. Using this information, the adhesion energy stored by the nanowire and substrate could be calculated according to the Euler–Bernoulli beam theory.

$$EI\frac{d^4u}{dx^4} = 0, \quad I = \frac{\pi d^4}{64}, \tag{4.1}$$

where E is the Young's modulus, I the beam's momentum of inertia according to the z-axis, $u(x)$ the bending line of the nanowire, and d is the thickness of the wire. Considering the fixed clamping of the nanowire, the boundary conditions

$$\left.\frac{du}{dx}\right|_0 = \left.\frac{du}{dx}\right|_s = 0, \quad \text{and} \quad u(0) = 0, u(s) = h, \tag{4.2}$$

are given taking into account a displacement of h and length of the nanowire s (cf. Figure 4.9). The specific solution of Equation (4.1) is

$$U_A = \frac{6\pi E h^2 d^4}{64 s^3} \tag{4.3}$$

In the experiments at hand, copper-oxide nanowires were used as handled objects. Their dimensions are a thickness of $d = 152\,nm$ and length of $l = 30\,\mu m$ (cf. Figure 4.9 lower image). The used nanowires were previously investigated in order to determine the Young's modulus of $E = 102.7\,GPa$ [204]. The placing and bending experiments were performed as described above and the resulting maximal interfacial adhesion energy was calculated according to Equation (4.3). The maximal applied energies measured in these experiments are shown in Figure 4.10 in dependency of the maximal displacement. The results clearly show that energy and displacement are quadratically dependent according to Equation (4.3). Mean adhesion energies and deviations are calculated for the two different scenarios i) flat surface placement and ii) placement with guiding structures and the results are given in Table 4.3. In direct comparison, structural design increases the maximal adhesion energy roughly by a factor of 6. Even if the variation also increases, both scenarios show statistically significant differences in interfacial adhesion energies[1].

[1] based on a significance level of α=0.05

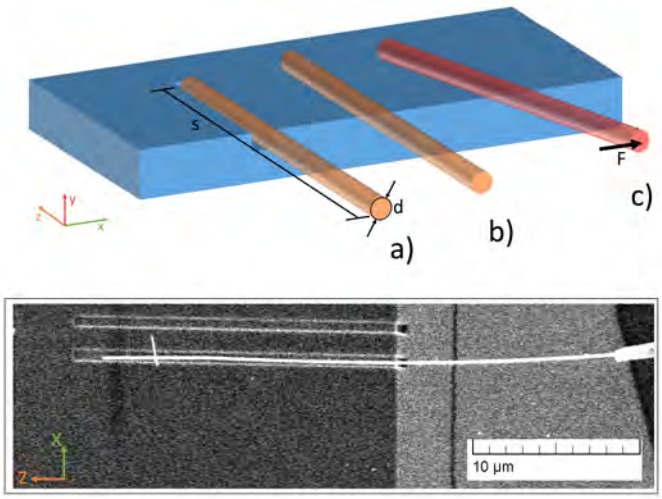

Fig. 4.9 Testing the improved handling by structural design. Upper image: A nanowire with length s and diameter d is mounted in a guiding trench structure a) and on a plain surface b). An additional force F perpendicular to the nanowire is applied and bends it until the nanowire misaligns with the original orientation c).
Lower image: SEM image of situation a). A nanowire is mounted in a silicon trench. It can be moved by an end-effector along the x-direction.

	mean energy μ_{U_A} / fJ	standard deviation σ_{U_A} / fJ
Plain substrate	2.3	1.6
Structural design	13.7	11.5

Table 4.3 Maximal interfacial adhesion energies for placing experiments.

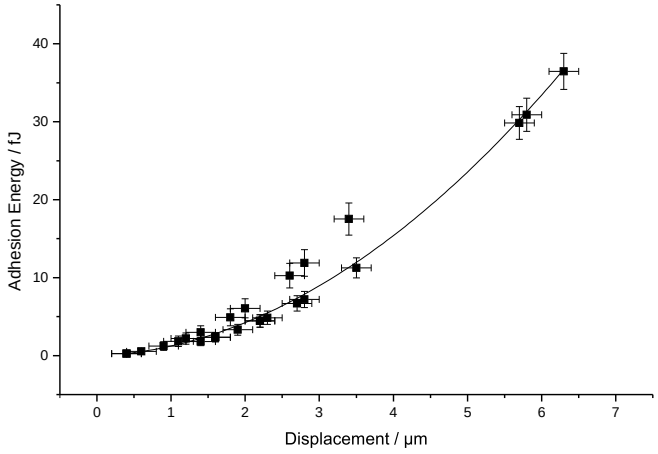

Fig. 4.10 Measurements of the maximal interfacial adhesion energy in dependency of the maximal displacement. The fitted curve represents the theoretical energy/displacement-dependency.

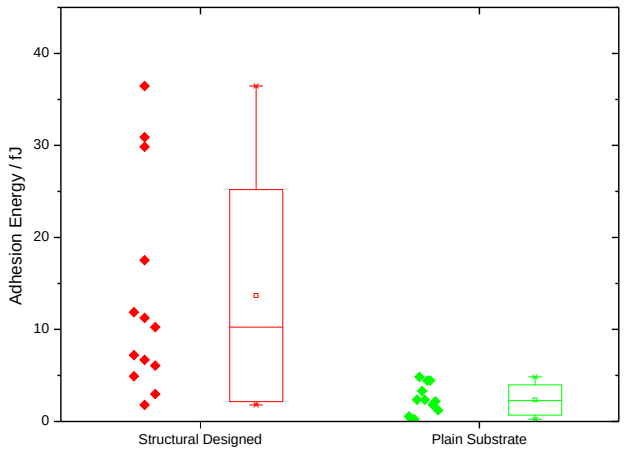

Fig. 4.11 Mean interfacial adhesion energy of a placed nanowire in a structural designed substrate (left) and a plain surface (right). Boxes mark the $\pm 1\sigma$ standard deviation.

Result As a result, it can be stated that structural design can improve handling and especially integration tasks on the micro-/nanoscale. It increases the interfacial adhesion energy of a handled object and a carrying or target substrate. This allows to apply larger forces to objects during their handling while preserving their intended position and orientation. Larger rotational uncertainties can be compensated during integration tasks and interfering parasitic forces (e.g. during the separation of a handled object and an end-effector) can be endured.

Improved Handling by Combined Techniques

The combination of other handling techniques with structural design allows to increase the controllable DOF (cf. Section 4.1.5). Since especially rotational DOF are lacking on the micro-/nanoscale, structural design is most beneficial for controlling these DOF.

A microgripper can be structurally designed in order to facilitate a turning movement of a flat gripped object as shown in Figure 4.8. Without structuring, the flat object either turns in an unpredictable direction or does not turn at all. The structural design of the gripper jaws predetermines the turning direction. The sequence shown in Figure 4.12 shows all phases of a gripping process with a microgripper. The object to be gripped is a flat piece of silicon, 2 x 5 µm^2 and 200 nm thick. The gripper's closing movement is in plane with the flat object. During their closing movement (b) - d)), the structure of the gripper jaws causes a turning movement of the flat object [37] .

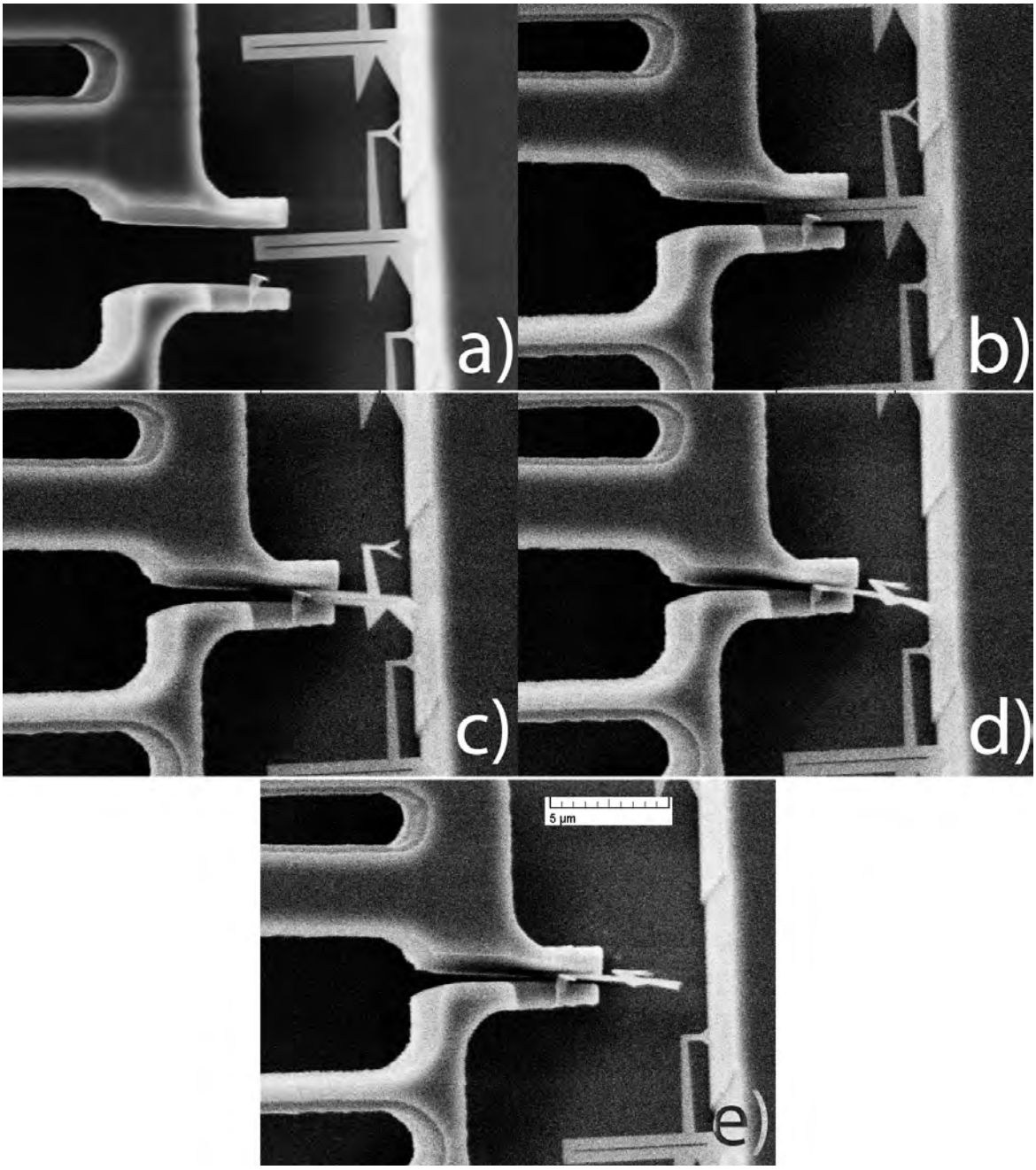

Fig. 4.12 Sequence of a gripping process inside the SEM: a) a structurally designed microgripper approaches an object attached to a surface. b) - d) The structure of the closing microgripper turns the object by 90°inside the gripper jaws. e) The object is completely turned and detached from the substrate.

Result In summary, structural design and its combination with other handling techniques allows to improve the capabilites of handling on the micro-/nanoscale. Increased surfaces and mechanically guiding structures can increase the tolerance against parasitic and disturbing forces. Furthermore, additional movements can be advantaged or constrained. Overall, a universal handling technique for the micro-/nanoscale does not exist. However, there is a variety of several different and complementing techniques that allow for serious and controlled handling on these scales.

4.2 Scanning Electron Microscope Effects

The SEM as a visualization system offers tremendous advantages, but is also accompanied by unavoidable side effects as introduced in Section 3.3.5. These side effects are widely seen as disturbing or even dismissive obstacles for the use of this system [154]. However, the surface charging effect can be exploited as a novel information source and applied to the robotic assembly tasks of nanoscale building blocks.

The electrical potential of each surface in SEM applications depends on several parameters but the electrical quantities of the sample are most important. Hence, the charge and the corresponding brightness information in scanning electron microscopy have been used to derive different pieces of information about the sample: In integrated circuits, the doping level of a sample can be investigated efficiently by charge observation [170]. Additional developed systems allow for failure detection by electron and ion beam irradiation [162]. In the latter, the negative correlation of the charging effect and scan-speed according to equation (3.7) has been discussed already.

4.2.1 Exploiting Scanning Electron Microscope's Effects for Assembly

The surface charging effect can be used to extract missing information about the relative depth of the objects. This precious information can be used for assembly control and automation.

According to equation (3.3), the grounding resistance R_G has a direct influence on the surface potential U_S. Hence, if the grounding resistance of a sample changes, the surface potential also changes, which leads to measurable aftereffects. Due to the working principle of the SEM, the change of the surface potential U_S leads to changes in brightness and image distortions such as a static image drift.

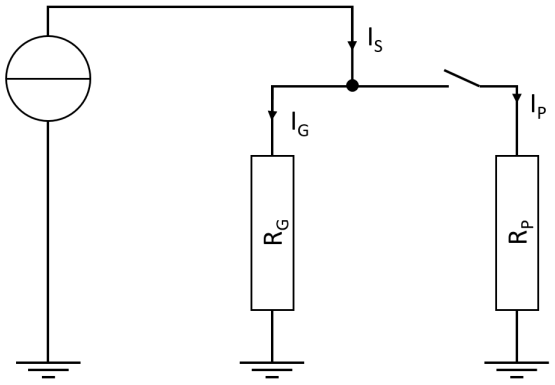

Fig. 4.13 Schematic equivalent circuit for a sample inside the SEM that is exposed to an electron beam with the current I_S. The sample is grounded by the resistance R_G leaking the corresponding current I_G. If a probe grounded via R_P touches the sample, an additional leaking current I_P occurs.

This can be exploited to derive significant information about the status of an assembly task. Figure 4.13 depicts an equivalent circuit of a sample during an assembly process inside the SEM. In its initial condition, the sample is exposed to the electron beam and a corresponding current I_S. The sample's surface potential U_S will be constant according to equation (3.7) if the conditions are preserved, but if another object or probe touches the sample, a further grounding resistance is applied to the sample by the probe R_P. According to equation (3.4), this directly changes the surface potential U_S. This is how a typical assembly task such as an insertion process can be monitored by means of visual information in the SEM-image. If the object to be inserted touches its target, a surface potential change will appear.

Negative side effects It is noteworthy that the surface charging effect can have negative side effects as well since the surface potential has a significant influence on all operational tasks of nano-assembly, which have to be considered during the development of the process. Different materials have different resistivity and permittivity; the resulting surface potential of different objects is not necessarily equal. This leads to major obstacle for assembly tasks: Two objects made of different materials that are exposed to the electron beam will have different potentials. On the micro-/nanoscale, this effect is even more apparent due to the large surface-to-volume ratio. The different charge of these two objects can cause major hurdles due to the electrostatic force and electrostatic discharge (ESD) (cf. Fig 4.14). Firstly, the electrostatic force causes an attractive force acting on the two objects. This can lead to misalignments during an assembly process. Secondly, the potential difference can result in discharge effects

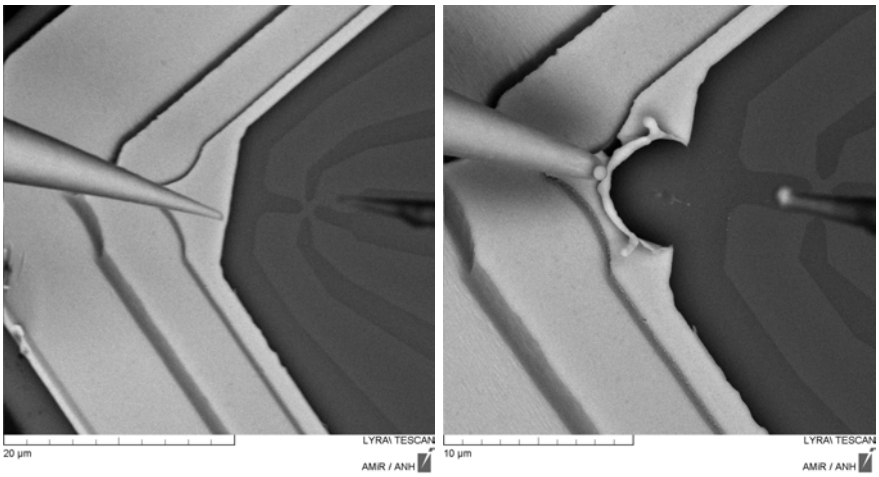

Fig. 4.14 Left: A tungsten tip hovers closely above a gold electrode. The potential of the two objects is different, although both are generated by the electron beam. Right: The tip touched the gold electrode and the resulting electrical current was large enough to evaporate the gold electrode due to joule heating.

that can cause severe damage to nanoscale samples. Since the potential differences can be in the range of a few thousand volts, the entire destruction of a charged nanoscale building block is likely to occur, when brought in contact with a grounded sample.

Material consideration The local surface potential of a sample depends mostly on its grounding resistance R_G. In all previous considerations, this resistance is assumed to be an effective resistance between the region of interest (ROI) and the ground level. This includes the resistance of the sample itself, grounding cables and contact resistances. Certainly, in many applications around micro-electromechanical system (MEMS) and nanoscale building blocks, silicon or other semiconductors are prominent materials. Semiconductors have an electrical resistivity, even though it is much higher than that of conductors (intrinsic silicon has a resistivity of 2.3 kΩm [79]). However, the overall electrical conductivity of semiconductors increases significantly under additional energy influence, as it occurs from the electron beam of the SEM: The incident electron beam generates charge carriers in the semiconductors that increase the conductivity. The generated carriers recombine in the vicinity of many micrometer [87]. The carriers density increases with the electron beam's current, while the range of generation increases in all three dimensions with the electron beam's energy. Hence, the actual local surface charge of silicon depends on the grounding resistance R_G, but also on the electron beam energy E and current I_P. As a consequence, semiconductors show a more complex surface charge behavior, since their initial grounding resistance

decreases under electron beam irradiation. This gives semiconductors self-limiting surface charge characteristics. Typical surface charge potentials for silicon are voltages of up to 50 V [193]. This makes semiconductors quite ingesting, since their surface potential can be exploited, but the self-limiting behavior prevents serious damage.

Touch Detection from Brightness

The surface potential change can lead to a brightness change in the SEM-image. This effect is extensively used to investigate the material properties of samples, also including probing for grounding purposes [162]. However, the brightness depends on several other parameters as well, and can change even if the surface potential does not. For example, and as mentioned in Section 2.1, the geometrical conditions can have a direct influence on the local brightness of an object. Hence, the touch detection from brightness technique is related to the depth-from-focus approach. In general, it can be used as information source for assembly tasks, but it is not applicable in every case.

Experimental Validation The usage of the touch detection from brightness approach is tested with regard to its applicability for automation. For this, automated approaches are performed, while output signals are monitored in order to detect touch events. The adjusted independent parameters are

- the electron beam scanspeed,
- the size of the ROI,
- and the position of the end-effector;

while the dependant, monitored, or calculated parameters are

- the brightness of the image and significance of changes,
- the precision of the technique, assessed by measuring the repeatability,
- the needed time and success rate of touch detection by discharge.

An exemplary signal sequence of a repetitive touching and retracing end-effector is shown in Figure 4.15. Each touch causes a significant change of brightness, while each retraction leads to a return to the original brightness level (cf. Figure 4.20 in upcoming section).

Figure 4.16 shows an exemplary position/brightness-plot for optimal conditions. Here, the uncertainty of the touch detection can be estimated to be about 50 nm over several

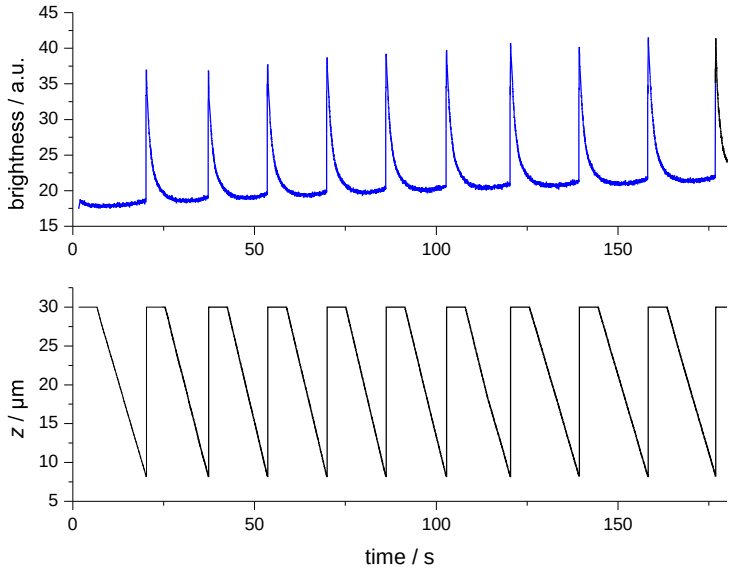

Fig. 4.15 Position and brightness signal during repetitive approaches of the end-effector to the surface. Each time the end-effector touches the surface, a significant brightness change is observable. If the end-effector is retracted, the surface charges slowly toward the original equilibrium state.

approaches. The signal seems to have a strong hysteresis, which is actually induced by the rapid retraction of the end-effector and the larger relaxation time of the surface charge.

Table 4.4 shows the results of an automated touch detection evaluation based on brightness changes. For this experimental series, brightness and contrast are set to the same values before starting the experiments. A general brightness change of at least 20% in comparison to the initial value is used as criteria for a successful approach. A grounding end-effector approaches the sample with in 200 nm steps, while all crucial values are monitored and calculated. Using the given configuration, the overall results show a high success rate of nearly 100% in almost all cases. The approach is counted as fail if the surface's position, which is determined in advance, is passed by more than a micrometer without touch detection by the automation software.

The dependencies of process time, scan-speed and ROI-size are obvious:

- Slower scan speeds and larger ROI show a linear increase in the approach-time. This is evident, since the overall frame-rate as a product depends on both parameters. Larger deviations form this linear dependency can be found for large scan speeds (<2 µs/px) and small ROI, since in those cases the PC-based image processing is slower than the frame-rate.

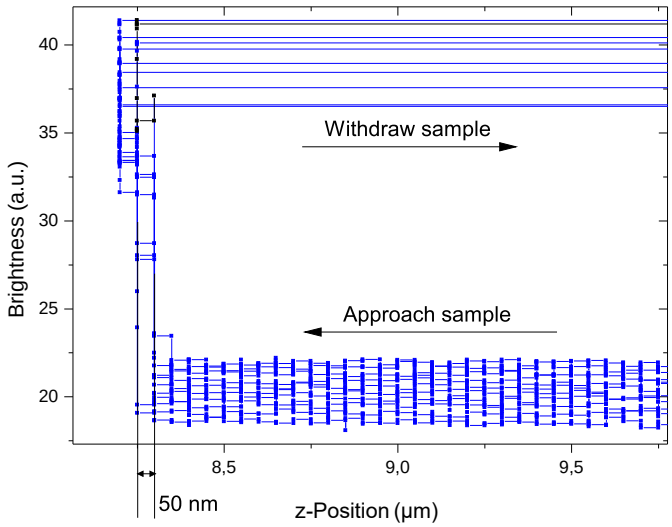

Fig. 4.16 Exemplary brightness values of an observed touching experiment in dependency of the end-effector's positions for several repetitions. The maximal position uncertainty for the corresponding significant brightness scale change determines the precision. In this case it is 50 nm.

- The success rates drops for large scan speeds (<2 µs/px) and small ROI. This is caused by the increased signal-to-noise ratio of these images, which leads to less significant brightness changes and makes false negative detections more likely.
- The final touch position changes due to setup variations during the experimental procedure. The given standard deviation is statistically calculated based on all approaches of one set. A standard deviation of zero indicates that the corresponding variance of measured values is less than the step-width during the automated approach.

In conclusion, it can be stated that the touch detection from brightness method allows an automated detection of touching events during the assembly of two objects inside the SEM. Hence, it provides a powerful technique for deriving crucial information for the assembly process out of the SEM's distortion effects.

Touch Detection from Image Shift

The surface potential affects the electron beam, not only by retarding the electron's landing energy but also in terms of deflecting the electron's optical path. The surface charge of a sample induces an electric field in its vicinity. The electron beam of the

Table 4.4 Automated touch detection using different image parameters. The starting position is always a height of 50 µm.

Scan Speed [µs/pxl]	ROI Size [pxl]	Frame-time [µs]	Final Position [µm]	σ [µm]	Time [s]	Success-rate %
0.2	32	205	6.59	0.166	4.17	47
0.6	32	614	6.31	0.125	4.29	100
1.8	32	1843	6.20	0.000	4.37	100
5.4	32	5530	6.13	0.308	5.64	100
16.2	32	16589	6.55	0.150	147.76	100
0.2	64	819	6.40	0.356	4.09	65
0.6	64	2458	6.15	0.198	4.28	95
1.8	64	7373	5.84	0.294	5.45	85
5.4	64	22118	6.56	0.123	9.02	100
0.2	128	3277	6.34	0.092	4.60	90
0.6	128	9830	6.41	0.137	4.81	100
1.8	128	29491	6.70	0.121	9.38	100
5.4	128	88474	6.80	0.000	27.26	100
0.2	256	13107	6.58	0.058	6.07	100
0.6	256	39322	6.60	0.000	11.77	100
1.8	256	117965	6.66	0.190	31.21	83
5.4	256	353894	6.62	0.067	92.69	100
0.2	512	52429	6.38	0.063	16.73	100
0.6	512	157286	6.51	0.107	39.51	100

SEM travels through this electron field and, hence, the electron's impulse vector is subjected to changes. In general, these changes can affect value and direction [52]. More concrete, on non-flat samples, the field-vectors $\vec{E}$ of the electric field are not parallel to the impulse vector of the incident electrons. Hence, the incident electron beam is deflected by the electric field. This deflection appears in the SEM-image as a drift of the point of view. Figure 4.17 sketches characteristic conditions inside the SEM during an assembly sequence. Figure 4.17a is the theoretical situation using a perfectly grounded sample without any surface charge, so before the first electron beam exposure. The incident electron beam hits the sample without any deflection and the optical path is straight. Figure 4.17b shows a typical situation with a charged sample - typical for enduring image acquisition. The electrostatic field deflects the electron. The optical path is curvilinear, which shifts the virtual point of view to the left. However, this shift is stable and static if the conditions don't change. Figure 4.17c depicts the

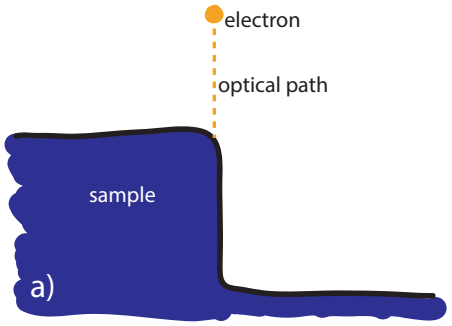

(a) Status for an initially non-exposed and, hence, non-charged sample. There is no generated field and, hence, the optical path is straight.

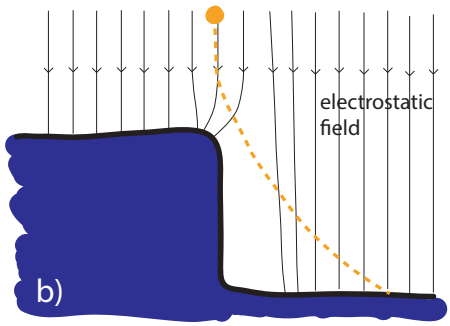

(b) The sample is charged and the electrical field has components that are not parallel to the incident electron impulse: the beam is deflected.

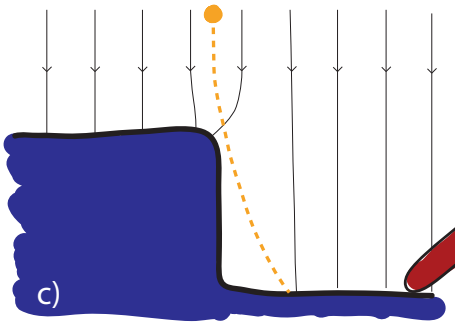

(c) The sample has additional grounding by another probe (red). This reduces the surface charge, the field and, hence, the resulting deflection.

Fig. 4.17 Sketch of the electron beam (yellow) hitting a sample (purple) under different conditions.

same sample touched by another grounding device. In a robotic assembly sequence, this is typically an end-effector carrying an object to be assembled. The additional contact reduces the overall grounding resistance and consequently the surface charge. The deflection of the electron beam is reduced and the virtual point of view shifts to the right in direct comparison to the condition depicted in Figure 4.17b.

The technique to detect a contact between two assembly objects solely relies on two physical effects. Firstly, the *local surface potential* as the fundamental physical effect in the SEM (introduces in Section 3.3.5) and secondly, the image shift by discharge effect, which is a direct consequence of the first. Generally, the local surface potential occurs only in the direct vicinity of the ROI scanned by the electron beam. However, the level of the potential still depends on the grounding of the entire sample. Hence, it can be concluded:

The touch-induced discharge effect can be observed even if the touching end-effector is not in the direct view-field of the ROI.

Evaluation of Touch Detection The working principle to detect the status of an assembly process by discharge observations is evident in theory. However, the predicted effects must be significant in order to be used as feedback signal in practical applications. As described in Section 4.2.1, brightness changes can be expected, but they suffer from other influences such as geometrical shading and, therefore are not universally applicable. In contrary, during an assembly task an image shift induced by the local surface charge does not depend directly on other uncontrollable factors. Hence, using the image shift as touch detection – hereinafter called *depth-from-discharge method* – is more robust. However, the applicability of the depth-from-discharge method depends on its magnitude: The image shift has to be significantly larger than the corresponding position detection uncertainty of the SEM image.

Estimation by FEM The magnitude of the surface charge-induced image shift depends on the entire electrical field in the SEM chamber that can be quite complex. The electrical field, induced by the surface charge within the grounded chamber, is generally inhomogeneous. Furthermore, the electron beam travels around 9 mm from the electron lens to the sample and is exposed to the field along this way. An analytic calculation of the electrostatic field and the resulting beam deflection is impossible due to the complexity of the geometrical conditions of the chamber. However, the finite element method (FEM) allows the calculation of an accurate approximation that takes all geometrical conditions into account. Figure 4.18 shows a scaled sketch of the geometrical condition that is used for the FEM simulation: A conventional 1/2 inch specimen mount stub with a 45°taper made of aluminum (TED PELLA Inc. Prod. No. 16102-9 [105]) is mounted onto the regular stage of the SEM. The stub carries a silicon chip ending with a thin cantilever of 50 µm width and 2 µm thickness (NanoWorld CONT [32]). The distance between the electron gun and the target is 9 mm. Stage, stub, and the entire chamber of the SEM are grounded, while the silicon cantilever is set to a varying potential. As discussed in Section 4.2.1, surface potentials of U_S up to 50 V are realistic but can also be assumed as the upper limit for silicon surfaces. Furthermore, electron beam energies E between 2 and 30 keV are typical for SEM applications.

Results of FEM simulation Figure 4.19 shows the results of the beam shift simulation. The following results are noteworthy and important for the application of the touch by discharge detection:

1. The deflection of the electron beam (and hence the image shift) is in the range of up to 10 µm.
2. The electric field is highly localized and effects the electron only in the direct vicinity of the silicon cantilever. In this simulation, electric field strengths of up to some kV/m are reached.
3. Beam deflection and surface potential are strongly correlated.
4. The beam deflection correlates strongly and negatively with the electron beam's energy.

Outcomes 3 and 4 are already well-known phenomena from the classical cathode ray tube [52] and can be directly calculated in a homogeneous/simple field. However, the dependency of surface charge and beam deflection is still a noteworthy outcome of the simulation. The linearity is typical and can be assumed under the given conditions as long as $E >> U_S$. Outcome 2 is evident and caused by the large number of magnitudes that are involved. All grounding surfaces - mainly the SEM chamber - form a large electrode, while the charged cantilever is about three orders of magnitudes smaller. The most noteworthy outcome is the order of magnitude of the beam deflection: Under the assumed and realistic conditions of object sizes, viewfield, beam energy, and material, it is calculated that the beam deflection is in the micrometer range. A grounded touching end-effector, which reduces the electron beam induced local potential of silicon only by 10 volts, causes a significant beam and image shift. This is at least one order of magnitude larger than the resolution of the SEM.

Depending on the beam energy, the deflection sensitivity is between 40 and 166 nm/V. Assuming a coarse image resolution of 10 nm in the SEM, this leads to the deduction that even very small voltage changes can be detected as significant. It can be concluded:

The touch detection by discharge technique is based on image shifts that are caused by changes of few volts in the local surface potential.

Experimental Validation The FEM-based estimation of the touch detection by discharge technique is confirmed by experimental validations. Exemplary Figure 4.20 shows an experimental setup: A cantilever made of intrinsic silicon is exposed to the electron beam of the SEM. A grounded tungsten end-effector is mounted to a robotic

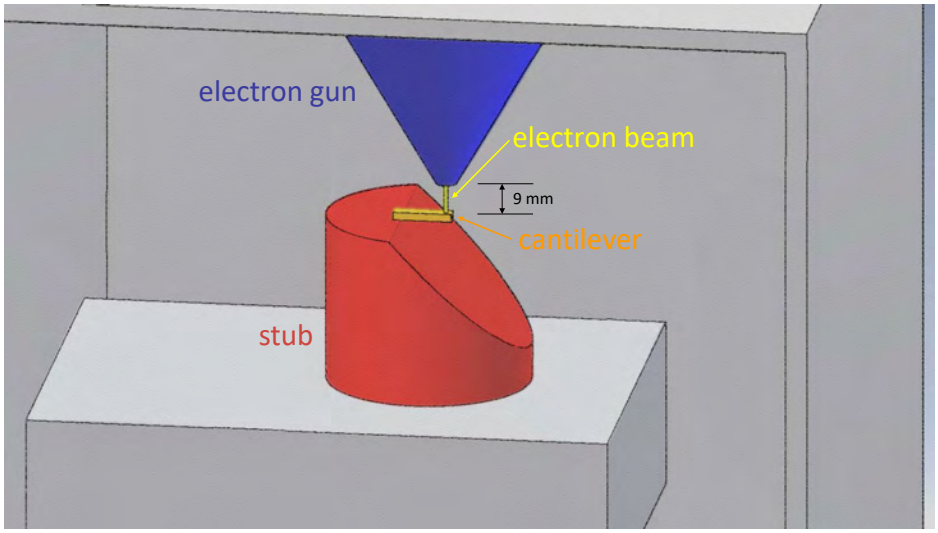

Fig. 4.18 Sketch (not true to scale) of the setup used for the FEM simulation. The cantilever (orange) is 50 µm long, 2 µm thick, and mounted on a 45°stub (red) at 9 mm focal distance to the electron gun (blue). The cantilever is set to different potentials in order to evaluate the electron beam's (yellow) deflection.

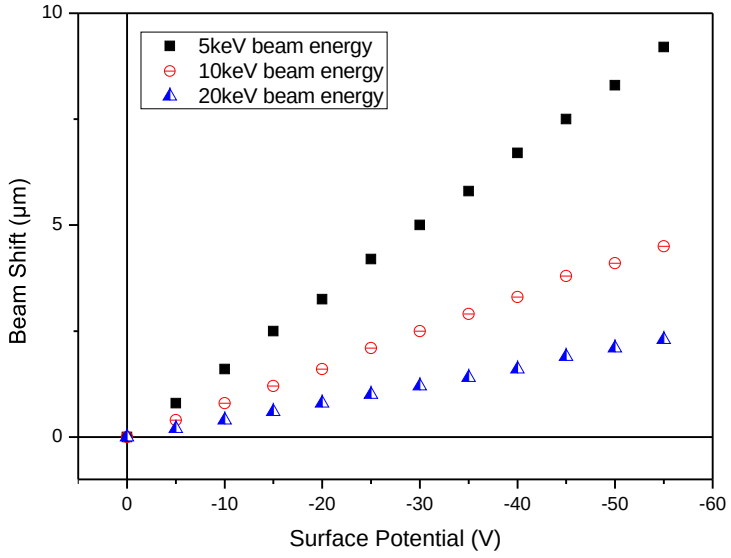

Fig. 4.19 The FEM simulated shift of the incident electron beam induced by different surface potentials for different exemplary electron energies.

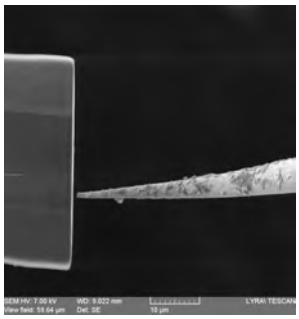

(a) A silicon cantilever (left) is exposed to the electron beam and carries a corresponding surface charge. A grounded end-effector (right) is in close proximity to the cantilever.

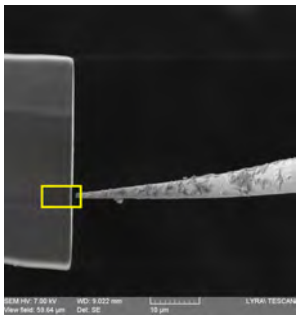

(b) The SEM scanning region is reduced to the yellow square. Consequently, the surface potential increases and the increasing beam deflection appears as an image shift to the left (part outside the yellow box is not updated and just shown as comparison).

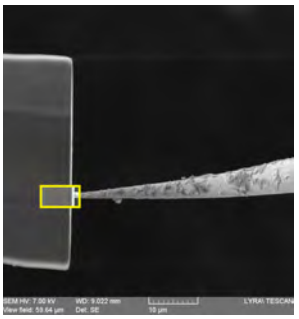

(c) The end-effector touches the sample. Hence, the surface potential decreases, so does the beam deflection, which appears as an image shift to the right. Furthermore, due to the reduced overall grounding resistance, the brightness of the image increases.

Fig. 4.20 Experimental validation setup for the touch detection by discharge approach. If the end-effector touches the cantilever, the image shifts sidewise.

fine-positioning system as described in Section 3.3.3. The edge of the cantilever is detected by image processing (cf. Section 4.3), while the end-effector is brought in contact with the charged surface. Figure 4.20a shows an overview of an exemplary experimental condition. In Figure 4.20b, the image acquisition of the SEM is reduced to a ROI. That increases the surface potential (cf. Section 3.3.5) and causes additional beam deflection to the right, which appears as an image shift to the left. If the end-effector touches the sample, it acts as additional grounding and reduces the surface potential. This leads to a reduction of the beam deflection, which appears as an image shift to the right; shown in Figure 4.20c. The adjusted independent parameters are

- E electron beam energy,
- I_P electron beam current,
- and the position of the end-effector;

while the dependent, monitored or calculated parameters are

- the position of the image and significance of changes,
- the precision of the technique, assessed by measuring the repeatability,
- the needed time and success rate of touch detection by discharge.

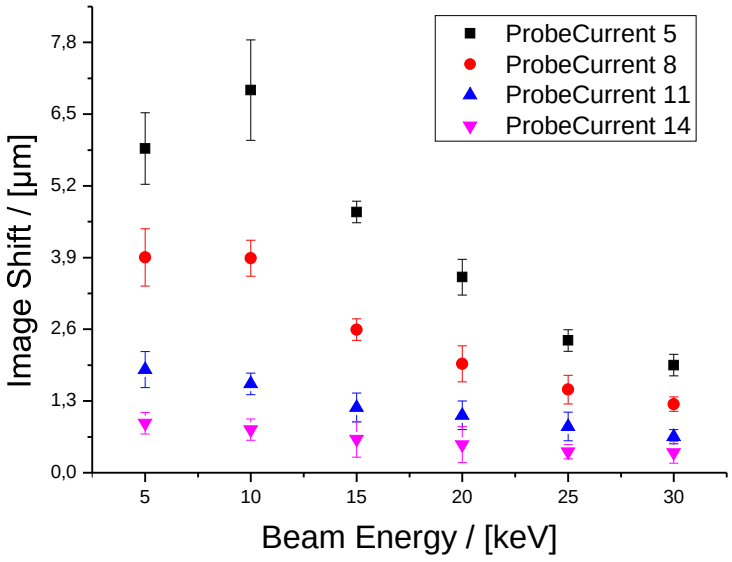

Fig. 4.21 Quantity of the image shift in dependency of the two major SEM parameters beam energy and probe current (smaller value means a higher electron irradiation). The dependency of the probe current is obvious. The inverse dependency on the beam energy is caused by the semiconducting sample, which reaches higher conductivity at higher irradiation energies.

For the image shift technique, template matching is used to track a significant feature of the sample. The position of this feature is monitored by software and significant movements are used as a touch indicator.

Result of Experimental Validation The results of all experimental series with focus on the parameter evaluation are shown in Figure 4.21. The linear dependency of image shift and beam current is evident and comprehensive, since more beam current I_P leads to a high amount of surface charge accumulation Q (cf. Equation (3.1)). On the other hand, the image shifts decrease with larger beam energies E. This is in full accordance to all assumptions above, since an increasing beam energy leads to increased conductivity of the semiconducting sample. Furthermore, the total image shift, which is in the range of $0.3 \ldots 8\,\mu m$, is consistent with the FEM-simulation.

For all sets of parameters, repeatability tests were performed to determine the precision of the technique. The maximal deviation of each set of approaches is used as uncertainty measure. Figure 4.22 shows a histogram of the resulting approach uncertainties. The average maximal miss-detection is about 8.8 nm, while the maximal uncertainty is 20 nm.

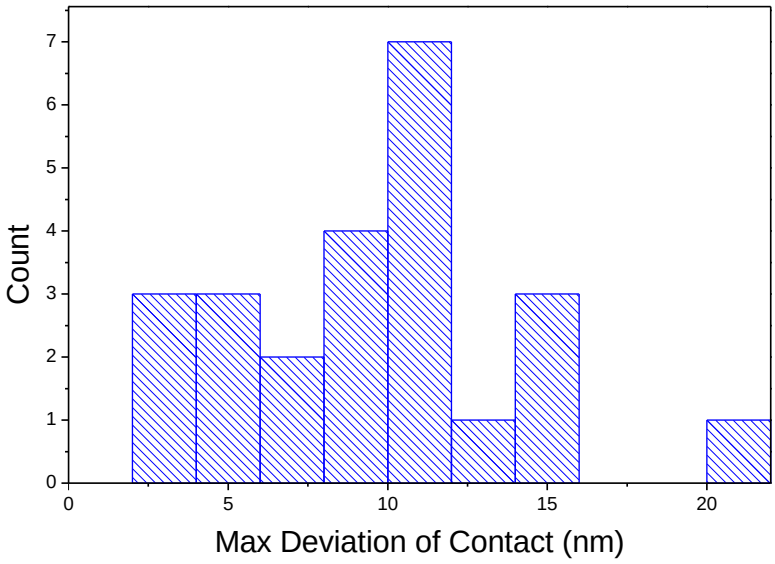

Fig. 4.22 Histogram of the deviation in contact detections for multiple approaches. An average deviation of 9 nm is typical with maximal values of 20 nm.

It can be concluded that the touch detection from image shift offers significant information if an end-effector or a handled object is in contact with a target substrate. This information is essential for integration tasks, where objects have to be integrated into receiving devices. Hence, this method can be used as a feedback method for micro-/nanointegration-tasks [39].

In direct comparison to the tough detection from brightness method, the image shift technique is slightly superior, since higher precision can be achieved. However, it poses more demands on the handling scenario, since clearly traceable markers are needed, which also involve the acquisition of larger images.

4.3 Software and Algorithm Implementations

Image-based data that offers status information on handling or integration scenarios is already based on digital image processing and an exploitation as feedback for automation is possible. The various introduced ways to derive image-based information on 2D-positions, 3D-positions, and assembly statuses all result in digital data streams. If applied in an automated process, these data streams are analyzed and used online by

a lab automation software. In this thesis, the *OFFIS automation framework* (OAF) is used as combined image processing and lab automation framework (cf. Section 3.4).

4.3.1 Image Processing Methods

Preprocessing of the acquired images is part of any image processing chain and consists of few fundamental filters. All SEM images are Gaussian filtered [212] in order to reduce *salt-and-pepper noise* that is especially typical for SEM images [160]. Furthermore, simple *threshold*-filters are applied to images that represent position likelihoods in order to consider only certain detection.

2D Tracking

Three different algorithms for object detection, position detection, and tracking are used in this thesis. They extract only 2D information in the image coordination system, which corresponds to the x/y-plane of the robotic setup. This 2D information has to be further processed to get 3D information or to convert them to meter-based scales.

Template matching Template matching is a standard algorithm for object detection [122]. It needs a template of the object that has to be identified in an image (stream). The template has to be smaller than the image in which it should be identified. The template matching algorithm simply calculates the cross-correlation of template and image for all possible positions that the template can have in this image. The result is a 2D map with values between 0 and 1, representing the correlation of template and image for all these positions. If a maximum with a high value can be identified in the image, the object is detected and its position in the image measured.

BLOB extraction binary large object (BLOB) extraction refers to methods that detect objects in an image that differ from the background - mostly by color or brightness [35]. The BLOB extraction algorithm operates on color or gray-scale images and converts them into a black/white image, where all pixels that fulfill a certain criteria are white, all others are black. Pixels, that are connected, are identified as one object that is labeled. This is how several objects can be identified in an image and properties such as size, center-of-gravity, inertia, and contours can be calculated subsequently. However, a prerequisite for BLOB extraction is a significant visual difference between the objects of interest and the background.

Line-scans In order to identify the edges of objects precisely, simple line-scan approaches can be used. Here, an object is characterized in an image line-by-line in order to identify the position with the largest elongation of the object.

3D Tracking and Detection

A single conventional camera system offers only 2D information and the third dimension has to be acquired using an additional system or has to be reconstructed from additional information. Only few methods exist for the acquisition or derivation of 3D information in SEM applications, since additional measuring systems are hardly implementable. Five examples are:

Depth-from-focus Relative depth differences of objects can be measured by varying the focal length of the SEMs objective lens. The gray-scale variance of the image is typically used as a measure of sharpness. However, due to the large depth of field of the SEM [160], this depth estimation has uncertainties of between several dozen micrometers [63, 64] and still few micrometers under optimized conditions [131].

It is noteworthy that the depth-from-focus method can be improved by further considerations of the physical image acquisition process. Due to the electron beam's Gaussian shape, the sharpness of the image is also Gaussian distributed around the focal plane. If the acquired sharpness values are used to calculate a Gaussian curve fit, the uncertainty can be reduced from about a micrometer to about 50 nanometer [77].

Stereo vision Stereo vision is a standard approach in conventional robotics to acquire the 3D information of a scenario. It can be applied to the micro-/nanoscale by using two or more beam sources or - more practically - two or more virtual beam sources. This can be achieved by using different optical paths of the electron beam which results in different incident angles. The two resulting images are separated in patches, whose position in the image are compared based on correlation. The result is a disparity map that represents the depth estimation. However, due to the working principle and the geometric conditions, the vergence is typically less than 10°and also depends on the magnification. Hence, this method is applicable for rather large height variances and has uncertainties of at least 0.5 µm [163].

Active triangulation Active triangulation is a common method in conventional robotics. It uses special light sources to project known lines, grids, or patterns on a scenery

from a different perspective than the observation perspective. The visible deviations from the original pattern are used to calculate 3D information [107]. Due to the different working principle of an SEM, a different electron detector appears as a different light source. This can be used to reconstruct 3D information with a resolution down to the nanometer scale [185, 173]. However, these methods either need samples that have observable and significantly different shading from each other, which does not apply to end-effectors several micrometers above a surface [185]; or they have a large instrumental effort [173].

Depth-from-focus is a method that is used by any operator doing teleoperated handling inside the SEM. Stereo vision is also used for teleoperated handling by using the FIB as the second image source.

Two more methods are used in this thesis based on the SEM specific effects (cf. Section 4.2.1).

Depth-from-shadow Depth-from-shadow uses the fact that a grounded object catches secondary electron from another object in its vicinity that cannot enter the SEMs detector anymore. Hence, a shading effect is observable in the SEM. This can be used as a detection method in order to measure if two objects are very close to each other - especially at the same height. The shading is detected by measuring the average gray-scale of the observed objects [198, 75].

Depth-from-discharge The last method uses the changing surface charge of samples when they are touched by an end-effector, which can cause brightness changes and image shifts (cf. sections 4.2.1 and 4.2.1). This can be directly used as touch detection sensing principle. The used algorithms simply have to detect rapid brightness changes of the sample. If the resulting image shift is used for touch detection, a rapid change of image positions has to be detected by the algorithm. This can be done by tracking any significant spot of the sample by template matching [69, 42]. It is noteworthy, that this tracked spot itself does not have to be of interest. It works as detection reference for the depth-from-discharge effect only - the spot has to be on the same sample and in the vicinity of an assembly target.

In summary, some concepts of conventional image processing are applicable to the tasks in micro-/nanointegration. The same algorithms can be used to derive information, but they are mostly applied to get different final information.

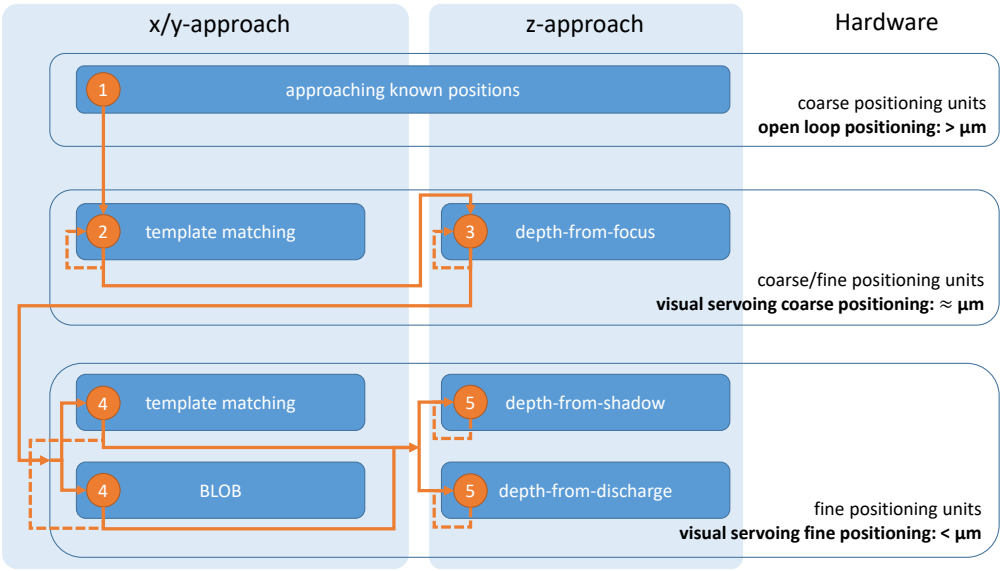

Fig. 4.23 Schematic sketch of an automation sequence on the micro-/nanoscale. Blue boxes indicate used algorithms, light blue boxes spacial movements, and orange circles indicate the order of the sequence. The first principle is that the used algorithms, as well as the used hardware units, start from coarse and get finer successively. The second principle is that x/y- and z-alignments are performed successively as well. Iterations with different parameters are optional.

4.3.2 Automated Handling Processes on the Micro-/nanoscale

The developed handling sequences, as well as their automation, all follow the same design concepts. Part of the initialization of the robotic and visual system is a calibration of all robotic axes. An actual automation sequence (without initialization) is depicted in Figure 4.23. Three fundamental design principles are applied: Firstly, coarse and fine positioning steps are performed in this order with the corresponding hardware axes (cf. Section 3.3.3). However, even in coarse alignment steps, it has to be considered that some types of axes (e.g. slip-stick) induce major vibrations that can destroy sample and end-effector if they are in some micrometers distance. Secondly, large positioning steps are performed before fine positioning steps. The coarser steps are in the range between several centimeters and few micrometers. Step-sizes are estimated from rather uncertain algorithms and safety clearances are applied - or even previously known positions can be addressed without feedback. Then, iterative fine positioning steps are performed using visual servoing based on more precise algorithms. Thirdly, all handling sequences are performed on the x/y-plane first and finished in the z-direction.

Depending on the actual scenario, x/y and z-alignment steps, as well as coarse/fine positioning steps can be performed iteratively, consecutively, or alternately.

Initialization

The initialization of the entire setup establishes the connections between all RC-units and the microscope. If necessary, the robotic axes are set to their zero-position. The SEM is set to all its initial parameters such as viewfield/magnification, scan-speed, resolution, and brightness/contrast.

A calibration is performed to map the robots' coordinate systems to the visual coordinate system that is based on orthogonal base vectors. Figure 4.24 shows the coarse positioning robot's coordinate system xyz_G, the fine positioning robot's coordinate system xyz_F, and their projections in the image plane. Due to imperfections in the mechanical setup, the coordinate systems are not collinear. The calibration however, allows to engage feed forward control of the robotic steps by means of visual servoing. Hence, all automation calculations can be performed in a Cartesian coordinate system and a simple transformation matrix for conversion. Since all handling steps in the x/y-plane are performed subsequently to steps in the z-direction in all sequences, 2D transformation matrices are sufficient in the demonstrated applications. Hence, a set of i transformation matrices T_i with $\vec{p}_{GI,FI} = T_{G,F}\vec{p}_{G,F}$ is needed where i equals the number of independent robotic axes systems.

Furthermore, a correction vector is needed for accurate z-positioning steps, due to the fact that all robotic z-axes are not perfectly aligned with the optical axis of the microscope. Hence, movement in the z-direction of a robotic axis causes movements in the x/y-image-plane. All needed correction factors are determined by calibration during the initialization as well. A defined movement along the z-axis is performed, while a significant marker on the sample/end-effector is tracked by template matching during this movement.

Automated x/y-Approach

The automation of alignment operations on the x/y-plane uses methods as developed in Section 4.2.1 and algorithms as introduced in Section 4.3.1. The overall design approach follows the two concepts of *center-and-zoom* steps and *detect-and-approach* steps:

Center-and-zoom steps Center-and-zoom steps are performed if several orders of magnitude in magnification have to be covered while visual servoing is needed. First, all objects of interest are placed close to the center of the visual image. Secondly, the

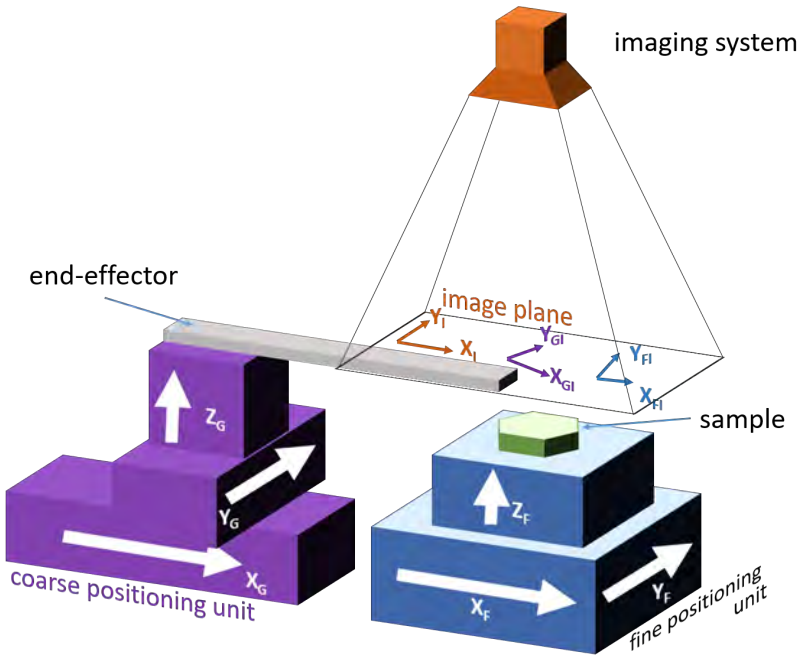

Fig. 4.24 Sketch of a robotic system using one coarse (purple) and one fine (blue) positioning system. The setup is mounted in a microscope (orange) that delivers a top view (e.g. an SEM). All three components have their own Cartesian coordinate system, but they are all not collinear, due to mechanical imperfection.

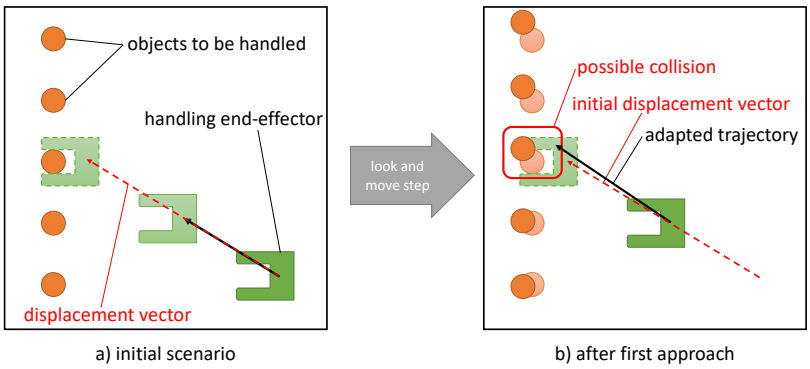

Fig. 4.25 Principle of detect-and-approach steps in a handling scenario in an SEM imaging system. The initial scenario (left) and the scenario after moving the end-effector (right) show different detected positions for the targeted objects, due to the beam-sample interaction. The initial trajectory corresponds to the measured displacement in the initial image, but is adjusted after a first intermediate step to avoid possible collisions.

magnification is increased enough to allow the identification of all objects. This kind of sequence is especially suitable for SEM based automation, since this instrument allows step-less zoom changes.

Detect-and-approach steps Detect-and-approach steps refer to the principle idea of visual servoing. However, as introduced in Section 4.2, all geometrical conditions and objects can interact with the imaging system of the SEM. Hence, detect-and-approach steps are performed iteratively until experimentally determined accuracy is achieved, which depends on the task. Figure 4.25 shows the principle of detect-and-approach steps with the example of a gripper picking a sphere. Firstly, the gripper and a target sphere are detected and their corresponding positions $\vec{p}_{gripper}$ and $\vec{p}_{sphere}$ are determined in the image. Secondly, the displacement vector $\vec{d} = \vec{p}_{sphere} - \vec{p}_{gripper}$ in the image is calculated. Thirdly, the image-based displacement vector is converted to a vector in the robotic axis coordinate system by $d_{G,F} = T^{-1}d$. But due to the assumable image distortions, this displacement vector is not used as trajectory directly. Rather an intermediate step is performed and the next displacement is determined on the new image. This sequence is performed iteratively and the trajectory is adjusted during each circle.

Object detection and position extraction All object detection tasks are performed exclusively with template matching, while their tracking is performed with template matching, line-scans, and BLOB extraction (cf. Section 4.3.1). Template matching is

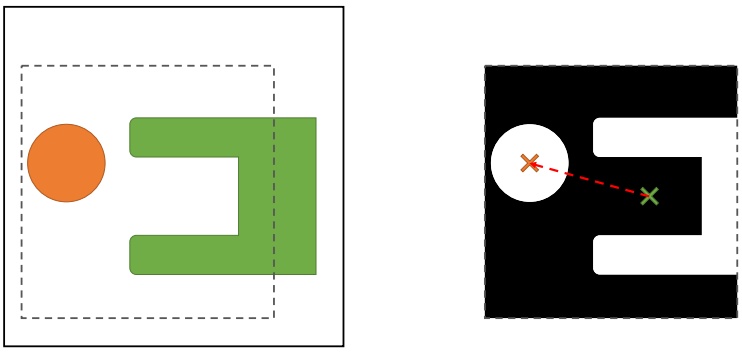

Fig. 4.26 Principle of BLOB extraction and tracking for visual servoing. a) Objects of interest are identified by template matching. A smaller ROI is acquired covering these objects. b) The BLOB extraction is applied to the RIO-image. The extracted objects and their corresponding center-of-mass (cross) is used for visual servoing operations.

used for coarser alignment tasks, where several pixels uncertainty are acceptable. For higher accuracy - especially in precise alignment tasks - BLOB extraction and tracking is used. However, BLOB extraction is used to detect and track the positions only after the identification by template matching. Figure 4.26 shows the schematic principle of this method: The objects of interest and their positions are identified in an overview image. A ROI covering the interesting objects is used for the BLOB extraction. One of the results of this extraction is the center-of-gravity, which represents the mechanical center for symetric objects. By using visual servoing and a detect-and-approach step, an alignment of the two objects can be achieved efficiently.

Automated z-Approach

The automation of alignment operations in the z-direction uses methods as developed in Section 4.2.1 and algorithms as introduced in Section 4.3.1. All steps in the z-direction are performed with simultaneous movements on the x/y-plane calculated by the correction vectors mentioned above. Hence, unintended movements on the image-plane can be compensated. This is crucial, since some fine detection methods for z-approaches rely on image changes in x/y-directions. Furthermore, the alignment in the x/y-projection is already performed and should not be changed anymore.

The z-alignment is performed until image processing detects a change of a monitored parameter, e.g. a brightness change or an image shift (cf. Sections 4.2.1 and 4.2.1).

4.4 Conclusions

The complexity and automation capability of a nanohandling strategy are interdependent. Automation becomes more challenging with the increasing complexity of a task and the complexity can only be increased only with automation.

There is a small selection of methods for handling on the nanoscale that have been used and demonstrated previously: Tip-based handling, whether it is with one or two tips, is the most common approach. In most cases, it has been combined with material-assisted handling methods, such as EBID joining or FIB cutting. Gripper-based handling has also been demonstrated successfully for nanomanipulations. However, all these fundamental methods can be improved by structural design of the end-effectors, which has been demonstrated by handling based on surface hierarchies.

Additional to these previously existing techniques, novel developments are presented based on structural design. The joining energy of a placed object can be increased with results in larger durability against mechanical influences. Furthermore, structurally improved end-effectors allow for better control of the DOF, which enables the actual assembly of nanoobjects. A cartridge system concept is the consequent continuation of this approach and, furthermore, expands the possibilities to handle nanoscale building blocks. Additionally, it offes control over more DOF. It also increases the reliability of nanohandling sequences, which is necessary for the automation.

In addition, assembly automation requires 3D information, which has insufficient accuracy when acquired by depth-from-focus and depth-from-shadow methods. Exploitation of the SEM specific charging effects by means of depth-from-discharge allows to gather information about the assembly status with increased accuracy.

A combination of conventional nanohandling methods with structural design and depth-from-discharge feedback enables automation capabilities for the reliable, precise and fast assembly of nanoscale building blocks.

5 Verification by Case Study I: Nanowire Integration

The investigation of nanomaterials as a crucial ongoing task is necessary to understand and use their tremendous potential. Nanowires in general are promising candidates for novel outstanding devices. However, solid and comprehensive knowledge about fundamental physical effects on these materials is still lacking. Since general investigation techniques on the nanoscale –especially multi-physical investigations– remain a challenge, many research depends on specially developed and tailored measuring setups.

Using microelectrical and MEMS-devices as fundamental test-bench is a widely-spread method to investigate nanomaterials (cf. Section 2.4.1). Electrical signals can be applied and monitored, while mechanical changes can be exerted on the sample. A MEMS-device is small enough to fit into many other instruments, which increases the field of investigations even more. These can be other microscopes (e.g. SEM/TEM/AFM), environmental control units (e.g. climate chambers, cryostats), or other environments (e.g. microfluidics). The investigated nanomaterials are either applied to an existing MEMS-device or an electrode structure is applied to a fabricated nanomaterial. In any case, the fabrication of the nanomaterials and the test-bench is not monolytic, which brings about the challenge to integrate a nanoscale component into a microscale device.

The techniques developed in this contribution and introduced in Chapter 4 allow to tackle these challenges successfully and facilitate the integration of nanocomponents – focusing on nanowires in this chapter.

5.1 Introduction & Motivation

A typical instrument for characterizations on the molecular level is the transmission electron microscope. It allows the acquisition of images with resolutions down to 50 picometer [169] and can reveal the crystal orientation of nanoscale samples [159]. In order to investigate more properties than just the nanoscale morphology of a sample and especially dependencies of these properties from the morphology, additional instrumental effort is needed to extend the TEM's abilites.

Traditionally, tensile testing is an established and common method for the mechanical characterization of bulk materials, as the interpretation of the data is simple and only few parameter assumptions are required in comparison to other mechanical tests. However, the tensile test poses high challenges on the nanoscale, since tensile forces down to few nanonewtons and sample strains of few nanometers must be solved. These challenges, which become more distinct when downscaling the samples, require a more delicate design of the test equipment. The technology of micro-electromechanical systems (MEMS) offers promising perspectives for the production of such testing components and also enables in-situ characterization inside the TEM, due to the small footprint of these devices (cf. Section 2.4.1). Here, a test-platform based on conventional MEMS-technology is used that is small enough to fit into an TEM and that can carry a nanowire. It can exert a tensile load to the nanowire while the an electrical current is driven through the wire. However, there is no standard technology to integrate a nanowire into this micro-test-platform.

5.1.1 Particular Challenges and Demands

The multi-physical characterization of nanowires inside the TEM using MEMS-devices needs methods to integrate these nanoscale objects on the microscale of the test-platform. Figure 6.1 shows an scanning electron microscope (SEM)-image of a typical MEMS-device for nanowire characterizations inside the TEM: Two plungers form a 5 µm gap and are equipped with gold electrodes. The electrodes can be used to drive a current through the nanowire during later characterizations. The lower plunger can be actuated by electrostatic comb drives that can be displaced up to several µm when about 100 V are applied [205].

The design of the test-platform dictates certain conditions for the nanowire integration:

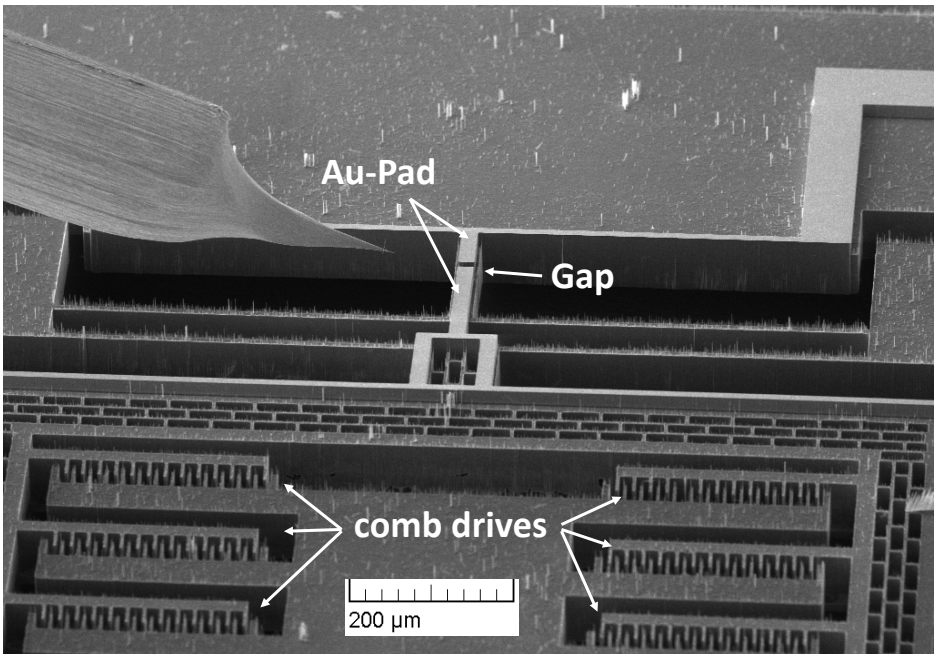

Fig. 5.1 SEM image of a MEMS testbench for multi-physical characterizations of nanowires inside the TEM: the 5 µm gap will be decorated with a nanowire that can be illuminated by the TEM later. The gap is created between two plungers that have gold electrodes to enable a current through the nanowire. The lower plunger can be actuated through the electrostatic comb drives.

Geometrical: The nanowire has to be mounted with its ends on the two plungers. Due to the design of the MEMS-device, the plungers should not be exposed to large forces since they are mounted on small silicon flexure hinges. Hence, the placement strategy of the nanowire has to be delicate and contacts between end-effectors and plungers should generally be avoided.

Connection: The mechanical and electrical connection of the nanowire to the electrodes is of major importance. The electrical connection is needed to drive a current, while the mechanical joining has to withstand the forces during tensile testing. While the electrical connection can be established reliably with electron beam induced depositions (EBIDs), the mechanical connection is much less certain to endure the mechanical stress.

Furthermore, additional conditions for the integration that have to be met when later conducting the experiment in the TEM:

Orientation: The position and orientation of the nanowire has to be well-defined. Even though the lateral position of the nanowire is of minor importance, the orientation of the nanowire is highly important. During the later investigations,

the nanowire should be exposed to a tensile load only and any bending momentum should be avoided. Hence, the nanowire has to be aligned along the actuation direction of the plunger. An alignment accuracy of at least one degree is desirable, which corresponds with a spacial placing accuracy of the nanowire of 88 nm on the plungers.

Stress free: A stress free mounting of the nanowire is desirable, since the morphological structure will be investigated in later experiments. Basically, this is an enhanced condition on the placing requirement.

Finally, the nanowire's preparation form is a general challenge for individual nanohandling and integration tasks: Many nanowires are offered in dilutions. This is not-adaptable for robotic handling and, hence, drying methods are necessary to get access to the wire.

Overall, the integration of nanowire into the MEMS-based tensile test-platform places strong demands on the mechanical accuracy. Due to the nature of fundamental research where this task originates from, speed and throughput requirements are less important.

5.2 Development of Advanced Integration Techniques

A nanowire integration technique is developed based on the fundamentals of i) the nanotip, ii) the material and iii) structural design handling (cf. Chapters 4.1.1-4.1.4).

5.2.1 Handling Setup

The robotic setup is designed with separated coarse- and fine-positioning units as explained in Chapter 3.3.3. The fine-positioning unit is a "Hera P-620" stage from Physikinstrumente (PI) with three linear orthogonal axes, that are equipped with capacitive sensors enabling a closed-loop positioning accuracy of about 1.6 nm. The working range is up to 100 by 100 by 50 μm^3. The system is closed-loop controlled by an analog "E-509" controller, which is fed by the automation-PC via a NationalInstruments AD PCI-card. This system is used to carry the end-effector and to perform all picking and placing tasks.

The coarse-positioning unit is a SmarAct slip-stick system with three linear orthogonal axes, that are equipped with optical encoders enabling a closed-loop positioning accuracy of several nanometers. The full traveling range is 21 by 21 by 21 mm^3. The

system is directly controlled by the automation-PC via USB. Due to large vibrations by the slip-stick actuation principle, this system is used for the manual pre-alignment of all components and for the automated sample exchange during the automation.

The robotic setup is integrated into the vacuum chamber of a conventional SEM. The system at hand is a SEM/FIB dual-beam microscope *Lyra* by Tescan. The electron gun uses a high resolution Schottky-electron-emitter, while the ion beam originates from a gallium liquid metal ion source. Furthermore, a gas injection system is attached, allowing to fed a precursor gas for material-based joining. The precursor gas is feed through a capillary needle and its concentration is regionally dependent. Therefore, the GIS capillary is supported by a simple motorized position stage, which stations the capillary few hundred micrometers close to the sample.

5.2.2 Nanowire Integration Sequence

The fundamental handling sequence is based on material-assisted handling, as introduced in Chapter 4.1.2 and depicted in Figure 4.5, substantiating, the actual integration sequence of the nanowire at hand can be classified into five main sub-tasks:

Picking-up the nanowire A thin tungsten tip is used as end-effector for the material based handling step. The wire is brought into contact with the nanowire on an insulated area, where no other surfaces are in the proximity of this juncture. An electron beam induced deposition is applied at this junction that mechanically joins the tungsten tip and the nanowire. This material-based joining is strong enough to tip up the nanowire from the carrying substrate by overcoming the adhesion forces.

Placing the nanowire The placement of the nanowire is performed by aligning the nanowire above the receiving structure. Secondly, the tungsten tip with the attached nanowire is lowered until the wire touches the target substrate. Receiving trenches in the substrate simplify the correct alignment of the nanowire according to the intended orientation. In respect to the nanowire's source substrate, the target sample is slightly tilted by 20°. Consequently, the nanowire touches the sample with its free end first and stays in the receiving trenches due to the adhesive forces, even if the tip moves sideways.

Joining the nanowire The first end of the nanowire, now laying in the receiving trench, is soldered there using an EBiD spot or line. A further lowering of the tip

places the other end of the wire right above the second receiving trench. Tension on the wire in any direction will be released in the next step that might be applied.

Detaching the nanowire The detachment of the nanowire from the tungsten tip is performed by a short and single FIB line exposure. Possible tensions in the wire, applied by the previous step, will be released since the nanowire is now fixed only on one end. Due to this relaxation, the nanowire touched the second receiving platform. If necessary, the free tungsten tip can now be used to correct the alignment by pushing the free end of the nanowire into its intended position.

Complete joining Finally, the second end of the nanowire can be joined in the trench with a third EBiD spot/line. Additional EBiD lines might be applied to booth junctions in order to increase the mechanical stability and to reduce the electrical contact resistance.

The sequence is performed with distinction in coarse and fine positioning steps (cf. Chapter 4.3.2): Coarse positioning is used to bring the end-effector or the grasped nanowire in proximity to the source or target substrate that is closer than 50 µm. Further approaching movements are executed by the fine positioning unit. The sequence is performed manually by engaging the methods and strategies given Chapter 4.1 and 4.3: xy-alignment tasks are conventionally performed by the operator. Z-alignment steps are performed by the operator as well, however, methods to derive depth information are needed. depth-from-focus is used to estimate the distances between tip/nanowire and substrate for the coarse positioning steps, while depth-from-shadow is performed during fine positioning steps. Xy- and z-positioning steps are performed iteratively, whereby the z-positioning always follows the xy-positioning. Joining step of tip/nanowire and nanowire/substrate are performed under touch detection based on the depth-from-brightness method (cf. Chapter 4.2.1).

5.2.3 Design of Mechanical Components

The concrete nanohandling sequence is based on material-assisted handling as introduced in Chapter 4.1.2 and depicted in Figure 4.5. However, this method is incapable of achieving precise nanowire integrations with determinable orientation. Additionally, the nanowires at hand are prepared as dilution in a liquid agent, which is an issue for the handling sequence. Firstly, if the nanowires were coated or dryed on simple flat surfaces, they could not be lifted by an end-effector since their diameter is in the same range as the end-effectors tip. Secondly, if the end-effector is in close proximity to the

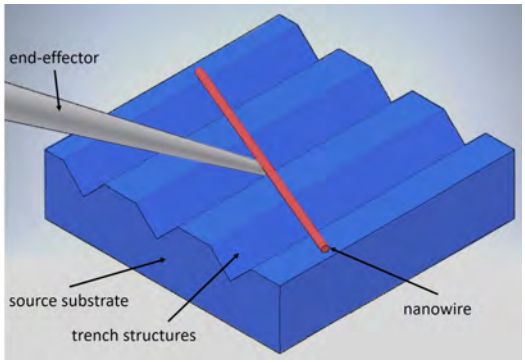

(a) Source substrate carrying nanowires. Small trenches are applied to the surface allowing the handling end-effector to lift the nanowire from underneath.

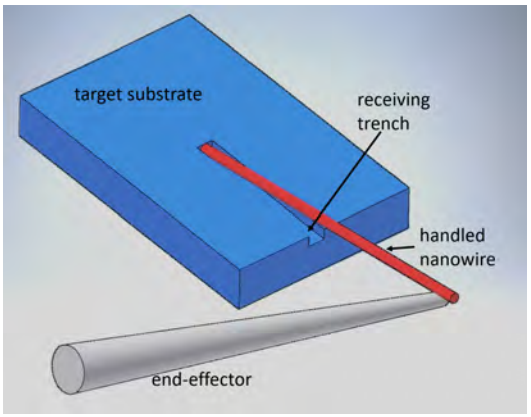

(b) Receiving substrate for the handled nanowires. The small trenches allow an accurate alignment of the nanowire according to an orientation predefined by the trenches.

Fig. 5.2 Structurally designed substrates facilitate handling and integration of nanowires with accurate final orientation.

nanowire and both are in close proximity to any other surface, the material deposition step can join all involved objects - including the carrying surface. And thirdly, full contact between the nanowire and the carrying substrate means large adhesion energy that has to be overcome during the picking step.

A structured substrate as nanowire carrier is used in order to allow lifting by the end-effector and a reduction of the adhesion energy: Figure 5.2a shows a sketch of this substrate, where triangular trenches are applied to the surface. The nanowires are dispensed form the liquid phase.

In order to achieve an integration with an accurate orientation of the nanowire, the target MEMS is structured as depicted in Figure 5.2b. Small receiving trenches are applied to the Au/Si-substrate and increase the interfacial adhesion energy between nanowire and target (cf. Chapter 4.1.5). In this way, the nanowire can maintain the position specified by the trench and withstand further mechanical influences even during subsequent manipulation steps.

5.3 Experimental Validation

The experimental realization is performed according to the sequence introduced in Chapter 5.2.2 and by means of structurally designed components as described in Chapter 5.2.3. Different types and thicknesses of nanowires are handled: Cu, Si, SiC

are used for the majority of the experiments, while the diameters vary between 100 and 300 nm.

Figure 5.3 shows different steps during an exemplate pick-up sequence. The trenched substrate allows the end-effector to lift the nanowire and an EBID junction can be applied without unintentionally joining the substrate. One or two FIB lines are used in order to cut the connected nanowire from the substrate. Depending on the individual situation and geometries, this separation method is necessary or dispensable. In general, for new samples with low electron beam exposure times, it is more likely that nanowires can be picked up without FIB cutting. Samples, that are extensively used and hence suffer from carbon depositions, have a strong substrate-nanowire bonding, which makes additional FIB cutting necessary. After successfully picking the nanowires, the actual sample exchange to the receiving MEMS substrate is executed automatically.

The integration into the MEMS substrate is performed in iterative xy- and z-positioning steps according to Chapter 5.2.2. Figure 5.4 shows a sequence of integration steps. In Figure 5.4a), the first free end of the nanowire is already joined to the target substrate. The inset shows previous stages of misalignment during the sequence. In Figure 5.4b), the nanowire is separated from the end-effector by a FIB line. In this stage, remaining mechanical stress is released. In Figure 5.4c), the second end of the nanowire is joined to the target substrate by EBiD. The particular MEMS sample shown in this figure has been used for several tensile tests that were conducted successively inside the SEM. These test were conducted until the nanowire breaks by tensile stress. For this reason, the sample shows various spots were nanowires had been placed.

5.3.1 Experimental Results

The proposed method of *material-assisted nanowire handling* improved with *structurally designed substrates* is a feasible approach to nanohandling and allows to integrate nanoobjects into existing microstructures. However, the performed integrations are still highly case-dependent: especially the pick-up process suffers from high uncertainties concerning the nanowire's adhesion energy. Furthermore, the orientations of the picked nanowires vary in dependency of the pickup process flow.

The actual integration step also depends on the accuracy of the pickup process, since it can be performed only if the free end of the picked nanowire is lower than the end-effector in the z-direction (in respect to the plane of the MEMS-device). The

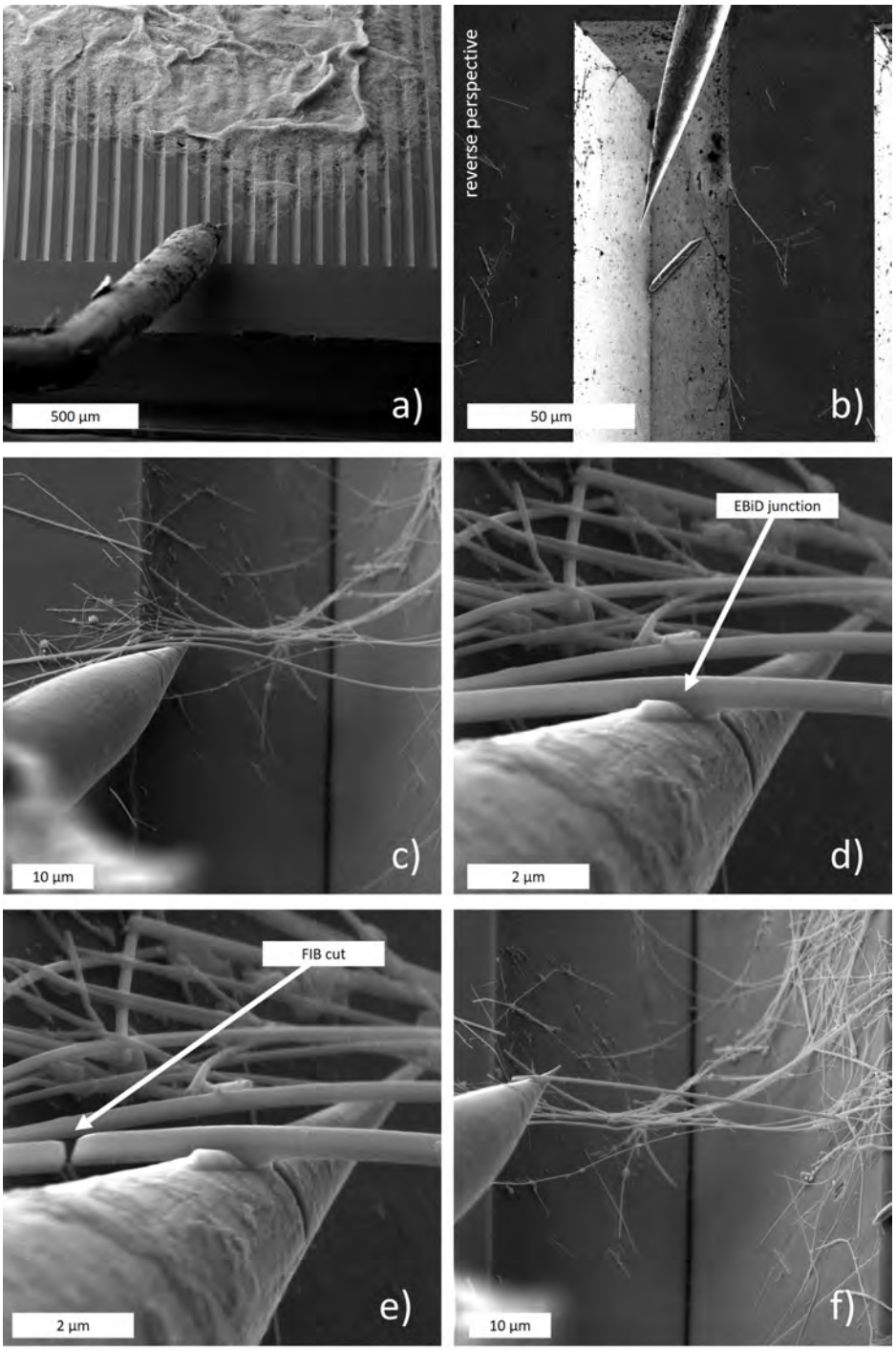

Fig. 5.3 Nanowire pick-up sequence. The trenches in the substrate allow the end-effector to lift the nanowire and prevent unintended EBiD junctions to the substrate. A FIB line is used to cut the nanowire for lift-off.

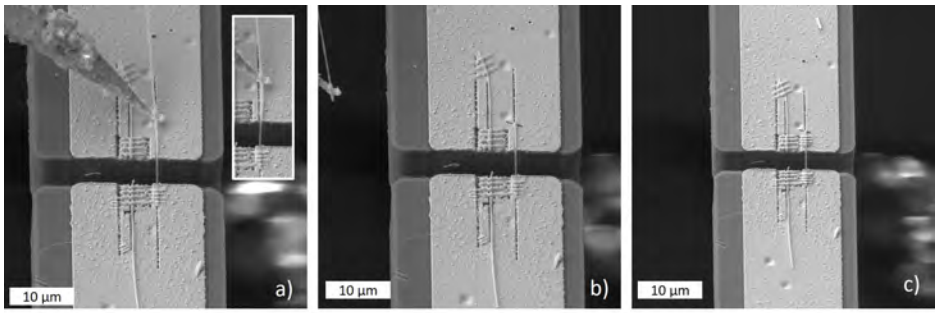

Fig. 5.4 Nanowire integration sequence. The trenches in the receiving substrate allow a precise alignment of the nanowire. a) The free end of the nanowire is already joint to the first MEMS stage, while the end-effector is still used to correct the alignment (compare misalignment in inset). b) A FIB line is used to seperate end-effector and nanowire. c) The second end of the nanowire is joined to the second MEMS stage. Comment: This particular MEMS-device has been used for invasive in-situ measurements and hence carries broken wires.

20° pre-tilting of the MEMS-device increases the chance to meet this geometrical condition.

Particular issues depend on the material that is handled: While conductive nanowires such as copper-nanowire can be handled without any additional effort, other material classes are more challenging: Insulating or semi-conducting nanowires, such as siliciumcarbid- or silicon-nanowires, suffer from a large surface charge by the electron beam (cf. E_2 energies in Chapter 3.3.5). This charging can lead to unintentional bending of the nanowire towards or away from the target substrate. Furthermore, SiC-nanowires are very brittle and break even when small orientation corrections are performed.

The success-rate of the entire handling sequence strongly depends on the particular material, scenario, and operator. For unknown conditions, a success-rates of less than 10% can be expected. After gaining more information about i) adhesion energy, ii) charging properties, and iii) mechanical stiffness, the process parameters can be optimized and the success-rate can increase by more than 50% for a nanowire-integration. The throughput of such an integration task (just integration without preparation such as seeking for a suitable nanowire) also depends on various parameters and varies between 5 and 20 minutes.

However, the main focus of nanowire integration is the exact geometric integration. Figure 5.6 shows eight exemplary integration results. All eight integrations are successfully performed regarding the fact that a nanowire is integrated and joined to the MEMS substrate. Figure 5.5a)-e) show integration results, where receiving trenches

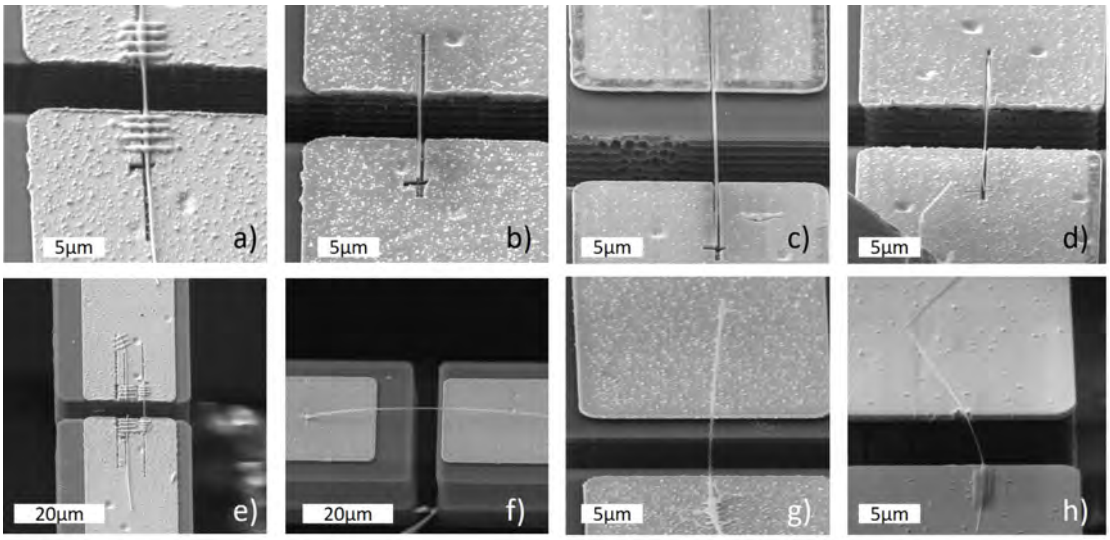

Fig. 5.5 Eight examples of successfully performed integration tasks: In a)-e) receiving trenches were used to align the nanowire, and f)-h) the nanowires are placed on the plain substrate without structured devices.

were used to align the nanowire. Figure 5.5f)-h) show examples in which the nanowires are placed on the plain substrate without structured devices.

A set of 24 successful experiments are used to compare the accuracy of the orientation of the integrated nanowire. The integrations using structural design achieve an average misalignment of $0.78 \pm 0.89°$, while the integrations on plain surface achieve $7.63 \pm 5.53°$. The deviation between these two sets of data are graphically shown in Figure 5.6 and are significant even for this limited amount of quantitative data.

5.4 Conclusions

The integration of the nanowire with orientation demands better than one degree is demanding but possible using conventional handling methods and structural design. However, a overall success is still lacking due to a variety of uncertainties. Therefore, the success depends on the skills of the operator. Hence, this integration technology is not very cost-efficient, since it is still operator-dependent and needs a cost-intensive instrumental effort (SEM with GIS and FIB).

So far, the automation capabilities of this sequence are limited to partly automated subsequences that support the operator making the overall process faster, but a fully automated task would have to be highly adaptable to a plurality of influences and

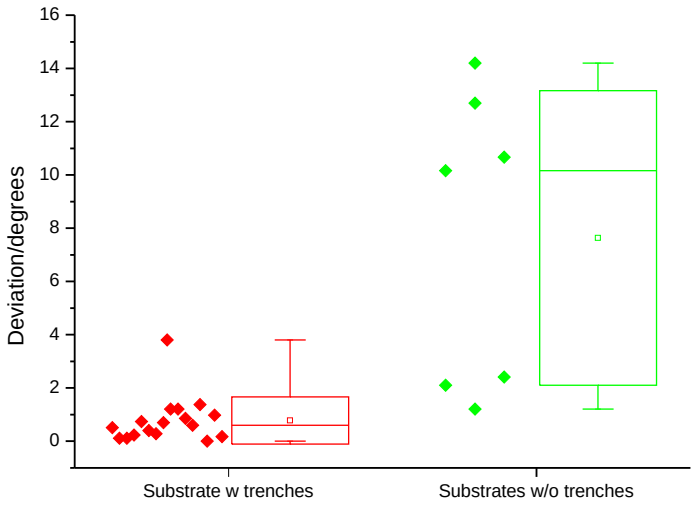

Fig. 5.6 Exemplary deviations of alignment for nanowires that are integrated in MEMS structures with and without receiving trenches.

decisions. Even though all needed instruments, information, and algorithms are available, an extensive effort would have to be invested in order to develop a fully automated sequence for several reasons:

1. The use of the complex and time-consuming joining and cutting methods EBID and focused ion beam (FIB), full automation is challenging, since different imaging perspectives have to be considered and the long-time stability of all steps is necessary.
2. Conventionally, the nanowires are delivered form the bottom-up production as unsorted loose material. This prohibits the use of grippers, which need a defined orientation of the nanowires for further pick-up operations.

Future developments for a high throughput assembly of nanowires should consider sorting or storing nanowires as a previous step.

Overall, the primary goal of this case study – the integration of nanowires into pre-existing MEMS-devices for metaphysical inventions – has been successfully achieved. The nanowires were transferred from a source substrate to the device and integrated into a predefined spot with predefined orientation in one dimension (one other is defined by the surface of the device itself and the second is along the longitudinal axis of the nanowire). Hence, four degrees of freedom (DOF) have been controlled. An average placing accuracy of less than one degree, corresponding to less than 90 nm spacial, has been achieved and facilitated subsequent investigations of nanomaterials: A variety experiments has been conducted in the TEM for different nanowires [40, 38, 204, 205].

6 Verification by Case Study II: NanoBits Assembly

NanoBits are a concept for exchangeable tips in scanning probe microscopy – especially in atomic force microscopy. It is a collaborative research project (no. 257244) in the funding scheme FP7 of the European Union. NanoBits are tiny flakes of few micrometers by around 100 nanometer, which are mounted on specialized cantilever structures. They can be produced with different kinds of lithography and come as batch products. However, before they can be used in a scanning probe microscope, they must be sorted into a cartridge system.

Filling a cartridge with NanoBits is a challenging task. It requires robotic handling with several degrees of freedom (DOF) and spacial precision on the sub-100 nm scale. Furthermore, another fundamental request for this task is a cost-efficient process, since the application is close to industrial application.

Thermoelectric grippers are used to pick, turn, and place each NanoBit. The prototypical cartridge is realized by means of focused ion beam (FIB) milling. By engaging only the advanced techniques for automated assembly (cf. Section 4), a fully automated process for cartridge filling is developed.

6.1 Introduction & Motivation

Today's processes in micro- and nanofabrication include several critical dimension (CD) metrology steps to guarantee the performance of produced devices. Especially in the manufacturing process of novel photonic devices and nanoelectronic circuit architectures, new 3D measuring and visualization techniques for metrology characterization have to be developed. This becomes increasingly challenging as the continuous

down-scaling of all dimensions tends to both require higher lateral resolution, and force the architectures to become more functional in all three dimensions. State-of-the-art for ultra precise metrology is still the atomic force microscope (AFM), which scans surfaces with a sharp tip at the end of a silicon cantilever beam. Since its invention in 1985, the AFM has become one of the most important tools in manufacturing micro- and nano technological devices. Fundamental figures such as surface roughness, precise distance measurements and calibrated topographic images can be acquired by the AFM. Depending on the kind of equipment used, much additional information can be gathered and specialized types of investigations can be performed by the AFM. Mechanical and magnetic information samples can be retrieved by the AFM without any additional instruments. Capacitance, charge, and workfunction can be measured by adding an electrical readout system to a conductive cantilever. In combination with an additional infrared spectroscopy unit, an AFM can be extended to a so called tip-enhanced raman-spectrometer (TERS), which is capable of measuring molecular configurations with the resolution a few nanometer lateral.

However, one of the most challenging aspects of the AFM-technology is to provide scanning probe tips that can probe smaller and smaller structures. Furthermore, due to their constructional conditions and working principles, two major limits of the atomic AFM-technology exist:

1. AFMs can acquire only 2.5D information; and this solely on rather flat surfaces. All acquired information is stored as 2D matrices representing a measured value (e.g. a height z) corresponding to a lateral position (x,y) on the projection of the real surface. As a result, the AFM is only able to measure information that can be represented as image function $z_{img} = f(x,y)$. Measurements producing actual 3D data are represented by functions such as $f(x,y,z) = 0$ are impossible. Hence, objects such as vertical walls, pendant or three dimensional complex structures cannot be measured, as depicted in Figure 6.1.
2. The scanning tip of the AFM is a geometrical object with special dimensions. Typically, AFM-tips have a pyramid shape with a face angle betwen 10° and 30° and, furthermore, the very end of the cantilever's tip has a natural curvature of few nanometers [13, 22, 11, 1]. Every part of the sample that has a larger local slope than these angles, cannot be approached by the tip and hence, cannot be measured at all. Generally, this problem can be described mathematically (cf. Figure 6.1) as follows: A function $z_{real}(x,y)$ describing the actual topology of a sample is measured by a scanning tip with a surface topology $g(x,y)$. Then the acquired

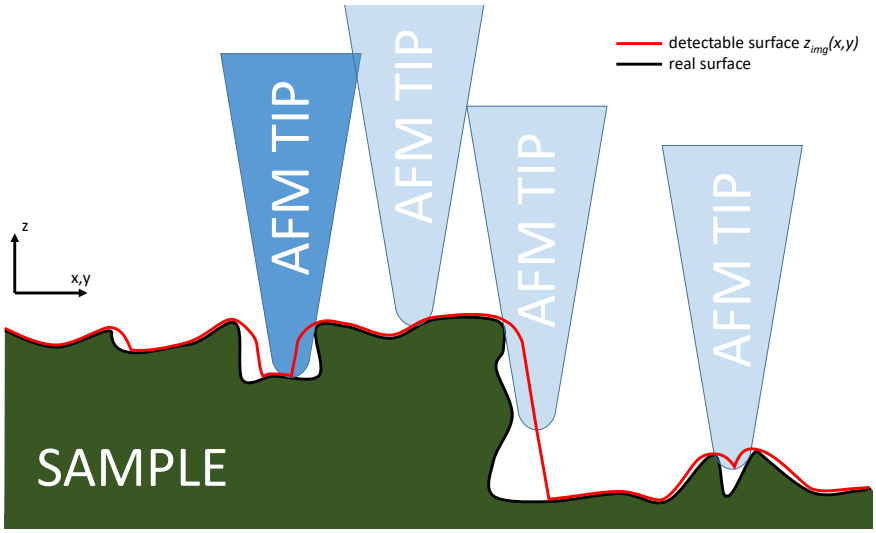

Fig. 6.1 Sketch of an AFM tip scanning a sample's surface (black line). The tip's geometry (conical shape and round apex) cause a distorted resulting image (red line). Vertical walls and fine structures cannot be accessed or resolved with non-ideal tips.

topological image $z_{img}(x,y)$ is determined by the convolution $z_{img}(x,y) = (-g * z_{real})(x,y)$.

The concept of the NanoBits-project is to offer a new class of scanning probe tips that allow not only for improved resolution but also novel AFM scanning techniques. This new approach contributes to more efficient manufacturing of e.g. disruptive nanooptical systems and novel CMOS devices. The NanoBits project uses novel customizable and exchangeable AFM tips and new AFM modes for the 3D characterization of critical dimension structures. The developed technique is especially used in sectors which depend on precise characterization of the morphology of micro- and nanooptical systems, as well as in the field of tip enhanced raman-spectroscopy measurements for nanomaterial and biomedical applications.

6.1.1 NanoBits

NanoBits is a novel concept for AFM probes. Their superiority arises from two major advantages:

Exchangebility The NanoBits-concept is designed to exchange the tip of an AFM cantilever *in-situ* – meaning inside the AFM without having to exchange the cantilever or even open the instrument. Consequently, the investigation of the very same spot of a sample with different specialized AFM modes is made

possible. These different investigations can be performed under preservation of the exact lateral position and orientation. Furthermore, the capability to exchange the scanning tip in-situ reduces measurement time and instrumental costs significantly.

Versatility Since NanoBits can be exchanged easily, each individual NanoBit can be chosen with regard to a very specific task. Furthermore, the production process of NanoBits makes it possible to fabricate them with respect to these specifics, as explained in the upcoming section.

The application of NanoBits as in-situ exchangeable components of the AFM tackles the aforementioned limits of the AFM technology in several ways. Three different types of possible NanoBits-designs are depicted in Figure 6.2 and allow for respective AFM modes:

HAR tips So called *high-aspect-ratio* (HAR) tips are designed to reach even into very narrow trenches of a sample as depicted in Figure 6.2a). They tip curvatures can be as narrow as 2 nm. They are 5 µm long and have a base-diameter of about 250 nm.

Side-Tip These NanoBits have a tip that is deflected by 45°of 90°allowing the cantilever to reach and scan vertical surfaces as depicted in Figure 6.2b). The tilted part is about 560 nm long. The same design can be realized as double-tip or as cross-tip.

Raman-Enhancer The concept of TERS is a scanning tip close to the surface, which leads to an increase of the electromagnetic field. Therefore, Raman measurements can be made using the near-field, which allows a bypass of the optical diffraction limit. Tips with a double-tip configuration are of particular interest, but generally challenging to fabricate. Using the NanoBits-concept, such double-tip configurations can be achieved with little instrumental effort as depicted in Figure 6.2c).

Design and Fabrication

NanoBits are designed according to their application as AFM tips and the necessity of being handled. Each NanoBit has four characteristic parts, which are indicated in Figure 6.3:

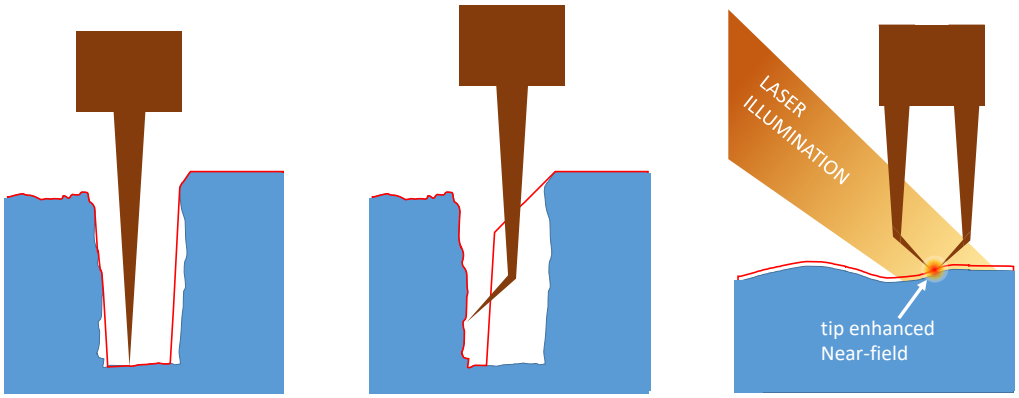

(a) A *high-aspect-ratio* tip scanning horizontal surfaces with narrow but deep trenches.

(b) A side-tip that is capable to acquire measurement on vertical surfaces.

(c) A double tip NanoBit that allows to acquire tip-enhanced raman images images.

Fig. 6.2 Schematic draw of different specialized NanoBits and their application in the AFM. The red lines indicate a reconstructed surface by the AFM.

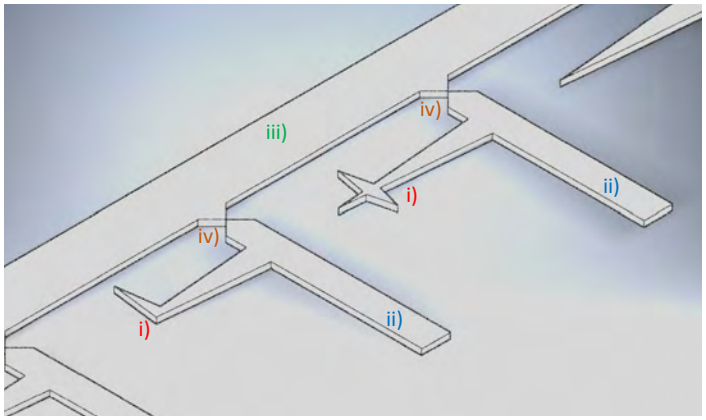

Fig. 6.3 Sketch of a NanoBits-production substrate. Each NanoBit has i) a tip for the actual scanning task and ii) a handle that is used to transfer the NanoBits. Each NanoBit is connected to iii) a carrying substrate by iv) breaking points.

i) Tip The tip of the NanoBit is the most important part due to its application. As mentioned above, different kinds of NanoBits have different geometrical designs. However, the overall dimensions are comparable: maximally 5 µm long and about 1 µm wide.

ii) Handle The handle of a NanoBit has to objectives. It is used during the manipulation to grabf and handle the NanoBit. Additionally, it acts as a support body for the tip to mount the NanoBit on a carrying cantilever. The handle is about 5 µm long and 1 µm wide.

iii) Log The NanoBit is connected to a carrying chip body. The actual dimensions of the log are of minor importance, but it has a narrowing, the predetermined breaking point.

iv) Breaking Point The predetermined breaking point is of high importance for the handling of NanoBits. In order to preserve the tip of a NanoBit, it is not allowed to touch any other object. Hence, NanoBits can not be used as loose building blocks. For this reason, all NanoBits have to remain on the carrying chip until a controlled release is intended. This is realized by a predetermined breaking point, which breaks under mechanical stress and releases the particular NanoBit.

NanoBits are made of rigid material, such as Si, SiO_2, and Si_3N_4 and are fabricated by two different approaches: The *microfabrication* processing based on standard microprocessing techniques. Photolithography as well as electron beam lithography are used to define the pattern for etching and deposition steps. Surface micromachining with e-beam and photoresists is used to define the geometry of the NanoBits as well the the carrying chip [158, 202]. This microfabrication approach allows the production of large quantities of NanoBits (>10.000 pieces) in standard clean-room processes.

In contrast, *focused ion beam milling* is used to cut NanoBits from pre-existing, thin membranes of poly-Silicon. Different techniques for the beam's path-planning can be applied in order to optimize the geometry and fineness of the NanoBit and its tip. This fabrication technique allows the fabrication of individual NanoBits with unique shapes and dimensions and HAR-tips with an aspect-ratio of 50 and tip diameters as small as 9 nm are achievable [168].

Most NanoBits used in this contribution were made with surface micromachining and polycrystalline silicon [202].

6.1.2 NanoBits-Application Scenario inside the AFM

NanoBits themselfes are merely probe tips, they have to be fed to the AFM environment in order to be exchanged on-spot. However, several demands and constraints have to be considered when developing the feeding technique:

1. Each NanoBit has to be mounted to the cantilever my means of an automatable and reliable process in the workspace of the AFM.
2. The concept has to be applicable to any AFM system with little additional instrumental effort, costs or modifications.
3. A further but essential limitation is the extreme mechanical sensitivity of NanoBits.

Considering these demands, the developed application scenario aims for a system that uses almost solely already existing hardware of the AFM. The overall scenario is the application of NanoBits inside the AFM and is illustrated in Figure 6.4. The system is designed to feed NanoBits while assuring physical inviolability and high accuracy. The final concept uses a microscale cartridge system that feeds several NanoBits to the AFM environment (Figure 6.4a). A specially designed cantilever –called plateau cantilever– collects the NanoBits presented by the cartridge (Figure 6.4b). Mechanical clamping is used to keep the NanoBit in a holding trench of the plateau cantilever. Due to the mechanical clamping, the NanoBit remains there during further measurements on the sample (Figure 6.4d). After using the cantilever - still holding the NanoBit- will move to a separation cartridge, which will pull off the NanoBit from the plateau cantilever (Figure 6.4e).

In this application scenario, the cartridge serves two purposes:

1. Each NanoBit is safely stored in a carrying system that defines is orientation.
2. Several NanoBits are collectively stored with well defined geometrical arrangements - possibly even in respect to a reference marker (cf. Figure 6.4a).

6.1.3 Peculiarities of the Assembly Scenario

The introduced application scenario inside the AFM demands a cartridge that is filled with NanoBits. Their resulting challenge of this demand is a filling process for the cartridge, since the NanoBits cannot be fabricated directly there. This filling process is a typical assembly task: Each NanoBit must be picked up from the fabrication substrate, transferred into the cartridge and inserted to it. The single functional requirement in

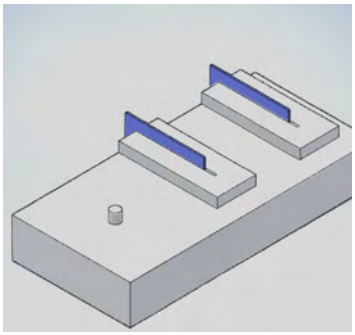

(a) Two NanoBits (blue) resting in a cartridge system. The small spot acts as spatial reference marker.

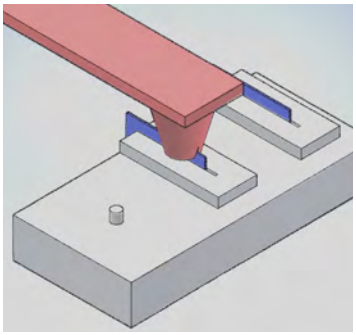

(b) A special cantilever (red) picks one of the NanoBits.

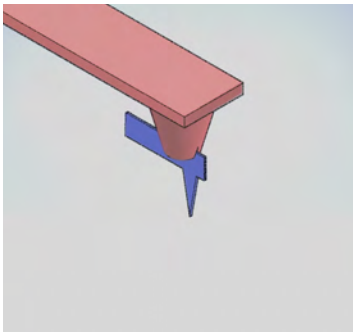

(c) The NanoBit remains in the cantilever due to clamping forces and can be extracted vertically from the cartridge.

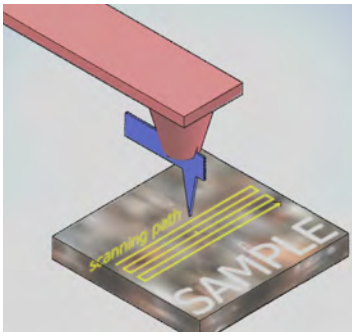

(d) The NanoBit can be used for AFM scans of a sample.

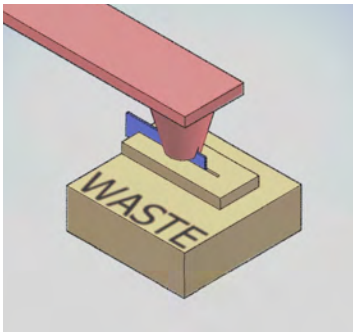

(e) After using the NanoBit, the cantilever places the it in a waste-cartridge system.

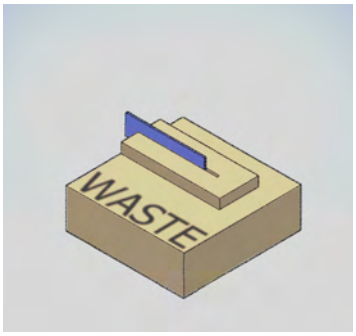

(f) The cantilever can be retracted horizontally. The NanoBit remains in the cartridge due to the structural design.

Fig. 6.4 Usage cylce of NanoBits inside the final application environment - the atomic force microscope. A special tip-less cantilever collects a single NanoBit from the cartridge system, uses it for conventional AFM scanning tasks and can release it in a waste-cartridge system.

this assembly sequence is that the cartridge must be filled with NanoBits. However, several non-functional requirements and peculiarities make this process challenging:

1. Accuracy and repeatability exist, due to the sensitive nature of the NanoBits and the fact that the AFM relies on the accuracy of the filled cartridge.
2. A reasonable throughput is necessary to realize this concept economically.
3. The assembly sequence has to be performed with reasonable costs to be economically viable in the AFM-cantilever market.

The first two requirements have to be met during and throughout the developed process. The last requirement however, is a restriction to the equipment used. Hence, very expensive scanning electron microscopes (SEMs) and complex assembly setups with several end-effectors are excluded. Technically, the entire sequence is intended to work in a low-budget, so-called *Desktop-SEM*, which has limited workroom and sensing capabilities. No cost-intensive additional equipment such as a FIB or gas injection system (GIS) units are necessary. Considering all these requirements and in order to fulfill the demands of the assembly process, a fully automated assembly process is developed. and presented in Section 6.2.

In summary, Figure 6.5 shows all three steps of the final NanoBits concept: fabrication, preparation and application. The fabrication of NanoBits is done with the MEMS technology in clean-room facilities – either by lithography or by FIB milling (cf. Chapter 6.1.1). The assembly of NanoBits into cartridges is done using microgrippers inside the SEM. And the final application is completely inside the AFM using the cartridges filled with NanoBits.

6.2 Development of a Fully Automated Assembly Process

The developments that are needed for a fully automated assembly process of a NanoBits-filled cartridge system consists of specially tailored mechanical components, the exploitation of physical effects, and specialized automation sequences.

Figure 6.6 shows the robotic setup, which is designed with separate coarse- and fine-positioning units as explained in Section 3.3.3: The fine-positioning unit is a "Hera P-620" stage from Physikinstrumente (PI) with three linear orthogonal axes, that are equipped with capacitive sensors enabling a closed-loop positioning accuracy of about

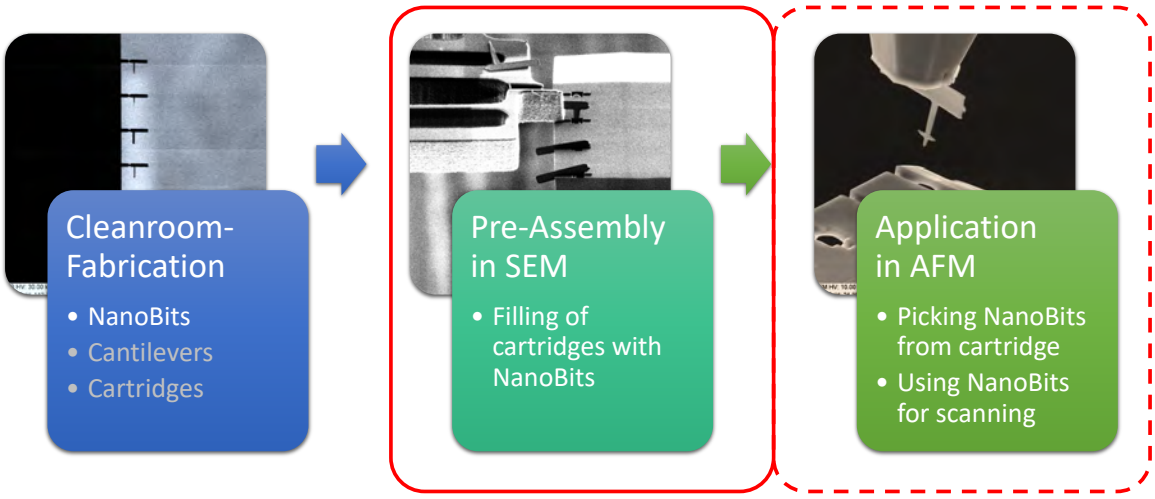

Fig. 6.5 Three preparation steps that are needed for the realization of the NanoBit-concept: 1^{st}: production of NanoBits (and other components) with the MEMS technology in cleanroom, 2^{nd}: assembly of NanoBits into cartridges inside the SEM, 3^{rd}: pickup and usage of NanoBit inside the AFM.

1.6 nm. The working range is up to $100 \times 100 \times 50\,\mu m^3$. The system is closed-loop controlled, by an analog "E-509" controller, which is fed by the automation-PC via a NationalInstruments AD PCI-card. This system is used to carry the gripper and to perform all approaching, gripping, and insertion tasks.

The coarse-positioning unit is a SmarAct slip-stick system with three linear orthogonal axes and a 360° rotatory axis. All are equipped with optical encoders enabling a closed-loop positioning accuracy of several nanometers and microdegrees, respectively. The full traveling range is $21 \times 21 \times 21\,mm^3$. The system is directly controlled by the automation-PC via USB. Due to large vibrations by the slip-stick actuation principle, this system is used for the manual pre-alignment of all components and for the automated sample exchange during the automation.

6.2.1 Design of Mechanical Components

The tailored mechanical design of tools and setup is used in order to facilitate all mechanical handling steps of the fully automated NanoBits-handling sequence. The microgrippers used are mechanically altered in order to control rotational DOF (cf. Section 4.1.6) and the cartridge is fully developed from the scratch in order to fulfill all requirements.

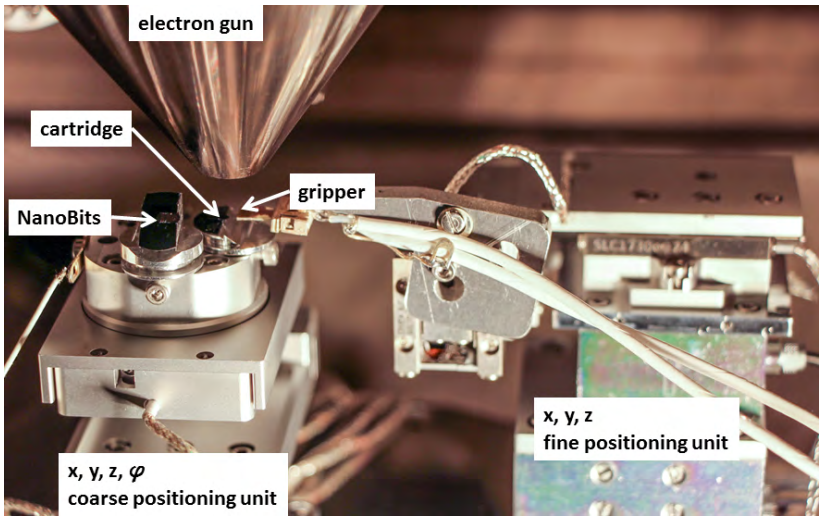

Fig. 6.6 Image of the robotic handling setup inside the SEM chamber. The x,y,z,ϕ-coarse-positioning stage carries both samples: the NanoBits-fabrication substrate and the cartridge. The x,y,z-fine-positioning stage carries the gripper. (Image from [42], ©2014 IEEE)

Gripper

The NanoBits offered are still attached to the carrying production substrate by the predetermined breaking point. This connection has to be separated in order to transfer each NanoBit to the cartridge system. Since the entire assembly sequence is intended to work economically, additional cost-intensive components such as FIB or GIS-systems are excluded and fast-working principles are preferable. Furthermore, the NanoBits are produced as horizontally mounted nanoscale building blocks, while their final orientation in the cartridge system is vertical. Hence, a handling approach based on structurally designed grippers (cf. Section 4.1.6) has been chosen for this task. The gripper and the NanoBits units are mounted rotated by 45°. This leads the gripper to apply an angular momentum to the NanoBit during the gripping process, which results in a rotation. However, caused by its fabrication technique[1] [33], the gripper has initially rough sidewalls that prevent a free-moving turning of the NanoBit inside the gripper jaws. For this reason, the gripper jaws are polished by FIB treatment.

The NanoBits have to be grasped and transferred to the cartridge system by the gripper. Initially, they are still mechanically connected to their fabrication substrate. In order to assess if the angular momentum applied by the gripper is sufficient to fracture the predetermined breaking point, a finite element method simulation of this process has been used. The typical forces of the thermal-electrical grippers are in the range of

[1] here reactive ion etching

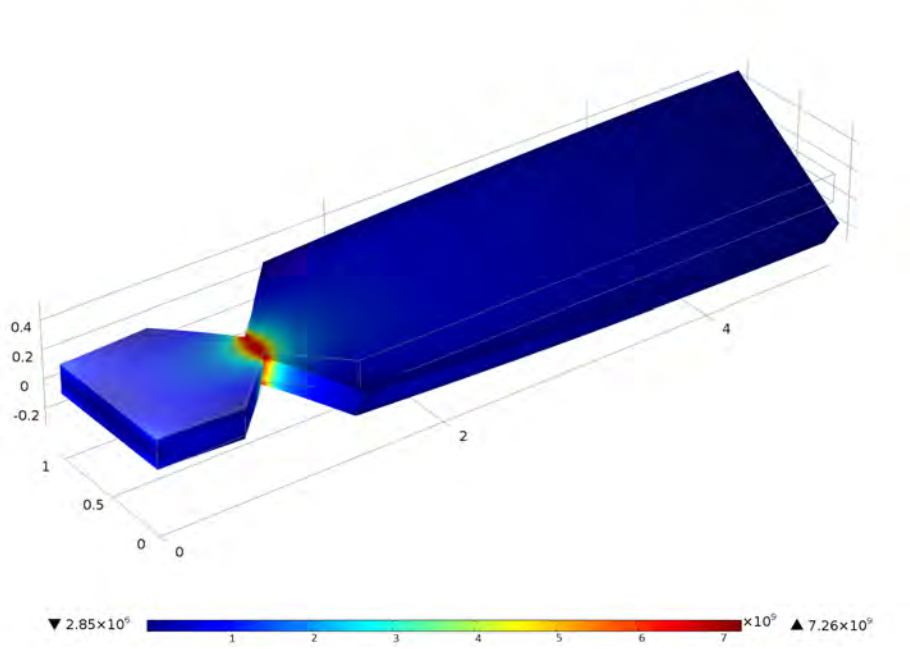

Fig. 6.7 Exemplary result of a finite element method simulation of the stress at the predetermined breaking point during the gripping process. The predetermined breaking point has a width of 200 nm and the stress reaches a peak level of 7.3 GPa.

1 µN to 10 µN [33]. All NanoBits are made of polycrystalline silicon or silicon nitride, which have fracture strengths of about 3 GPa and 6 MPa, respectively [135, 189, 136]. The FEM simulation is performed using a parametric variation of the width, while a gripping force of 1 µN is assumed. Young's modulus, poison ratio, and density in accordance with the COMSOL material library.

Figure 6.7 shows an exemplary result for this simulation: the stress reaches its maximal level at the predetermined breaking point as intend . In the given example with a width of the predetermined breaking point of 200 nm, the stress' peak level is 7.3 GPa, which exceeds the fracture strength of silicon.

A width variation between 200 nm and 800 nm has been performed and the results are shown in Figure 6.8. The result of this simulation is that the predetermined breaking point should be fabricated with width values of less than 400 nm in order to break reliably under mechanical torsion during the gripping process.

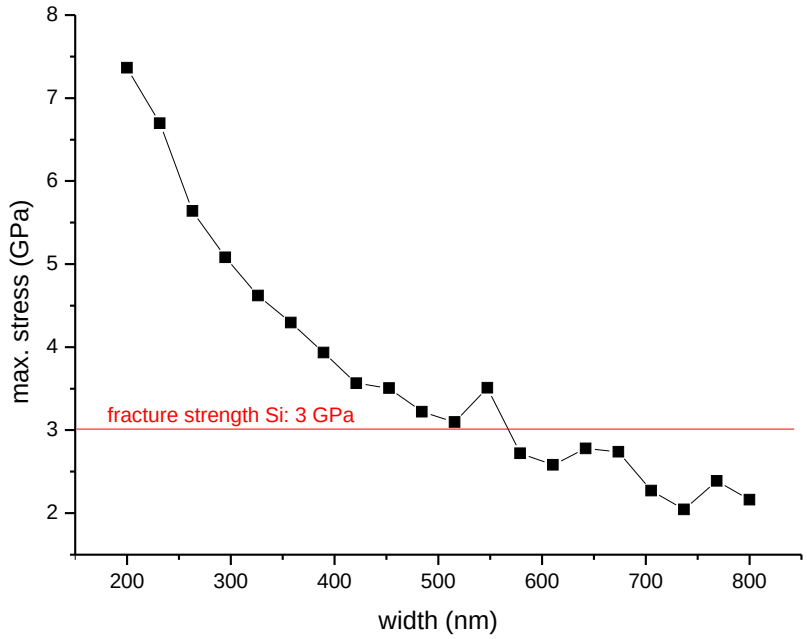

Fig. 6.8 Maximal stress level of the predetermined breaking point of a silicon NanoBit depending on its width. 3 GPa is the expected fracture strength of silicon.

Cartridge

The major purposes of the cartridge – carrying NanoBits i) damage-free and ii) with well-defined positions – can be achieved by a suitable design. A technical sketch of the final cartridge design is shown in Figure 6.9. The entire chip is about 2 x 3 mm^2 in size, with only a small part of it being formed by the actual cartridge. The design shown in Figure 6.9 can carry up to eight NanoBits. A small trench acts as a guiding structure for the inserted NanoBits and ensures the correct orientation during the filling and picking process (cf. Figure 6.9b). The larger aperture in the center enables to insert a NanoBit into the cartridge without touching the sensitive and fragile tip. Additionally, the conical opening on the backside prevents any damage to the tip during the later pick-up process by the cantilever in AFM conditions: The cantilever applies pressure to the NanoBit in order to clamp it. This can cause unintended movements and consequential tilting, which could damage the tip.

The cartridges are made of polycrystalline silicon and are fabricated by FIB-processing from conventional AFM cantilevers as blanks. The process consists of three steps: Firstly, the cantilever structure is milled down to the intended length and fine polished with the FIB in order to achieve sharp edges. Secondly, the backside is structured to fabricate the conical opening of the cavities. Thirdly, the guiding trench and the

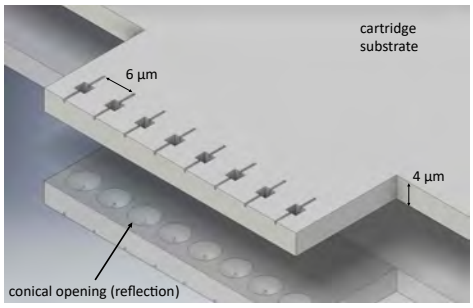

(a) Overview of a cartridge capable of carrying up to eight NanoBits. The conical opening of each cavity is visible in the reflection.

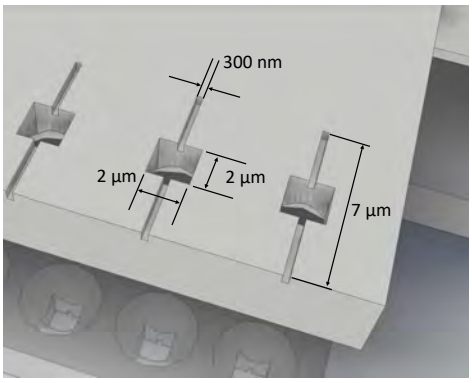

(b) Close-up of the cartridge's cavities and their dimension. The small gap guarantees the alignment of the NanoBits, while the large aperture and the conical backside opening preserves the NanoBit's tip during the assembly.

Fig. 6.9 Technical sketch of the cartridge's design. The overall size of the carrying chip is about 2 x 3 mm^2, while the actual cartridge part is about 50 x 20 μm^2.

larger aperture are fabricated on the topside. A final fabricated cartridge is shown in Figure 6.10.

The cartridge fabrication system at hand is a serial process and time consuming, due to the FIB writing process. Comparable results can be achieved with micromachining as a mass production technique.

6.2.2 Fully Automated Handling Sequence

The developed fully automated handling sequence exploits several SEM typical effects, which are introduced in Chapters 2.1 and 4.2.1, to gather sufficient information on the assembly status. The information of this data is processed using algorithms as introduced in Chapter 4.3.

In the NanoBits handling sequence, all steps are performed with the same SEM configuration: Beam energy, current, viewfield, and focal distance are constant. The only parameters that change during the sequence are i) the positions of the robot platforms, ii) the scanning speed of the SEM and iii) the region of interest (ROI). The latter corresponds with an image update rate between 0.5 Hz (first overview images) and about 10 Hz for small ROI.

Only a few manual preparation steps are required before the automation can take over:

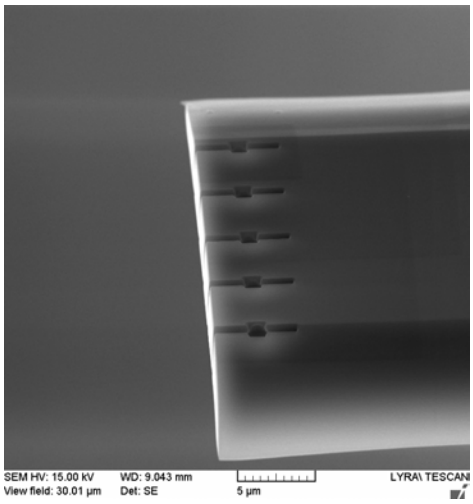

(a) Inclined view of a cartridge that can carry up to five NanoBits.

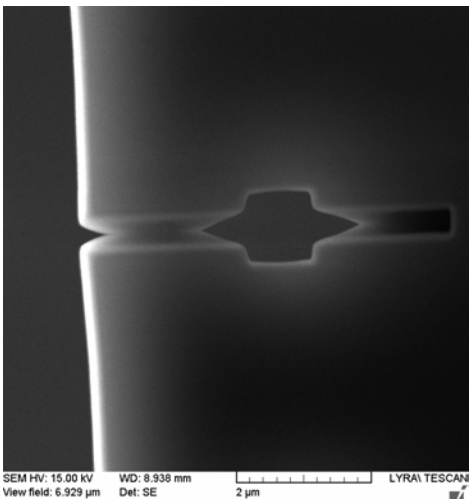

(b) Close-up of one of the cavities.

Fig. 6.10 Scanning electron microscope image of a fabricated cartridge system. Guiding trenches are about 6 µm long and 350 nm wide. The center aperture is about 1 x 1 μm^2.

1. The templates of all objects that will have to be detected: NanoBit, gripper jaws, and the reservoir's cavity
2. Two positions have to be determined and stored in the system: First, a pose of all positioning systems where i) NanoBits and gripper are visible at the intended magnification, while the reservoir and NanoBits have the same alignment and the NanoBits are definitely on a lower z-level than the gripper. Secondly, a position where the reservoir is visible at the left side of the overview image; the grippers uppermost position must be higher than the reservoir.
3. The automation sequence's first step is to move the gripper to a center position, at which the operator has had to center the stage of the SEM.

In general, the overall sequence is developed according to the fundamental process design rules as introduced in Section 4.3.2 and shown in Figure 6.11. The complete cycle of the automation process is represented in the flowchart in Figure 6.12, while details are given in Figures 6.13-6.16

The following conditions and design details are considered:

- Due to the image acquisition constraints for SEM-images introduced in Chapter 4.2, working using an absolute coordination system is not feasible for an accuracy below a few µm (due to drift, charging and beam deflection).

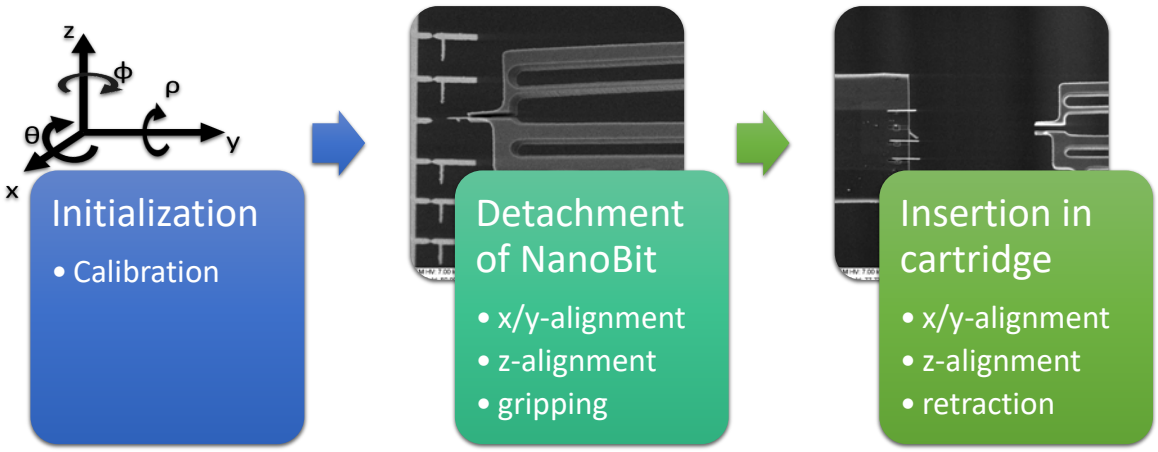

Fig. 6.11 The overall sequence of NanoBit-assembly. After initialization, each the NanoBit is collected from the production substrate and inserted into the cartridge.

- To perform positioning steps that require accuracies better than a few µm, the relative position information of two objects is derived. The relative displacement in an image can be translated into a relative displacement in the global coordination system. This approach is used for all fine positioning steps with an accuracy of a few tens of nanometers.
- The first positioning/alignment step is always performed in the x/y-plane only. This task is based on template matching or BLOB-detection.
- The second positioning/alignment step is performed in the z-direction. depth-from-shadow (cf. Section 4.2) and *touch-detection-from-discharge* (cf. Section 4.2.1) are used to gather sufficient information on the assembly status.

Calibration

The first step is to calibrate the visualization- and robotic system. During calibration, the NanoBits-sample as well as the reservoir is located near the overview part to create comparable conditions for the electron beam. This ensures that the calibration takes equivalent image distortions into account.

First, the gripper is moved to the center position - into the optical axis. Binary large object (BLOB)-detection is used to detect the upper and the lower gripper jaw. From these two objects the gripping point - the point exactly between the gripper jaws, is extracted by calculation of the point between both objects in alignment with the left edge.

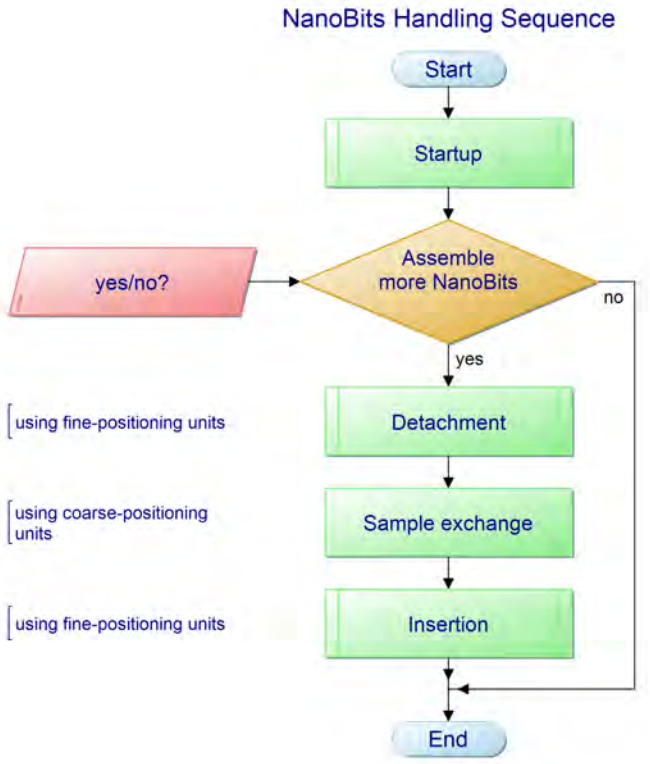

Fig. 6.12 Overview of the overall NanoBits handling sequence as flowchart. Details and sub-sequences are shown in Figures 6.13 and 6.16.

Secondly, the gripper is moved to three different points in the image, while the corresponding positions from the internal positioning sensors of the PI system and in the image are measured. Based on these, a transformation matrix is calculated, which allows the transformation of all positions from the image coordination system to the PI coordination system.

The entire setup is tilted by 5° to preserve sight in the tip of a grasped NanoBit, which would otherwise be exactly aligned to the optical axis and masked by the gripper jaws. Hence, every movement in the z-direction causes cross-dependent movements in the x/y-direction. In order to compensate these movements, the gripper is moved to the maximal and minimal z-position, while its corresponding x/y-positions are determined by template matching. A linear regression is used to calculate the dependency of the x/y-movements on the z-movement. Typical cross-dependencies of y/z-direction are about 100 nm/µm, which correspond to an inclination of 5°(87 nm/µm) and very small alignment uncertainties in the mechanical setup. From this point on, all z-actuations are performed with simultaneous x/y-corrections.

NanoBits-Detachment

The NanoBits-detachment sequence (cf. Figure 6.13) starts with initial conditions and positions: NanoBits and gripper are in view and at opposite ends of the image.

Firstly, NanoBits and gripper are recognized and their positions are determined by template matching. Secondly, the gripper is moved into a 3 µm vicinity of the selected NanoBit using the global coordinate system. With respect to the detected positions of the NanoBit and gripper, a ROI is activated, whose size is calculated in order to cover the gripper jaw's tips and the handle of the NanoBit. BLOB-detection is used to detect all three objects (both jaws and the NanoBit). Visual servoing (look-and-move steps) is performed until an alignment of gripper and NanoBit is achieved.

Thirdly, the depth-from-shadow method is used to align gripper and NanoBit in the z-direction. The gripper moves down in µm-steps until the jaws clearly shadow the handle of the NanoBit, which is indicated by a significant grayscale drop of at least 20 units. The downwards movement is continued until a minimum grayscale is found; the movement is stopped if the grayscale increases to 120% of the maximum grayscale drop. This ensures the detection of an actual minimum. This process is repeated from 3 µm below the determined position with maximum shading. In a second sweeping movement, the gripper is moved upwards in 100 nm steps until an exact minimum value is found; the NanoBit is presumably at the same height as the center of the

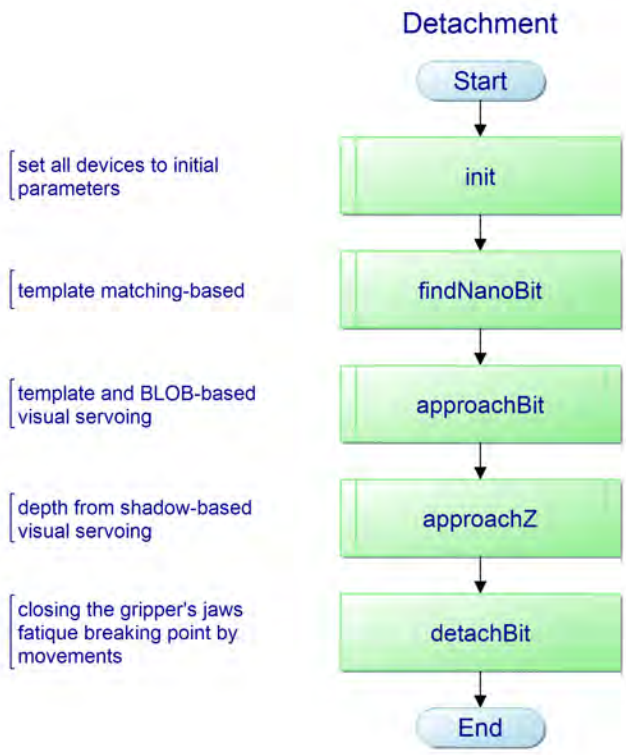

Fig. 6.13 Detachment sequence for a single NanoBit. Subsequences are shown in Figures 6.14 and 6.15.

gripper jaws. For a correct determination of the grayscale-levels, a scan speed of 4 and tenfold averaging are selected. Finally, the gripper is moved up by 1.5 µm to align the NanoBit at the lowest possible position between the jaws.

Fourthly, the gripper is closed and moved 20 times with increasing amplitude in the y-direction to break the predetermined breaking point of the NanoBit. A slight retraction of the gripper by 400 nm is performed during this breaking-movement in order to compensate the thermal expansion of the gripper and to avoid any contact of the freed NanoBit with the substrate.

Finally, the gripper and the grasped NanoBit are retracted.

NanoBit-Insertion

The NanoBit-insertion sequence starts in the overview position and with initial SEM parameters: cartridge, gripper and gripped NanoBit are visible at opposite ends of the

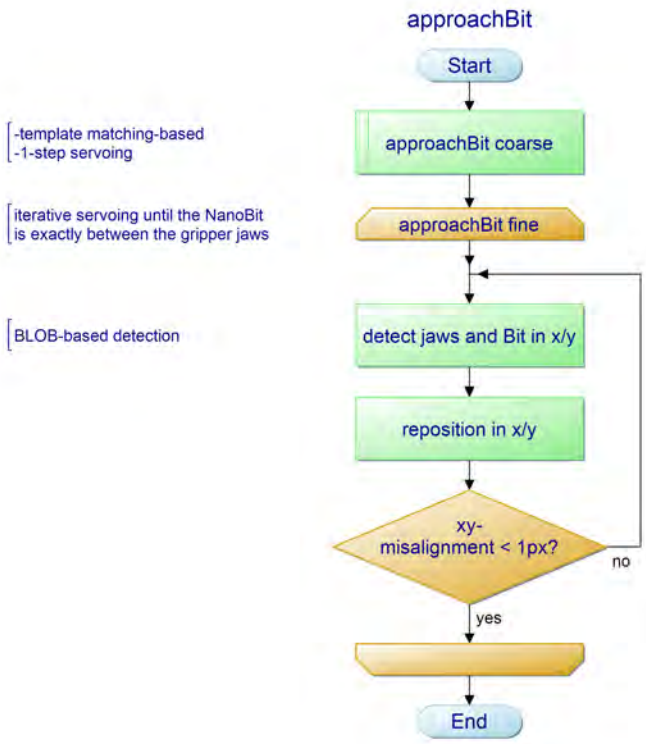

Fig. 6.14 Approach-subsequence in x/y-plane for a NanoBit within the detachment-sequence.

image. The position of the cartridge's cavity that is aimed for insertion is determined by template matching.

First, an individual calibration for the tip of the NanoBit at hand is performed: A ROI on the left of the jaw is scanned line by line to determine the tip of the NanoBit (see Chapter 4.3.2). This achieves a relative x/y-calibration for the NanoBit's tip in relation to the gripper jaws. In parallel, a template of the NanoBit is captured for later purposes.

Second, the NanoBit must be aligned in the x/y-plane hovering above the cartridge. The NanoBit is placed with a 2.5 µm clearance to the detected cavity so that the NanoBit does not mask the sight on the cavity. Using a new ROI, a new determination of the NanoBits tip and the cavity is performed, which is used for another visual servoing step that exactly positions the NanoBit above the cavity.

Third, the actual insertion of the NanoBit is performed based on the depth-from-discharge method. As explained in Chapter 4.1.4, the primary goal during insertion is to avoid any damage to the handled NanoBit. In contrast to the depth detection during the gripping process, contact-detection failures during the insertion process can lead to severe damage to all involved components. For this reason, a high image update rate

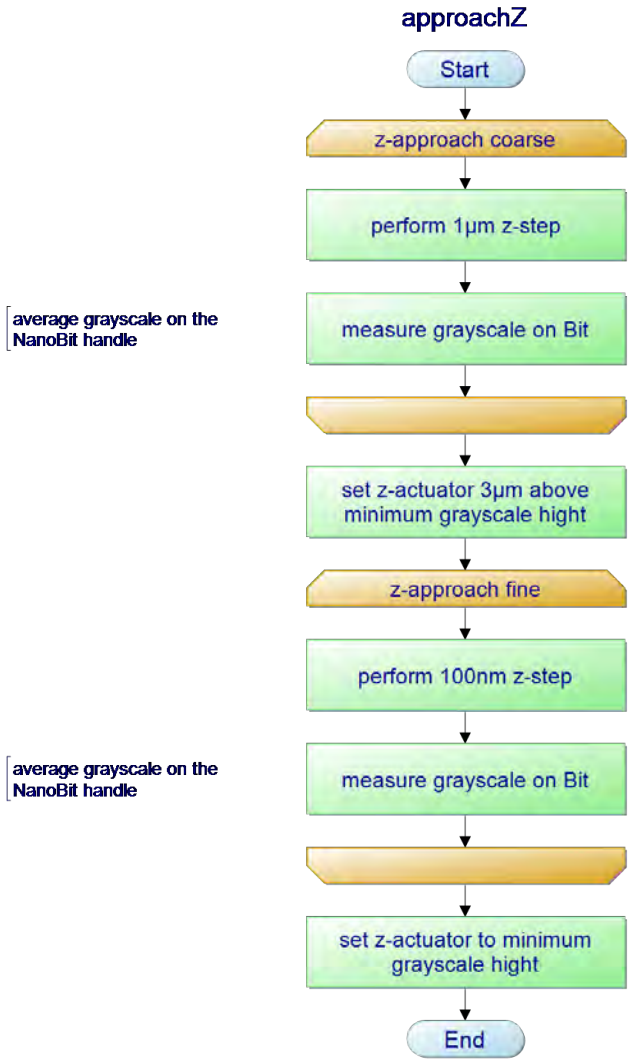

Fig. 6.15 Approach-subsequence in z-direction for a NanoBit within the detachment-sequence.

and small movements are used. A ROI of only a few µm length around the cavity is used to observe the insertion of the NanoBit. The NanoBit is then lowered in 100 nm steps, while the NanoBit's position is monitored by template matching. If the NanoBit or the gripper touches the surface of the cartridge, the resulting discharge leads to a significant shift of the image (cf. Section 4.2.1).

As final step, the gripper is opened and retracted. While opening, only the actuated right gripper jaw moves. The NanoBit moves to the right and touches the cartridge, which limits its movement. The resulting contact area between cartridge and NanoBit is larger than the contact area beween gripper jaw and NanoBit, which allows for the retraction of the gripper without moving the NanoBit (cf. Section 4.1).

6.3 Experimental Validation

The developed automated NanoBit-assembly sequence was tested in over 140 assembly events. Different cartridges and a variety of NanoBit-samples have been used [42].

The constant SEM parameters are 7 kV of beam energy, a probe current of 350 pA, an viewfield of 50 µm, and the focal distance 9 mm. After the first manual adjustments, the sequence works fully automated for one NanoBit. Each additional NanoBit to be handled must be confirmed by the operator.

The Figures 6.17 and 6.18 show exemplary situations and the series of the detachment and insertion step, whose details are explained in the following section.

6.3.1 Experimental Results

The experiments show affirmative results, namely feasibility and reasonable success rates of the fully automated process. An overall average success rate of 80% is achieved for a fully automated sequence that handles about one NanoBit per minute with sub-100 nm accuracy.

However, various steps strongly depend on the quality of the involved microsystem components and the most important part is a well-manufactured predetermined breaking point of the NanoBit.

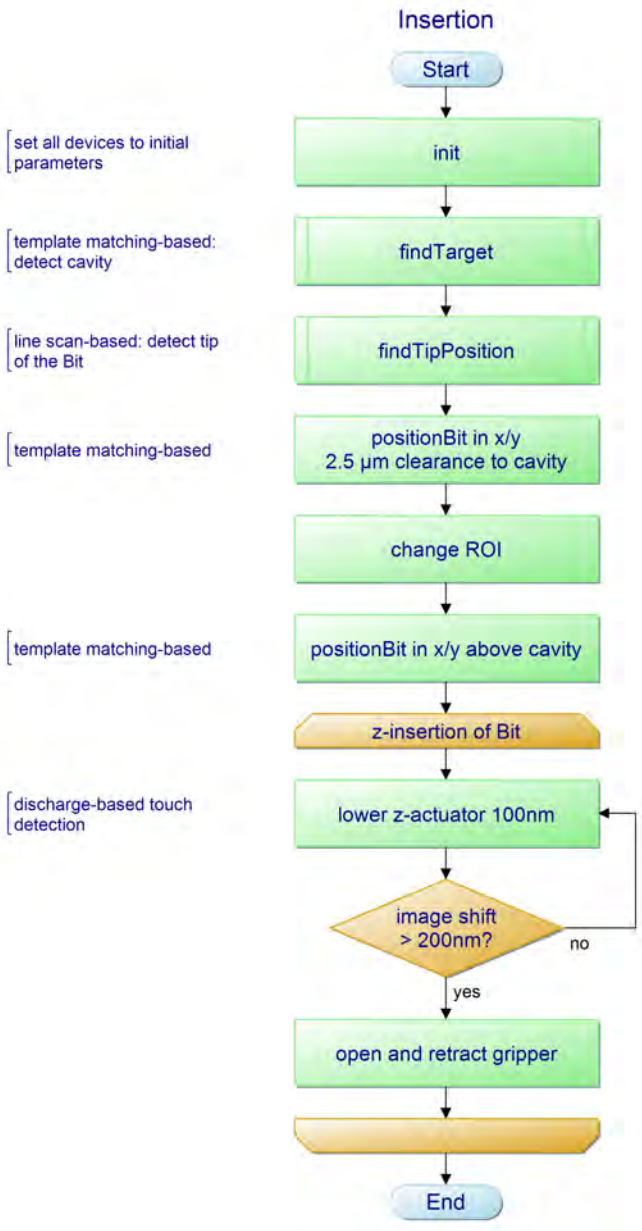

Fig. 6.16 Insertion sequence for a NanoBit.

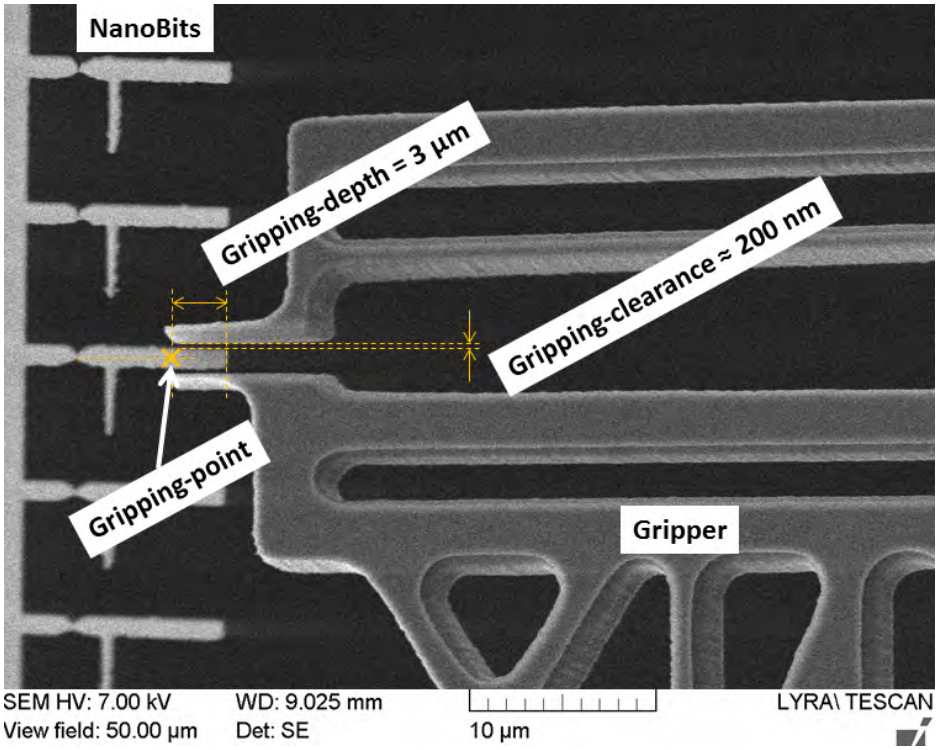

Fig. 6.17 Gripping procedure: gripping point is automatically determined and aligned with the center axis of the NanoBit. Clearance between jaws and NanoBits is about 200 nm. Gripping depth is predetermined with 3 µm. (Image from [42], ©2014 IEEE)

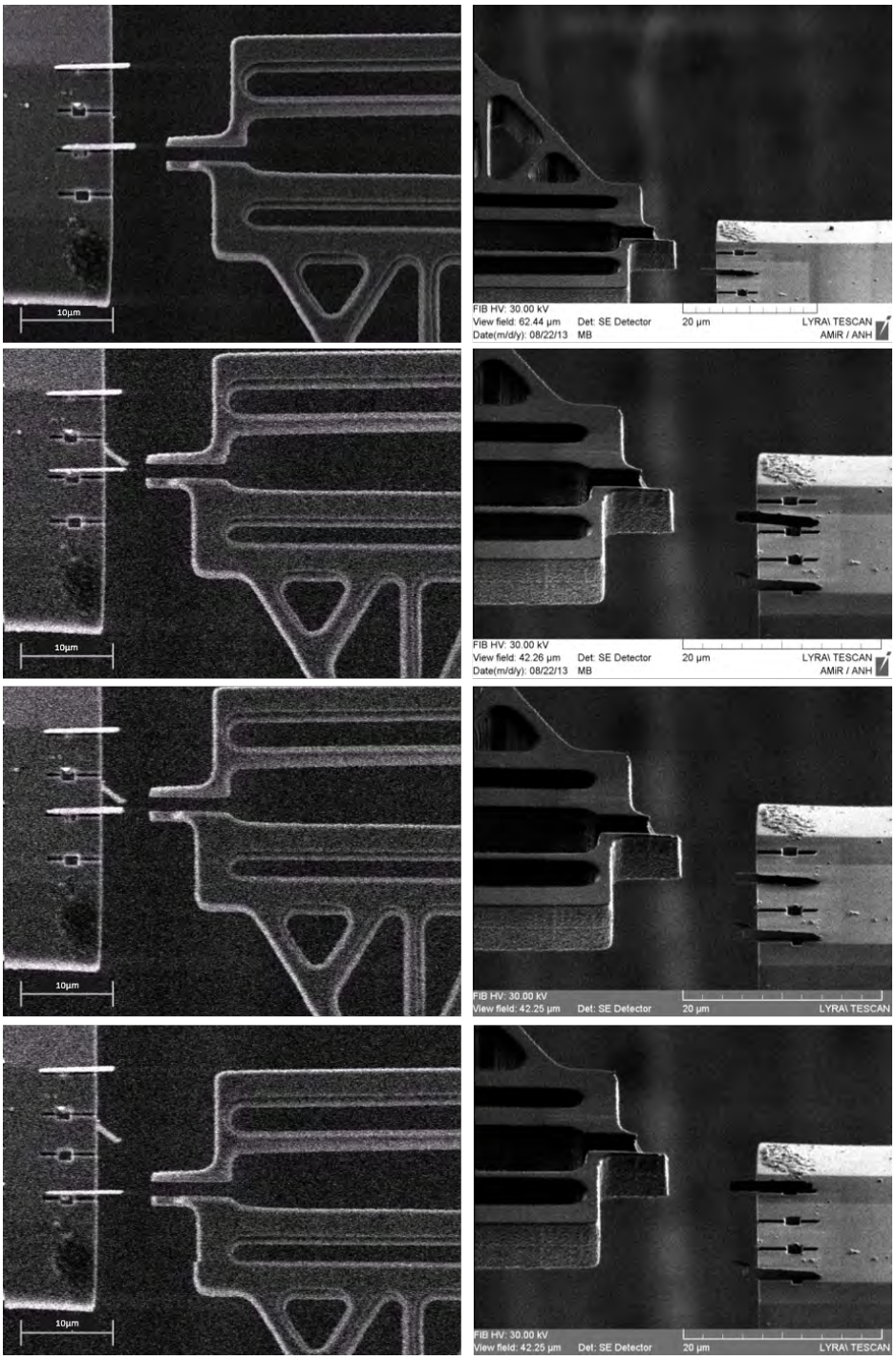

Fig. 6.18 Top- and corresponding sideview perspective of three exemplary insertion approaches. The NanoBit is successfully inserted into the cavity and is released. (Image from [42], ©2014 IEEE)

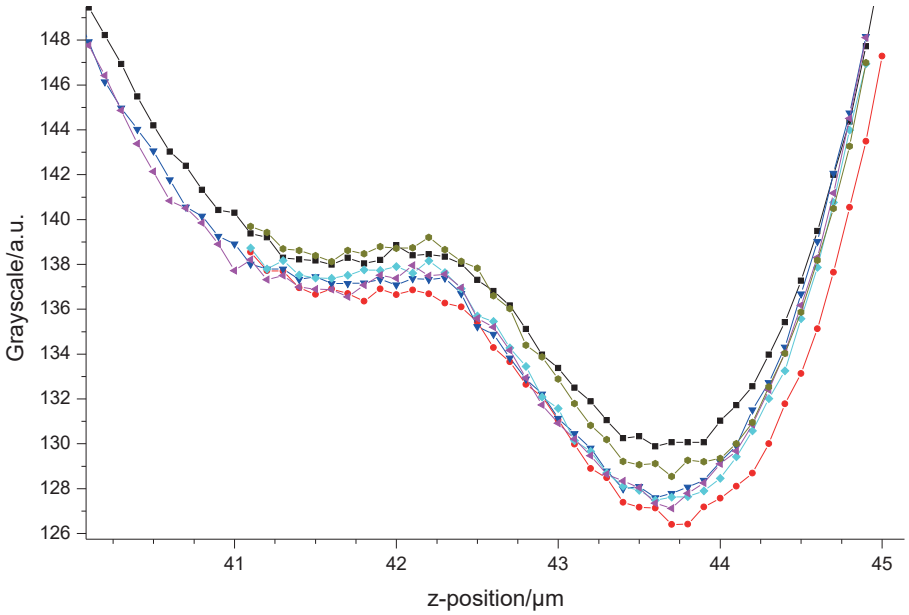

Fig. 6.19 Comparison of six different z-approaches. The minimum grayscale around 43.7 µm indicates a maximal shadowing of the NanoBit, which corresponds to a fully centered position. Maximal deviation is less than 200 nm. (Image from [42], ©2014 IEEE)

NanoBit-Detachment

The detachment of the NanoBits is the most critical step during the process. As mentioned above, the predetermined breaking point has to be fabricated precisely. If this is the case, the detaching sequence shows a success rate of nearly 100%. The overall success rate, including badly fabricated predetermined breaking points, is 80%.

The x/y-alignment based on BLOB-detection works perfectly with only 200 nm clearance between gripper jaws and NanoBit. The z-alignment approach also shows a very high repeatability: Figure 6.19 shows the grayscale values depending on the z-position of the gripper, which are used to determine the optimal gripping position. The deviation of all detected minimum are less than 200 nm, which is more than sufficient for all subsequent tasks (cf. Figure 6.17). This result is confirmed by non-automated measurements by FIB images with a sideview perspective: The deviation of z-positions is about 100 nm.

The required process time for the detaching sequence varies between 30 and 50 seconds, which mainly depends on the initial and unknown height difference of gripper and NanoBit (cf. Section 6.3.1 for details).

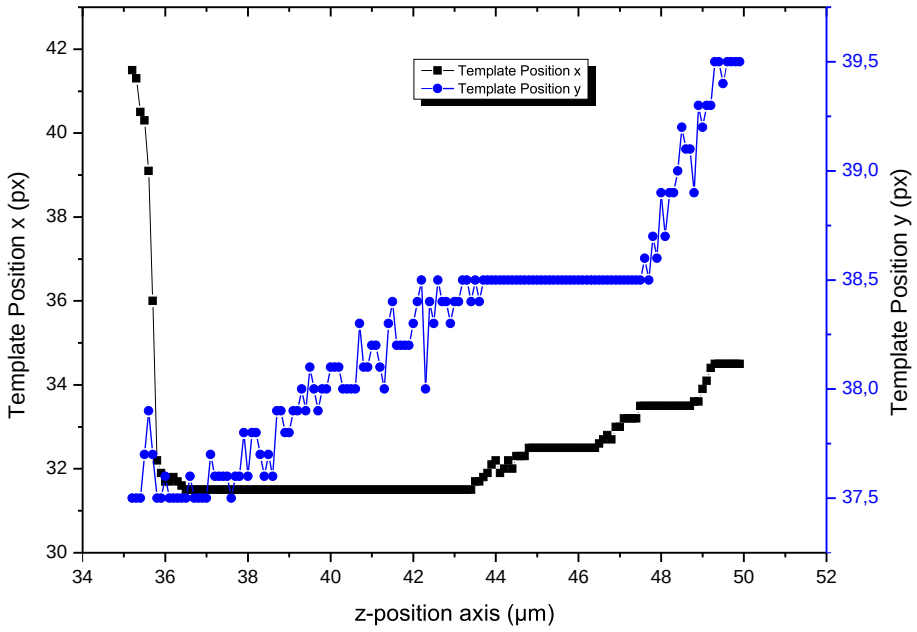

Fig. 6.20 x/y-position of the NanoBit measured by template matching during the insertion process. Touch detection from discharge is used to determine the point of contact. (Image from [42], ©2014 IEEE)

NanoBit-Insertion

The insertion sequence shows the same high success rate as the detachment sequence: nearly 100%. Here, the rating *success* also includes that the NanoBit's tip did not come in contact with anything during the assembly insertion sequence.

The x/y-alignment by template matching allows for an insertion of the NanoBit into the cartridge's cavity. Due to geometric constraints – the size of the NanoBit and the cavity – the precision can be determined to be better than 400 nm.

The actual insertion in the z-direction is measured by *touch-from-discharge* detection (cf. Section 4.2.1). An exemplary measurement of an approach is shown in Figure 6.20. The absolute movement of the template in the x/y-direction shows significant changes caused by corresponding z-approaches of the surface. The z-position measurable uncertainty for the detected position change is 100 nm, which corresponds to the step-width of the z-axis during this approach.

Overall, the NanoBit aligns with the reservoir with an average deviation of less than 5° in the x/y-plane and less than 7° in the z-direction.

Process Times and Success Rate

The overall time requirements for all process steps are shown in Table 6.1 and are visualized in Figure 6.21.

Table 6.1 Time requirements of the fully automated NanoBits assembly process.

Task:	avg. time / sec	σ / sec
find Bits by TM	3.93	1.59
grippers x/y-approach towards Bit by BLOB	5.50	2.09
grippers z-approach towards Bit - coarse (in sec/µm distance)	1.59	0.60
grippers z-approach towards Bit - fine	15.32	5.80
gripping of Bit	1.99	0.47
seperation and retraction	6.53	2.86
find cavities	3.66	0.87
determine Bit's tip position	8.37	2.24
x/y-alignment of tip and cavity	9.61	1.14
z-approach towards cavity (in sec/µm distance)	0.70	0.13
Sum	**65.20**	**8.18**

The time consumption for all coarse positioning approaches is calculated in relation with the traveled distance. The actual times for the coarse alignment of gripper and NanoBit were between 2 and 8 seconds and the actual times for the z-approach to the cavity were between 3 and 15 seconds. The time consumption of all other process steps is independent of the distances that have to be covered and they take a few seconds. All process steps take a reproducible amount of time; while the standard deviations are between 12% and 44%. The overall resulting assembly time for the entire assembly process is (65 ± 8) seconds.

The overall success rate of the NanoBit assembly is about 80%. However, the different process steps have unequal contributions to this rate. Table 6.2 shows the process' success rate broken down by the respective step. X/y-alignment steps based on visual servoing show success rates of nearly 100%. The z-alignment of gripper and NanoBit also works perfectly. All other process steps are more error-prone and depend on the success of the previous steps. Furthermore, the given values in Table 6.2 also depend on the respective definition of success.

The grasping process highly depends on the quality of the predetermined breaking point. If the fabricated process provides NanoBits with predetermined breaking points larger than 300 nm, the detachment from the fabrication substrate fails and the NanoBit cannot be grasped. Hence, the the success rate refers to experiments, where the

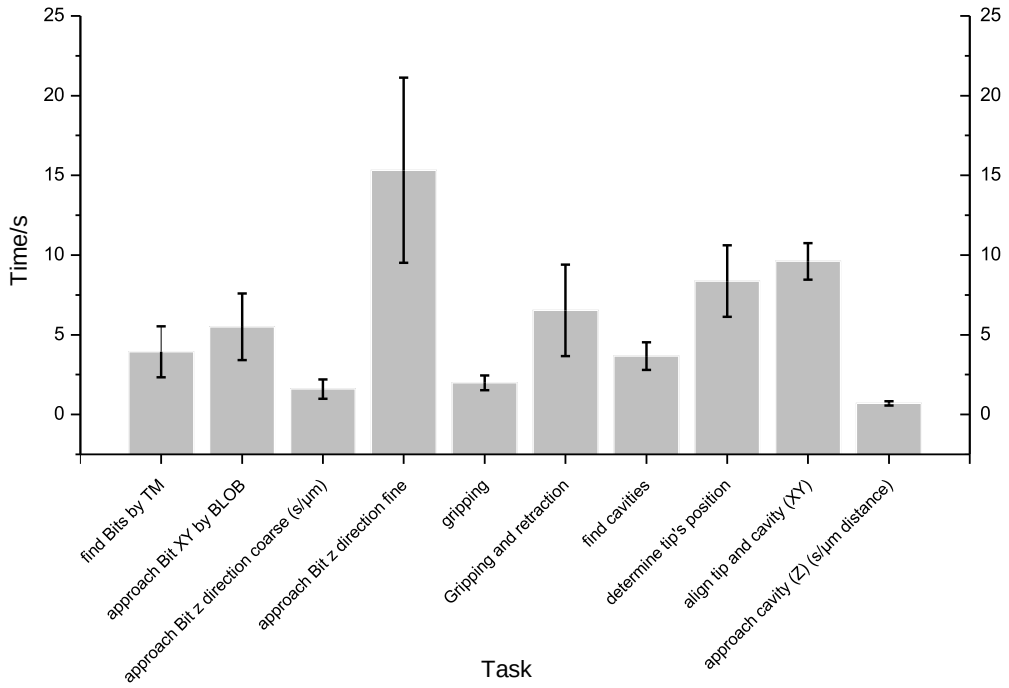

Fig. 6.21 Required times for all different steps of an NanoBits assembly sequence.

predetermined breaking point can be cracked by the gripper. The failure rate of 5% comes from gripping processes, where the predetermined breaking point is cracked, but the NanoBit is misaligned between the gripper jaws in a way that no longer allows insertion into the cartridge's cavity.

The z-alignment success rate during the NanoBit's insertion depends on the accuracy of the gripping process. The insertion is most likely to fail, if the orientation of the gripped NanoBit deviates from the gripper's orientation by more then about 5°, since the NanoBits cannot be inserted into the cartridge's cavity without touching it, which leads directly to a full misalignment. NanoBits that are well-aligned when gripped can be inserted with about 90% success rate.

Releasing the NanoBit and retracing the gripper is comparably safe, if the previous process step is successful. The remaining uncertainty of 5% refers to incidents, where the NanoBit's adhesion to the gripper is larger than to the cartridge.

The success rates of all individual steps are different, but not independent, and they mostly can be reduced by the predetermined breaking point's precision. In general, the grasping's uncertainty is caused by hardly breaking predetermined breaking points. Since the magnitude of the movements during the gripping process are determined

Table 6.2 Success rate of the NanoBit assembly by the process steps.

Detachment		**Insertion**	
x-y alignment	100%	x-y alignment	100%
z-alignment	100%	z-alignment	90%
grasping	95%	releasing	95%
		Overall	81%

experimentally, they imply uncertainty. In combination, this leads to the given success-rate of 95%. Since the insertion step relies on proper grasping, it also depends directly on the predetermined breaking points. And the last crucial step, the retraction of the gripper, is more likely to work if the NanoBit is correctly inserted. Hence, it too relies on the quality of the predetermined breaking points directly.

Finally, its can be stated that positioning and handling tasks themselves are manageable, but the feasibility of the integration strongly depends on an accurately control of all degrees of freedom. This challenge has been successfully tackled for this particular work, but in general, controlling all degrees of freedom as accurate as possible will be a remaining challenge in micro-/nanointegration.

6.4 Conclusions

This case study – the fully automated NanoBit-assembly – demonstrates the potential and possibilities of automated robotic integration on the nanoscale. Nanoscale building blocks – so-called NanoBits – are detected, gripped, rotated, and placed in a cartridge system with a throughput of about one piece per minute. The controlled translational and rotational DOF are 3 and 2, while lateral and rotational accuracies are 100 nm and <7°, respectively. Furthermore, the developed assembly sequence relies on rather cost-efficient instruments. Only regular nanopositioning stages and a standard SEM are required in addition to the cleanroom-devices. The entire process works fully automated (without any user interaction after initialization) and achieves a success rate of 80%,

In summary, this work exceeds all comparable efforts in the field of automated micro-/nanointegration in terms of complexity, speed, and accuracy. The combination of a large amount of controlled DOF with a limited instrumental effort; a manipulation range and achieved precision that covers five orders of magnitudes as well as full automation has been unachieved so far. The final results show the potential of automated robotic

nanohandling for research and industrial purposes. Automated handling is achievable and can transform a time-consuming and unreliable method into an economically reasonable technology. Automated NanoBits integration is faster than any integration of NanoBits performed manually.

In general, the demonstrated methods are applicable to any other in-SEM integration task, but they are not sufficiently adaptable to be applied as “off-the-shelf” method. Hence, case-related development is still necessary based on the developed methods and this requires an economical evaluation of the effort.

7 Conclusions and Outlook

7.1 Conclusions

Nanomaterials and nanoobjects possess unique physical properties, which makes them promising candidates for any kind of future devices. Their potential is best used if they are used as functional building blocks that contribute their functionality individually. Hence, nanoobjects can be treated as crucial nanoscale building blocks in future devices for research and future innovations in technology.

Since there is a large interest in nanoobjects, researchers have already been using nanomanipulaton inside the scanning electron microscope (SEM) for years in order to investigate them directly or to prepare samples for subsequent investigations. Some handling tasks inside the SEM are even performed on a daily basis. However, most of these processes are performed manually.

The automation of handling nanoscale objects is rare. A comprehensive toolkit with methods and instruments is far from available and even profoundly gathered figures of merit of the few automation approaches are lacking. Nevertheless, fundamental research, as well as industrial innovations, would benefit from automation and integration capabilities on the nanoscale, because accuracy, speed, and success rate can be improved by automation. However, the more complex an integration task is, which mostly refers to the amount of degree of freedom (DOF) that have to be controlled, the more challenging is the automation. Vice versa, automation can help to realize complex handling tasks and make them possible in the first place.

In order to increase the control of as many DOF as possible, existing handling methods can be improved by structuring the used robotic end-effectors and samples. By doing

this, rotational uncertainties can be reduced and even complex rotational tasks become possible and can compensate the lack of robotic rotational DOF. However, controlling rotational DOF is still the most error-prone operation in nanohandling. Finally, structural design even allows the realization of micro-cartridge systems for nanoscale building blocks.

The presented nanowire integration task demonstrated the improvements by the structural design of sample and end-effector. Nanowires have been integrated into MEMS devices with an orientation precision of less than one degree and a corresponding lateral precision of 90 nm. However, due to the large uncertainties of the source materials, the time-intensive process steps, and the instrumental effort, a fully automated process remains a challenge for this task.

In contrast, the presented integration of NanoBits demonstrated the ability of structurally designed samples, end-effectors and the exploitation of SEM typical side-effects as useful information source. The developed micro-cartridge system can be filled in a fully automated process by a sequence that controls five DOF and achieves handling accuracies of 100 nm and 7°, respectively. Sufficient information on the handling status is derived from the SEM by the developed depth-from-discharge method, which allows a throughput of about one piece per minute. These results are outstanding in micro-/nanointegration and demonstrate the potential and capabilities of automation in nanorobotics.

In summary, it has been demonstrated that serious automation can be achieved on the nanoscale. In order to achieve that, the tailored design of samples and end-effectors is as important as gathering as much sensor information as possible.

7.2 Outlook

Further demonstration of the potential of automation in robotic nanohandling is highly important to increase the visibility of this technology, in order to contribute to the research community and assist industrial innovation in the long term view. In order to substantiate the benefits of the technology, development must be further based on the demands.

Programming In order to increase reliability and throughput of automated nanohandling, an adaptive sequence can be applied. The assessment of the result of a performed

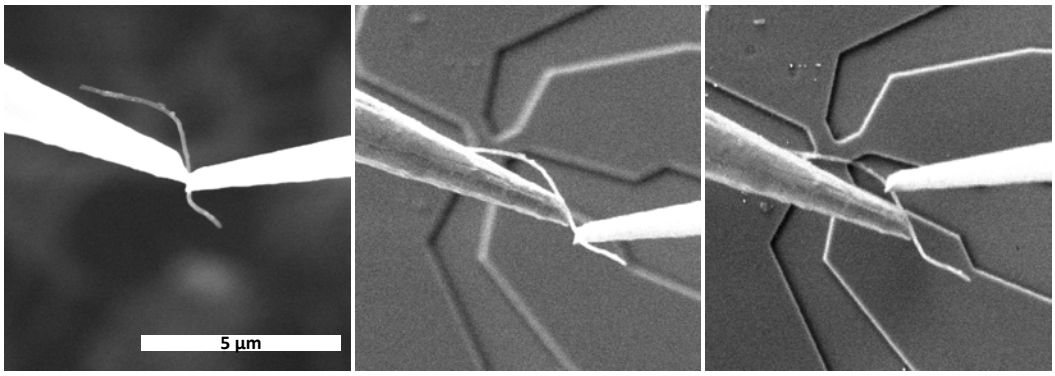

Fig. 7.1 Stages of a dual tip handling sequence. Left: The two tips act as a gripper-like end-effector. Center: Small positioning changes of one tip allow an orientation control of the nanowire. Right: During placement, one of the tips can be used to push the nanowire to the sample as well.

assembly step can be performed as kind of online quality control and possible corrections such as re-positionings could be performed. This is a logical next step and it follows known concepts in conventional robotics [99]. Nowadays, artificial intelligence approaches are widely discussed - also in robotics. Today, it is vague, whether this technology can help nanorobotics. Most artificial intelligence approaches need a large amount of data, which is contradictory to the challenges in nanorobotics, where sensors' information have low density. However, image-based classifications seem to be realistic.

Negative ROI The presented studies already make use of a region of interest (ROI), where the electron beam is reduced to a certain region. This leads to an increased framerate. In most experiments and also in the demonstrated automated sequence, the ROI is set dynamically to different positions. However, the ROI also cause a larger exposure and especially precious samples suffer from the electron bombardment. Unfortunately, the samples' place is mostly the region where the manipulation takes place. The depth-from-discharge approach already allows to monitor the proximity of the handling region instead of the sample/end-effector, still gaining the important information. However, future developments could consider a *negative ROI*: A rectangular ROI with a masked region inside: a negative ROI. This would be a way for the vicinity around a sample to be monitored without exposing the sample to the electron beam.

Dual Tip Handling Further developments of dual tip handling could facilitate more interesting possibilities for nanohandling and automation (cf. Section 4.1.1). First, dual tip manipulation with two end-effectors that both have three DOF allows to combine

different functionalists. Just like a gripper, the two tips can be used to increase the interaction surface between end-effector and object, but the flexibility during release steps is much higher. Second, independently movable tips can be used to control the orientation of the handled nanoobject. Due to the dominant adhesion force, the object follows both tips and can be rotated in all 3 dimensions. Third, by using two tips additional functionality might be integrable in the end-effector, such as electrical characterization measurements.

As a summary of these potential developments that include topics from computer science, measurement instrumentation, and physics, it can be concluded that research in automated nanoassembly will be become more interdisciplinary. Considering this, automated nanoassembly will be able to demonstrate its abilities and potential better and better, maturing it into an important standard technology.

References

[1] NT-MDT Spectrum Instruments Ltd., editor. Nt-mdt afm probes catalogue. URL http://www.ntmdt-tips.com/data/media/nt-mdt_afm_probes_29_03_12.pdf. [Accessed on: 2018-05-23].

[2] *HAZARDOUS AREA TECHNICAL GUIDE*. Darlaston Central Trading Estate Salisbury Street, Darlaston West Midlands. WS10 8XB United Kingdom, 2007. URL https://www.redapt.co.uk/assets/186/redapt_hazardous_area_guide.pdf.

[3] LLC Zyvex Instruments, editor. Zyvexs200 nanomanipulator, 2009. URL http://www.zyvex.com/Documents/S200.pdf. [Accessed on: 2018-08-22].

[4] Xidex Corporation, editor. Xidex nanobot system - nx-2000, 2011. URL http://xidex.com/images/stories/PDF_Files/The_NanoBot_-_Transform_your_SEM_or_FIB_into_a_workshop_for_nanodevice_fabrication_and_testing_-_110322.pdf. [Accessed on: 2018-08-22].

[5] Staffan Elfving, editor. Iso 8373:2012 robots and robotic devices – vocabulary, 2012. URL https://www.iso.org/standard/55890.html. [Accessed on: 2018-08-31].

[6] International Technology Roadmap for Semiconductors (ITRS 2013), 2013. URL http://www.itrs.net.

[7] Preparation Of TEM-Samples. Product Advertisement, 07 2014. URL http://www.nanomotor.de/aa_tem.htm.

[8] Din cen iso/ts 80004-1: Nanotechnologien - fachwörterverzeichnis. Technical report, German Institute for Standardization, 2016.

[9] AMETEK Arizona Instrument, editor. Jerome, 2018. URL https://www.azic.com/jerome/. [Accessed on: 2018-08-27].

[10] Aerotech Inc., editor. Piezo controls and software, 2018. URL https://www.aerotech.com/product-catalog/piezo-nanopositioners/piezo-controls-and-software.aspx. [Accessed on: 2018-08-23].

[11] Bruker AFM Probes International, editor. Rtesp-300 product description:, 2018. URL https://www.brukerafmprobes.com/Product.aspx?ProductID=3905. [Accessed on: 2018-05-23].

[12] Basler AG, editor. Basler software, 2018. URL https://www.baslerweb.com/en/products/software/original-software/. [Accessed on: 2018-08-23].

[13] BudgetSensors, editor. Afm probes catalogue, 2018. URL https://www.budgetsensors.com/uploads/pdf/budgetsensors-brochure.pdf. [Accessed on: 2018-05-23].

[14] Chronogrip - robotic structure, 2018. URL http://www.percipio-robotics.com/index.php/en/systems/chronogrip/80-chrono-robot. [Accessed on: 2018-08-15].

[15] FemtoTools AG, editor. Ft-g microgripper, 2018. URL http://www.femtotools.com/products/previousproducts/ft-g-microgripper/. [Accessed on: 2018-08-16].

[16] FLIR Integrated Imaging Solutions GmbH, editor. Flycapture sdk, 2018. URL https://www.ptgrey.com/flycapture-sdk. [Accessed on: 2018-08-23].

[17] GETec Microscopy GmbH, editor. Did you know your sem could do this...?, 2018. URL http://www.getec-afm.com/fileadmin/content/Brochure_AFSEM_v2016-06-30.pdf. [Accessed on: 2018-08-22].

[18] Häcker Automation GmbH, editor. Automation / applications, 2018. URL https://haecker-automation.de/en/applications/. [Accessed on: 2018-08-22].

[19] The Imaging Source Europe GmbH, editor. The imaging source software, 2018. URL https://www.theimagingsource.com/products/software/. [Accessed on: 2018-08-23].

[20] Imina Technologies SA, editor. mibot bt-14, 2018. URL https://www.imina.ch/sites/default/files/product_pdf/iminatechnologies_mibot_technicalspecifications_en_web.pdf. [Accessed on: 2018-08-22].

[21] Kleindiek Nanotechnik GmbH, editor. Micromanipulator for electron microscopy, 2018. URL https://www.nanotechnik.com/mm3a-em.html. [Accessed on: 2018-08-22].

[22] NanoWorld AG, editor. Pointprobe® silicon afm probes general description, 2018. URL http://www.nanoworld.com/pointprobe-afm-tips-general-description. [Accessed on: 2018-05-23].

[23] Nenovision - litescope data, 2018. URL http://www.nenovision.com/litescope/litescopetm/technical-specification/#tabs. [Accessed on: 2018-08-22].

[24] Oxford Instruments Group, editor. Omniprobe 400, 2018. URL https://nano.oxinst.com/products/omniprobe/omniprobe-400#product-information-tabs. [Accessed on: 2018-08-22].

[25] GmbH & Co. KG, editor. Pi software tools for precision motion control / positioning, 2018. URL http://www.pi-usa.us/products/Software/index.php. [Accessed on: 2018-08-23].

[26] Smart equipment technology, 2018. URL http://www.set-sas.fr/en/ctl-Products.html. [Accessed on: 2018-08-16].

[27] SmarAct GmbH, editor. Product catalog volume 16, 2018. URL http://www.smaract.com/SmarAct_Catalog_v16.pdf. [Accessed on: 2018-08-22].

[28] Toronto Nano Instrumentation, editor. Lifeforce nanomanipulation system: Lf-2000, 2018. URL https://docs.wixstatic.com/ugd/56af0c_88a4d4884771450bb259e9dd36162c17.pdf. [Accessed on: 2018-08-22].

[29] dSPACE GmbH, editor. Controldesk, 2018. URL https://www.dspace.com/en/pub/home/products/sw/experimentandvisualization/controldesk.cfm. [Accessed on: 2018-08-23].

[30] Abbott, Jake J. and Nagy, Zoltán and Beyeler, Felix and Nelson, Bradley J. Robotics in the Small, Part I: Microbotics. *IEEE Robot. Automat. Mag.*, 14(2): 92–103, 2007. doi: 10.1109/mra.2007.380641. URL http://dblp.uni-trier.de/db/journals/ram/ram14.html#AbbottNBN07.

[31] Jean-Ochin Abrahamians, Bruno Sauvet, Jérôme Polesel-Maris, Rémy Braive, and Stéphane Régnier. A nanorobotic system for in situ stiffness measurements on membranes. *IEEE Transactions on Robotics*, 30(1):119–124, 2014.

[32] NanoWorld AG. *AFM-Tip - CONT - Pointprobe Series - NanoWorld*, 2017. URL http://www.nanoworld.com/contact-mode-pointprobe-afm-tip-cont.

[33] K. N. Andersen, D. H. Petersen, K. Carlson, K. Mølhave, O. Sardan, A. Horsewell, V. Eichhorn, S. Fatikow, and P. Bøggild. Multimodal Electrothermal Silicon Microgrippers for Nanotube Manipulation. *IEEE Transactions on Nanotechnology*, 8(1):76–85, January 2009. doi: 10.1109/TNANO.2008.2006558.

[34] Ph Avouris, T Hertel, R Martel, THRHS Schmidt, HR Shea, and RE Walkup. Carbon nanotubes: nanomechanics, manipulation, and electronic devices. *Applied Surface Science*, 141(3-4):201–209, 1999.

[35] Donald G. Bailey. *Blob Detection and Labelling*, pages 416–. Wiley-IEEE Press, 2011. ISBN 9780470828519. doi: 10.1002/9780470828519.ch11. URL https://ieeexplore.ieee.org/xpl/articleDetails.jsp?arnumber=6016318.

[36] M. Bartenwerfer and S. Fatikow. Robotic dual-tip assembly for nanowire handling and integration. In *Nanotechnology (IEEE-NANO) , 2015 IEEE 15th International Conference on*, pages 1497–1500, July 2015. doi: 10.1109/NANO.2015.7388926.

[37] M. Bartenwerfer, V. Eichhorn, D. Jasper, S. Fatikow, A. Savenko, D. H. Petersen, B. Malm, and P. Bøggild. Automated Handling and Assembly of Customizable AFM-Tips. In *Proceedings of the IEEE International Symposium on Assembly and Manufacturing (ISAM'11)*, pages 1–6, Tampere, Finland, May 25-27 2011. doi: http://dx.doi.org/10.1109/ISAM.2011.5942350.

[38] Malte Bartenwerfer and Sergej Fatikow. Nanorobot-Based Handling and Transfer of Individual Silicon Nanowires. *International Journal of Intelligent Mechatronics and Robotics*, 2(2):34–46, 2012. doi: 10.4018/ijimr.2012040103.

[39] Malte Bartenwerfer and Sergej Fatikow. Exploitation of SEM charging effects for monitoring robotic assembly tasks. In *2016 IEEE/RSJ International Conference on Intelligent Robots and Systems (IROS)*. Institute of Electrical and Electronics Engineers (IEEE), oct 2016. doi: 10.1109/iros.2016.7759761.

[40] Malte Bartenwerfer, Sergej Fatikow, Hongjiang Zeng, Tie Li, and Yuelin Wang. Individual Nanowire Handling for NEMS Fabrication. In *Proceedings of IEEE/ASME International Conference on Advanced Intelligent Mechatronics, AIM2012*, pages 562–567, 2012.

[41] Malte Bartenwerfer, Volkmar Eichhorn, Sergej Fatikow, Marco Becker, Alexey Savenko, Izzet Yildiz, and Peter Bøggild. Design of a Micro-Cartridge System for the Robotic Assembly of Exchangeable AFM-Probe Tips. In *Proc. of IEEE International Conference on Robotics and Automation (ICRA)*, pages 1722–1727, Karlsruhe, Germany, May 6-10 2013.

[42] Malte Bartenwerfer, Claas Diederichs, and Sergej Fatikow. Automated Robotic Assembly for a Micro-Cartridge System inside the Scanning Electron Microscope. In *Proc. of IEEE International Conference on Robotics and Automation (ICRA)*, pages 5197–5202, Hong Kong, China, May 31st - June 7th 2014.

[43] F Bauer, S Sitzman, C Lang, C Hartfield, and J Goulden. Advancing materials characterization in the fib-sem with transmission kikuchi diffraction. *Microscopy and Microanalysis*, 20(S3):326–327, 2014.

[44] Dominik J Bell, Lixin Dong, Bradley J Nelson, Matthias Golling, Li Zhang, and Detlev Grützmacher. Fabrication and characterization of three-dimensional ingaas/gaas nanosprings. *Nano Letters*, 6(4):725–729, 2006.

[45] Felix Beyeler, Simon Muntwyler, and Bradley J Nelson. Wafer-level inspection system for the automated testing of comb drive based mems sensors and actuators. In *Automation Science and Engineering (CASE), 2010 IEEE Conference on*, pages 698–703. IEEE, 2010.

[46] G. Binnig and H. Rohrer. Scanning tunneling microscopy. *Surface Science*, 126 (1-3):236–244, mar 1983. doi: 10.1016/0039-6028(83)90716-1.

[47] G. Binnig, C. F. Quate, and Ch. Gerber. Atomic force microscope. *Physical Review Letters*, 56(9):930–933, mar 1986. doi: 10.1103/physrevlett.56.930.

[48] Miltiadis A. Boboulos. *Automation and robotics*. Bookboon.com Ltd, [London], 2010. ISBN 8776816966.

[49] Peter Bøggild. Nanogrippers. *Encyclopedia of Nanotechnology*, pages 1552–1569, 2012.

[50] Aude Bolopion, Christian Dahmen, Christian Stolle, Sinan Haliyo, Stéphane Régnier, and Sergej Fatikow. Vision-based haptic feedback for remote micromanipulation in–sem environment. *International Journal of Optomechatronics*, 6(3):236–252, 2012. doi: 10.1080/15599612.2012.701370. URL https://doi.org/10.1080/15599612.2012.701370.

[51] Gary Bradski. The OpenCV library. *Dr. Dobb's Journal of Software Tools*, 25 (11):120, 122–125, November 2000. ISSN 1044-789X. URL http://www.ddj.com/ftp/2000/2000_11/opencv.txt.

[52] KARL Ferdinand Braun. Electrical oscillations and wireless telegraphy. *Nobel Lecture, December*, 11(1909):226–245, 1909.

[53] Benoit Brazey, Redwan Dahmouche, Jean-Antoine Seon, and Michael Gauthier. Experimental validation of in-hand planar orientation and translation in microscale. *Intelligent Service Robotics*, 9(2):101–112, Apr 2016. ISSN 1861-2784. doi: 10.1007/s11370-015-0183-0. URL https://doi.org/10.1007/s11370-015-0183-0.

[54] David C. Brock, editor. *Understanding Moore's law: Four decades of innovation*. Chemical Heritage Press, Philadelphia, Pa., 2006. ISBN 0-941901-41-6. URL http://www.loc.gov/catdir/enhancements/fy0643/2006010387-b.html.

[55] A Brooks, T Kaupp, A Makarenko, S Williams, and A Oreback. Software engineering for experimental robotics. *Software Engineering for Experimental Robotics. Springer Tracts in Advanced Robotics*, pages 231–251, 2007.

[56] Alberto Cagliani, Rafal Wierzbicki, Luigi Occhipinti, Dirch Hjorth Petersen, Karin Nordstrøm Dyvelkov, Özlem Sardan Sukas, Berit G Herstrøm, Tim Booth, and Peter Bøggild. Manipulation and in situ transmission electron microscope

characterization of sub-100 nm nanostructures using a microfabricated nanogripper. *Journal of Micromechanics and Microengineering*, 20(3):035009, 2010.

[57] Patrick C Chaumet, Adel Rahmani, and Manuel Nieto-Vesperinas. Optical trapping and manipulation of nano-objects with an apertureless probe. *Physical review letters*, 88(12):123601, 2002.

[58] B. K. Chen and Y. Sun. A mems microgripper with changeable gripping tips. In *2011 16th International Solid-State Sensors, Actuators and Microsystems Conference*, pages 498–501, June 2011. doi: 10.1109/TRANSDUCERS.2011.5969619.

[59] B.K. Chen, Yong Zhang, and Yu Sun. Active release of microobjects using a mems microgripper to overcome adhesion forces. *Microelectromechanical Systems, Journal of*, 18(3):652–659, 2009. ISSN 1057-7157. doi: 10.1109/JMEMS.2009.2020393. URL https://ieeexplore.ieee.org/document/4914836/.

[60] Brandon K Chen, Yong Zhang, Doug D Perovic, and Yu Sun. From microgripping to nanogripping. In *Micro Electro Mechanical Systems (MEMS), 2010 IEEE 23rd International Conference on*, pages 296–299. IEEE, 2010.

[61] Gabriela Conache, Struan M Gray, Aline Ribayrol, Linus E Fröberg, Lars Samuelson, Håkan Pettersson, and Lars Montelius. Friction measurements of inas nanowires on silicon nitride by afm manipulation. *Small*, 5(2):203–207, 2009.

[62] J Corbett, PA McKeown, GN Peggs, and R Whatmore. Nanotechnology: international developments and emerging products. *CIRP Annals-Manufacturing Technology*, 49(2):523–545, 2000.

[63] Christian Dahmen. Focus-based depth estimation in the sem. In *Optomechatronic Technologies 2008*, volume 7266, page 72661O. International Society for Optics and Photonics, 2008.

[64] Christian Dahmen. Defocus-based threedimensional tracking in sem images. In *Informatics in Control Automation and Robotics*, pages 243–254. Springer, 2011.

[65] Robert W Deller and Joon H Lee. Acceptance testing of actuators using backlash and stiction measurements, 6 2007. US Patent 7,292,954.

[66] B.V Derjaguin, V.M Muller, and Yu.P Toporov. Effect of contact deformations on the adhesion of particles. *Journal of Colloid and Interface Science*, 53(2):314 – 326, 1975. ISSN 0021-9797. doi: https://doi.org/10.1016/0021-9797(75)90018-1. URL http://www.sciencedirect.com/science/article/pii/0021979775900181.

[67] Rosen Diankov and James Kuffner. Openrave: A planning architecture for autonomous robotics. *Robotics Institute, Pittsburgh, PA, Tech. Rep. CMU-RI-TR-08-34*, 79, 2008.

[68] Claas Diederichs, Christian Dahmen, Malte Bartenwerfer, and Sergej Fatikow. Tracking Algorithms for Closed-Loop Positioning of Mobile Microrobots. In *Proceedings of IEEE/ASME International Conference on Advanced Intelligent Mechatronics, AIM2012*, pages 568–573, 2012.

[69] Claas Diederichs, Malte Bartenwerfer, Manuel Mikczinski, Sören Zimmermann, Tobias Tiemerding, Christian Geldmann, Ha Nguyen, Christian Dahmen, and Sergej Fatikow. A rapid automation framework for applications on the micro- and nanoscale. In *Proc. of the Australasian Conference on Robotics and Automation 2013*, page 8, December 2013.

[70] Xiaoyun Ding, Sz-Chin Steven Lin, Brian Kiraly, Hongjun Yue, Sixing Li, I-Kao Chiang, Jinjie Shi, Stephen J Benkovic, and Tony Jun Huang. On-chip manipulation of single microparticles, cells, and organisms using surface acoustic waves. *Proceedings of the National Academy of Sciences*, 109(28): 11105–11109, 2012.

[71] Mohamed Dkhil, Aude Bolopion, Stéphane Régnier, and Michaël Gauthier. Analysis of the influence of inertia for non-contact micromanipulation. *Journal of Micro-Bio Robotics*, 13(1-4):15–26, 2017.

[72] K. Eric Drexler. *Engines of creation*. Doubleday, New York NY u.a., 1987. ISBN 0-385-19973-2.

[73] Christoph Edeler. *Modellierung und Validierung der Krafterzeugung mit Stick-Slip-Antrieben für nanorobotische Anwendungen*. Verlag Dr. Hut, 2011.

[74] V. Eichhorn, S. Fatikow, T. Wich, C. Dahmen, T. Sievers, K. N. Andersen, K. Carlson, and P. Bøggild. Depth-detection methods for microgripper based CNT manipulation in a scanning electron microscope. *Journal of Micro-Nano Mechatronics*, 4(1-2):27–36, 2008. doi: 10.1007/s12213-008-0001-2.

[75] Volkmar Eichhorn. *Nanorobotic handling and characterization of carbon nanotubes inside the scanning electron microscope*. Verlag Dr. Hut, 2011.

[76] Donald M Eigler and Erhard K Schweizer. Positioning single atoms with a scanning tunnelling microscope. *Nature*, 344(6266):524, 1990.

[77] Patrick Elfert, Malte Bartenwerfer, and Sergej Fatikow. Wafer-scale automation of electron beam induced depositions. In *2016 IEEE International Conference on Advanced Intelligent Mechatronics (AIM)*. Institute of Electrical and Electronics Engineers (IEEE), jul 2016. doi: 10.1109/aim.2016.7576792.

[78] J Elliott, A Kor, and OA Omotosho. Energy consumption in smartphones: An investigation of battery and energy consumption of media related applications on android smartphones. In *International SEEDS Conference*, December 2017. URL http://eprints.leedsbeckett.ac.uk/4703/.

[79] Golla Eranna. *Crystal Growth and Evaluation of Silicon for VLSI and ULSI*. Taylor and Francis, Hoboken, 2014. ISBN 9781482232813. URL http://search.ebscohost.com/login.aspx?direct=true&scope=site&db=nlebk&AN=916038.

[80] F. Faggin. The mos silicon gate technology and the first microprocessors. *Nuovo Cimento Rivista Serie*, 38:575–621, 2015. doi: 10.1393/ncr/i2015-10119-7.

[81] S. Fatikow, V. Eichhorn, and M. Bartenwerfer. Nanomaterials Enter the Silicon-Based CMOS Era. *IEEE Nanotechnology Magazine*, 6(1):14–18, March 2012. doi: 10.1109/MNANO.2011.2181735.

[82] Richard P. Feynman. Plenty of Room at the Bottom, December 1959. URL https://www.its.caltech.edu/~feynman/plenty.html. Lecture given at an American Physical Society meeting at the California Institute of Technology. [Accessed on: 13.07.2016].

[83] CAM Fraunhofer. Nanoprobing sem solution for in situ semiconductor failure analysis. 2018. URL https://www.imina.ch/sites/default/files/use_case_files/iminatechnologies_appnote_semicon-failure-analysis.pdf. [Accessed on: 2018-08-31].

[84] Takafumi Fujiwara, Masahiro Nakajima, Akihiko Ichikawa, Kenichi Ohara, Yasuhisa Hasegawa, and Toshio Fukuda. Electrostatic actuation of folded multi-graphene structure for nano-gripper. In *Nanotechnology (IEEE-NANO), 2016 IEEE 16th International Conference on*, pages 34–35. IEEE, 2016.

[85] Toshio Fukuda, Fumihito Arai, and Lixin Dong. Assembly of nanodevices with carbon nanotubes through nanorobotic manipulations. *Proceedings of the IEEE*, 91(11):1803–1818, 2003.

[86] T Furukawa, K Ishida, and E Fukada. Piezoelectric properties in the composite systems of polymers and pzt ceramics. *Journal of Applied Physics*, 50(7): 4904–4912, 1979.

[87] Takashi Fuyuki, Hayato Kondo, Tsutomu Yamazaki, Yu Takahashi, and Yukiharu Uraoka. Photographic surveying of minority carrier diffusion length in polycrystalline silicon solar cells by electroluminescence. *Applied Physics Letters*, 86(26):262108, 2005.

[88] B. Gady, R. Reifenberger, D. S. Rimai, and L. P. DeMejo. Contact electrification and the interaction force between a micrometer-size polystyrene sphere and a graphite surface. *Langmuir*, 13(9):2533–2537, 1997. doi: 10.1021/la960656z. URL https://doi.org/10.1021/la960656z.

[89] Michaël Gauthier, David Hériban, Dominique Gendreau, Stéphane Régnier, Nicolas Chaillet, and Philippe Lutz. Micro-factory for submerged assembly: Interests and Architectures. In *Proceedings of the 5th International Workshop on MicroFactories, IWMF'06.*, volume 1, Besanćon, France, 2006.

[90] Brian Gerkey, Richard T Vaughan, and Andrew Howard. The player/stage project: Tools for multi-robot and distributed sensor systems. In *Proceedings of the 11th international conference on advanced robotics*, volume 1, pages 317–323, 2003.

[91] Hans-Jürgen Gevatter and Ulrich Grünhaupt, editors. *Handbuch der Mess- und Automatisierungstechnik in der Produktion*. VDI-Buch. Springer-Verlag Berlin Heidelberg, Berlin, Heidelberg, 2., vollst. bearb. aufl. edition, 2006. ISBN 9783540212072. doi: 10.1007/3-540-34823-9. URL http://site.ebrary.com/lib/alltitles/docDetail.action?docID=10183162.

[92] Ahmad Ghanbari and Ehsan Qaredaghi. Simulation and analysis of three finger micro/nano gripper using different materials. In *Advanced Materials Research*, volume 622, pages 665–670. Trans Tech Publ, 2013.

[93] L. A. Giannuzzi. *Introduction to Focused Ion Beams: Instrumentation, Theory, Techniques and Practice*. Springer, 2006. ISBN 978-0-387-23313-0.

[94] Zheng Gong, Brandon K Chen, Jun Liu, and Yu Sun. Robotic probing of nanostructures inside scanning electron microscopy. *IEEE Trans. Robotics*, 30 (3):758–765, 2014.

[95] Andreas Graff, Christian Grosse, Michel Simon, and Frank Altmann. New Tool for In-Situ Lift Out of TEM Samples. *Microscopy and Microanalysis*, 13:88–89, 2007. doi: 10.1017/S1431927607080440.

[96] Felix Greiner and Helmut Schlaak. Mikro-nano-integration, 2011. URL https://www.technologieland-hessen.de/mm/Broschuere_Mikro-Nano-Integration_web.pdf. [Accessed on: 2018-07-13].

[97] Elnaz Haddadi, Hadi Ghattan Kashani, Hasan Nahvi, et al. On the sensitivity of nanogripper-carbon nanotube friction to contact area. *e-Journal of Surface Science and Nanotechnology*, 15:81–86, 2017.

[98] HC Hamaker. The london—van der waals attraction between spherical particles. *physica*, 4(10):1058–1072, 1937.

[99] Veit Hammerstingl and Gunther Reinhart. Fähigkeiten in der montage, 2017. URL http://mediatum.ub.tum.de/?id=1370174. Version 1.0. [Accessed on: 2017-07-01].

[100] J. G. Hanse. Honeywell mems inertial technology product status. In *PLANS 2004. Position Location and Navigation Symposium (IEEE Cat. No.04CH37556)*, pages 43–48, April 2004. doi: 10.1109/PLANS.2004.1308972.

[101] Wolfgang M Heckl. Visualization and nanomanipulation of molecules in the scanning tunnelling microscope. In *Pioneering ideas for the physical and chemical sciences*, pages 179–191. Springer, 1997.

[102] Georg Wilhelm Friedrich Hegel. *Wissenschaft der Logik: Erster Teil: Die objektive Logik Zweiter Teil: Die subjektive Logik*. Contumax and Hofenberg, Berlin, 1. auflage edition, 2016. ISBN 3843091668.

[103] Tina Horstmann. Bosch sensortec sets size, performance and integration benchmarks in consumer mems. *www.bosch-press.com*, 2013. URL http://www.bosch-presse.de/pressportal//zip?country=de&language=en&docId=42031.

[104] S. Hutchinson, G. D. Hager, and P. I. Corke. A tutorial on visual servo control. *IEEE Transactions on Robotics and Automation*, 12(5):651–670, Oct 1996. ISSN 1042-296X. doi: 10.1109/70.538972.

[105] Ted Pella Inc. *SEM Supplies and Accessories Overview*, 2018. URL http://www.tedpella.com/SEM_html/SEMpinmount.htm.

[106] Jacob N. Israelachvili. *Intermolecular and Surface Forces*. Academic Press, 2011. ISBN 978-0-12-375182-9. URL https://www.amazon.com/Intermolecular-Surface-Forces-Jacob-Israelachvili-ebook/dp/B004HD63LG?SubscriptionId=0JYN1NVW651KCA56C102&tag=techkie-20&linkCode=xm2&camp=2025&creative=165953&creativeASIN=B004HD63LG.

[107] Bernd Jähne. *Digitale bildverarbeitung*. Springer-Verlag, 2013.

[108] Jae Eun Jang, Seung Nam Cha, Youngjin Choi, Dae Joon Kang, David G Hasko, Jae Eun Jung, Jong Min Kim, and Gehan AJ Amaratunga. A nanogripper employing aligned multiwall carbon nanotubes. *IEEE Transactions on Nanotechnology*, 7(4):389–393, 2008. doi: 10.1109/TNANO.2008.926331.

[109] I Joachimsthaler, R Heiderhoff, and L J Balk. A universal scanning-probe-microscope-based hybrid system. *Measurement Science and Technology*, 14(1):87, 2003. URL http://stacks.iop.org/0957-0233/14/i=1/a=313.

[110] K. L. Johnson, K. Kendall, and A. D. Roberts. Surface energy and the contact of elastic solids. *Proceedings of the Royal Society of London A: Mathematical, Physical and Engineering Sciences*, 324(1558):301–313, 1971. ISSN 0080-4630. doi: 10.1098/rspa.1971.0141. URL http://rspa.royalsocietypublishing.org/content/324/1558/301.

[111] D. C. Joy. Smart - a program to measure sem resolution and imaging performance. *Journal of Microscopy*, 208(1):24–34, 2002. ISSN 0022-2720. doi: 10.1046/j.1365-2818.2002.01062.x.

[112] Sylvain Joyeux and Jan Albiez. Robot development: from components to systems. In *6th National Conference on Control Architectures of Robots*, pages 15–p, 2011.

[113] Yuejun Kang, Dongqing Li, Spyros A Kalams, and Josiane E Eid. Dc-dielectrophoretic separation of biological cells by size. *Biomedical microdevices*, 10(2):243–249, 2008.

[114] Suenne Kim, Farbod Shafiei, Daniel Ratchford, and Xiaoqin Li. Controlled afm manipulation of small nanoparticles and assembly of hybrid nanostructures. *Nanotechnology*, 22(11):115301, 2011.

[115] Tae-Hwan Kim, Zhouhang Wang, John F Wendelken, Hanno H Weitering, Wenzhi Li, and An-Ping Li. A cryogenic quadraprobe scanning tunneling microscope system with fabrication capability for nanotransport research. *Review of Scientific Instruments*, 78(12):123701, 2007.

[116] J Klöber-Koch, J Pielmeier, S Grimm, M Miličić Brandt, M Schneider, and G Reinhart. Knowledge-based decision making in a cyber-physical production scenario. *Procedia Manufacturing*, 9:167–174, 2017.

[117] V. Koledov, V. Shavrov, M. Fawzy, M. Blumenthal, S. von Gratowski, A. Irzhak, A. Shelyakov, and M. Topic. Nano-nanomanipulation of cdse nanowires using nano-tweezers based on shape memory alloys. In *2015 International Conference on Manipulation, Manufacturing and Measurement on the Nanoscale (3M-NANO)*, pages 69–73, Oct 2015. doi: 10.1109/3M-NANO.2015.7425500.

[118] Bonjin Koo, Xuemeng Zhang, Jingyan Dong, Srinivasa M Salapaka, and Placid M Ferreira. A 2 degree-of-freedom soi-mems translation stage with closed-loop positioning. *Journal of Microelectromechanical Systems*, 21(1): 13–22, 2012.

[119] Axel Kortschack and Sergej Fatikow. Development of a mobile nanohandling robot. *Journal of Micromechatronics*, 2(3-4):249–269, 2004.

[120] Gilbert Lecarpentier and Joeri De Vos. Die-to-die and die-to-wafer bonding solution for high density, fine pitch micro-bumped die. In *8th International Conference and Exhibition on DEVICE PACKAGING*, 2012. URL http://proxy.siteo.com.s3.amazonaws.com/www.set-sas.fr/file/imaps-dp2012-d2wbonding2012-03-08.pdf.

[121] Jon C Lee and BH Lee. The versatile application for in-situ lift-out tem sample preparation by micromanipulator and nanomotor. In *Proceedings of ISTFA*, 2005.

[122] John P Lewis. Fast template matching. In *Vision interface*, volume 95, pages 15–19, 1995.

[123] Mingwei Li, Rustom B Bhiladvala, Thomas J Morrow, James A Sioss, Kok-Keong Lew, Joan M Redwing, Christine D Keating, and Theresa S Mayer. Bottom-up assembly of large-area nanowire resonator arrays. *Nature nanotechnology*, 3(2):88, 2008. doi: 10.1038/nnano.2008.26.

[124] Xinyu Liu, Keekyoung Kim, and Yu Sun. A mems stage for 3-axis nanopositioning. *Journal of Micromechanics and Microengineering*, 17(9):1796, 2007.

[125] Tianming Lu. *Design and Realization of a Desktop Micro-Manipulation Cobotic Platform*. Theses, Université Pierre et Marie Curie - Paris VI, March 2016. URL https://tel.archives-ouvertes.fr/tel-01363790.

[126] Zhe Lu, Xuping Zhang, Clement Leung, Navid Esfandiari, Robert F Casper, and Yu Sun. Robotic icsi (intracytoplasmic sperm injection). *IEEE Transactions on Biomedical Engineering*, 58(7):2102–2108, 2011.

[127] A. Lugstein, M. Steinmair, A. Steiger, H. Kosina, and E. Bertagnolli. Anomalous piezoresistance effect in ultrastrained silicon nanowires. *Nano Letters*, 10(8): 3204–3208, 2010. doi: 10.1021/nl102179c. URL https://doi.org/10.1021/nl102179c. PMID: 20698638.

[128] Eric Marchand. Visp: A software environment for eye-in-hand visual servoing. In *IEEE Int. Conf. on Robotics and Automation, ICRA'99*, volume 4, pages 3224–3229, 1999.

[129] PG Martin, I Griffiths, CP Jones, CA Stitt, M Davies-Milner, JFW Mosselmans, Y Yamashiki, DA Richards, and TB Scott. In-situ removal and characterisation of uranium-containing particles from sediments surrounding the fukushima daiichi nuclear power plant. *Spectrochimica Acta Part B: Atomic Spectroscopy*, 117:1–7, 2016.

[130] Naresh Marturi. *Vision and visual servoing for nanomanipulation and nanocharacterization in scanning electron microscope.* PhD thesis, Université de Franche-Comté, 2013.

[131] Naresh Marturi, Sounkalo Dembélé, and Nadine Piat. Depth and shape estimation from focus in scanning electron microscope for micromanipulation. In *Control, Automation, Robotics and Embedded Systems (CARE), 2013 International Conference on*, pages 1–6. IEEE, 2013.

[132] D. Maugis and B. Gauthier-Manuel. Jkr-dmt transition in the presence of a liquid meniscus. *Journal of Adhesion Science and Technology*, 8(11):1311–1322, 1994. doi: 10.1163/156856194X00627. URL https://doi.org/10.1163/156856194X00627.

[133] Daniel Maugis. Adhesion of spheres: The jkr-dmt transition using a dugdale model. *Journal of Colloid and Interface Science*, 150(1):243 – 269, 1992. ISSN 0021-9797. doi: https://doi.org/10.1016/0021-9797(92)90285-T. URL http://www.sciencedirect.com/science/article/pii/002197979290285T.

[134] Joachim Mayer, Lucille A. Giannuzzi, Takeo Kamino, and Joseph Michael. TEM Sample Preparation and FIB-Induced Damage. *MRS Bulletin*, 32:400–407, 2007. doi: 10.1557/mrs2007.63.

[135] J.C. McLaughlin and A.F.W. Willoughby. Fracture of silicon wafers. *Journal of Crystal Growth*, 85(1):83 – 90, 1987. ISSN 0022-0248. doi: https://doi.org/10.1016/0022-0248(87)90207-7. URL http://www.sciencedirect.com/science/article/pii/0022024887902077.

[136] B. Merle and M. Göken. Fracture toughness of silicon nitride thin films of different thicknesses as measured by bulge tests. *Acta Materialia*, 59(4):1772 – 1779, 2011. ISSN 1359-6454. doi: https://doi.org/10.1016/j.actamat.2010.11.043. URL http://www.sciencedirect.com/science/article/pii/S1359645410007986.

[137] Pascal Metzger, Joseph Macheda, Michael D Stead, Keith A Cooper, and SET North America. Development done on device bonder to address 3d requirements in a production environment. In *International Wafer Level Packaging Conference (IWLPC) November*, pages 11–13, 2014.

[138] David Michael. Iso/tc 229 nanotechnologies. Technical report, International Organization for Standardization, 2005.

[139] Uwe Mick, Volkmar Eichhorn, Tim Wortmann, Claas Diederichs, and Sergej Fatikow. Combined nanorobotic afm/sem system as novel toolbox for automated hybrid analysis and manipulation of nanoscale objects. In *Robotics and Automation (ICRA), 2010 IEEE International Conference on*, pages 4088–4093. IEEE, 2010.

[140] Stefan Miltenyi, Werner Müller, Walter Weichel, and Andreas Radbruch. High gradient magnetic cell separation with macs. *Cytometry: The Journal of the International Society for Analytical Cytology*, 11(2):231–238, 1990.

[141] Yifei Mo and Izabela Szlufarska. Roughness picture of friction in dry nanoscale contacts. *Physical Review B*, 81(3):275, 2010. ISSN 1098-0121. doi: 10.1103/PhysRevB.81.035405.

[142] R Sri Muthu Mrinalini and GR Jayanth. A system for replacement and reuse of tips in atomic force microscopy. *IEEE/ASME Trans. Mechatronics*, 21(4):1943–1953, 2016.

[143] Xuan Mu, Wenfu Zheng, Jiashu Sun, Wei Zhang, and Xingyu Jiang. Microfluidics for manipulating cells. *Small*, 9(1):9–21, 2013.

[144] P. Muller. Glossary of terms used in physical organic chemistry (iupac recommendations 1994). *Pure and Applied Chemistry*, 66(5):1077–1184, 1994. ISSN 1365-3075. doi: 10.1351/pac199466051077.

[145] LA Nagahara, T Thundat, and SM Lindsay. Preparation and characterization of stm tips for electrochemical studies. *Review of scientific instruments*, 60(10): 3128–3130, 1989.

[146] Masahiro Nakajima, Fumihito Arai, and Toshio Fukuda. In situ measurement of young's modulus of carbon nanotubes inside a tem through a hybrid nanorobotic manipulation system. *IEEE transactions on nanotechnology*, 5(3):243–248, 2006.

[147] Keir C Neuman and Steven M Block. Optical trapping. *Review of scientific instruments*, 75(9):2787–2809, 2004.

[148] Ha X Nguyen, Elena Teidelt, Valentin L Popov, and Sergej Fatikow. Modeling and waveform optimization of stick–slip micro-drives using the method of dimensionality reduction. *Archive of Applied Mechanics*, 86(10):1771–1785, 2016.

[149] A Nikoobin and M Hassani Niaki. Describing the effective parameters in grippers, and designing the novel micro-nano gripper. In *Control, Instrumentation and Automation (ICCIA), 2011 2nd International Conference on*, pages 957–963. IEEE, 2011.

[150] G Pahl and W Beitz. *Konstruktionslehre; Handbuch für Studium unds Praxis, zweite, neuerabeitete und erweiterte Auflage*. Springer Verlag Berlin, 1986.

[151] *Precision Thick Film Chip Resistors*. Panasonic, 3 2018. URL https://industrial.panasonic.com/cdbs/www-data/pdf/RDA0000/AOA0000C304.pdf.

[152] Dirch Hjorth Petersen, Rong Lin, Torben Mikael Hansen, Erik Rosseel, Wilfried Vandervorst, Christian Markvardsen, Daniel Kjær, and Peter Folmer Nielsen. Comparative study of size dependent four-point probe sheet resistance measurement on laser annealed ultra-shallow junctions. *Journal of Vacuum Science & Technology B: Microelectronics and Nanometer Structures Processing, Measurement, and Phenomena*, 26(1):362–367, 2008. doi: 10.1116/1.2794743. URL https://avs.scitation.org/doi/abs/10.1116/1.2794743.

[153] S Philippi, U Weißker, T Mühl, A Leonhardt, and B Büchner. Room temperature magnetometry of an individual iron filled carbon nanotube acting as nanocantilever. *Journal of Applied Physics*, 110(8):084319, 2011.

[154] Michael T Postek, Karen S Howard, Arthur H Johnson, and Kathlyn L McMichael. The scanning electron microscope. *Handbook of charged particle optics*, pages 363–399, 1997.

[155] Kari Pulli, Anatoly Baksheev, Kirill Kornyakov, and Victor Eruhimov. Real-time computer vision with OpenCV. *Communications of the ACM*, 55(6):61, jun 2012. doi: 10.1145/2184319.2184337.

[156] Shengyong Qin, Tae-Hwan Kim, Zhouhang Wang, and An-Ping Li. Nanomanipulation and nanofabrication with multi-probe scanning tunneling microscope: From individual atoms to nanowires. *Review of Scientific Instruments*, 83(6): 063704, 2012.

[157] Morgan Quigley, Ken Conley, Brian P. Gerkey, Josh Faust, Tully Foote, Jeremy Leibs, Rob Wheeler, and Andrew Y. Ng. Ros: an open-source robot operating system. In *ICRA Workshop on Open Source Software*, 2009.

[158] R. T. Rajendra Kumar, S. U. Hassan, O. Sardan, V. Eichhorn, F. Krohs, S. Fatikow, and P. Bøggild. Nanobits: customisable scanning probe tips. *Nanotechnology*, 20(39):395703 (6pp), 2009. doi: 10.1088/0957-4484/20/39/395703.

[159] EF Rauch, M Véron, J Portillo, D Bultreys, Y Maniette, and S Nicolopoulos. Automatic crystal orientation and phase mapping in tem by precession diffraction. *Microscopy and Analysis-UK*, 128:S5–S8, 2008.

[160] Ludwig Reimer. *Scanning Electron Microscopy: Physics of Image Formation and Microanalysis*, volume 45 of *Springer Series in Optical Sciences*. Springer, 2nd edition, 1998.

[161] Eric Rohmer, Surya PN Singh, and Marc Freese. V-rep: A versatile and scalable robot simulation framework. In *Intelligent Robots and Systems (IROS), 2013 IEEE/RSJ International Conference on*, pages 1321–1326. IEEE, 2013.

[162] Ruediger Rosenkranz. Failure localization with active and passive voltage contrast in fib and sem. *Journal of Materials Science: Materials in Electronics*, 22(10):1523, Jul 2011. ISSN 1573-482X. doi: 10.1007/s10854-011-0459-x. URL https://doi.org/10.1007/s10854-011-0459-x.

[163] S. Roy, J. Meunier, A. M. Marian, F. Vidal, I. Brunette, and S. Costantino. Automatic 3d reconstruction of quasi-planar stereo scanning electron microscopy (sem) images*. In *2012 Annual International Conference of the IEEE Engineering in Medicine and Biology Society*, pages 4361–4364, Aug 2012. doi: 10.1109/EMBC.2012.6346932.

[164] Changhai Ru, Yong Zhang, Yu Sun, Yu Zhong, Xueliang Sun, David Hoyle, and Ian Cotton. Automated four-point probe measurement of nanowires inside a scanning electron microscope. *IEEE Transactions on Nanotechnology*, 10(4): 674–681, 2011.

[165] Changhai Ru, Xinyu Liu, and Yu Sun. *Nanopositioning Technologies: Fundamentals and Applications*. 1st ed. 2016 edition, 2016. ISBN 9783319238524. URL http://dx.doi.org/10.1007/978-3-319-23853-1.

[166] Bert Sakmann and Erwin Neher. Patch clamp techniques for studying ionic channels in excitable membranes. *Annual review of physiology*, 46(1):455–472, 1984.

[167] Bal S Sandhu. An overview of mems sensors - whitepaper. 2015. URL https://community.arm.com/cfs-file/__key/telligent-evolution-components-attachments/01-1998-00-00-00-00-68-58/Whitepaper-_2D00_-An-Overview-of-MEMS-Sensors.pdf. [Accessed on: 2018-08-31].

[168] Alexey Savenko, Izzet Yildiz, Dirch Hjorth Petersen, Peter Bøggild, Malte Bartenwerfer, Florian Krohs, Maria Oliva, and Torsten Harzendorf. Ultra-high aspect ratio replaceable afm tips using deformation-suppressed focused ion beam milling. *Nanotechnology*, 24(46), 2013. doi: 10.1088/0957-4484/24/46/465701.

[169] Hidetaka Sawada, Naoki Shimura, Fumio Hosokawa, Naoya Shibata, and Yuichi Ikuhara. Resolving 45-pm-separated si–si atomic columns with an aberration-corrected stem. *Microscopy*, 64(3):213–217, 2015.

[170] C. P. Sealy, Martin Castell, and Peter Wilshaw. Mechanism for secondary electron dopant contrast in sem. 49:311–21, 02 2000.

[171] Wanfeng Shang, Haojian Lu, Wenfeng Wan, Toshio Fukuda, and Yajing Shen. Vision-based nano robotic system for high-throughput non-embedded cell cutting. *Scientific reports*, 6:22534, 2016.

[172] Qing Shi, Zhan Yang, Yana Guo, Huaping Wang, Lining Sun, Qiang Huang, and Toshio Fukuda. A vision-based automated manipulation system for the pick-up of carbon nanotubes. *IEEE/ASME Transactions on Mechatronics*, 22 (2):845–854, 2017.

[173] Qiwei Shi, Stéphane Roux, Félix Latourte, François Hild, Dominique Loisnard, and Nicolas Brynaert. Measuring topographies from conventional sem acquisitions. *Ultramicroscopy*, 191:18 – 33, 2018. ISSN 0304-3991. doi: https://doi.org/10.1016/j.ultramic.2018.04.006. URL http://www.sciencedirect.com/science/article/pii/S0304399118300263.

[174] Torsten Sievers and Sergej Fatikow. Real-Time Object Tracking for the Robot-Based Nanohandling in a Scanning Electron Microscope. *Journal of Micromechatronics - Special Issue on Micro/Nanohandling*, 3(3-4):267–284(18), 2006.

[175] Torsten Sievers, Marco Jähnisch, Christian Schrader, and Sergej Fatikow. Vision feedback in an automatic nanohandling station inside an SEM. *Optomechatronic Micro/Nano Devices and Components II*, 6376(1):63760B, 2006.

[176] M. Sitti. Micro- and nano-scale robotics. In *Proceedings of the 2004 American Control Conference*, volume 1, pages 1–8 vol.1, June 2004. doi: 10.23919/ACC.2004.1383571.

[177] Richard E. Smalley. Of chemistry, love and nanobots. *Scientific American*, 285 (3):76–77, 2001. ISSN 0036-8733. doi: 10.1038/scientificamerican0901-76.

[178] Damon A Smith, Vincent C Holmberg, Doh C Lee, and Brian A Korgel. Young's modulus and size-dependent mechanical quality factor of nanoelectromechanical germanium nanowire resonators. *The Journal of Physical Chemistry C*, 112(29): 10725–10729, 2008.

[179] Peter A Smith, Christopher D Nordquist, Thomas N Jackson, Theresa S Mayer, Benjamin R Martin, Jeremiah Mbindyo, and Thomas E Mallouk. Electric-field assisted assembly and alignment of metallic nanowires. *Applied Physics Letters*, 77(9):1399–1401, 2000.

[180] William R. Smythe. *Static And Dynamic Electricity*. CRC Press, 1989. ISBN 9780891169178. URL https://www.amazon.com/Static-Dynamic-Electricity-William-Smythe/dp/0891169172?SubscriptionId=0JYN1NVW651KCA56C102&tag=techkie-20&linkCode=xm2&camp=2025&creative=165953&creativeASIN=0891169172.

[181] Peter Soetens and Herman Bruyninckx. Realtime hybrid task-based control for robots and machine tools. In *Robotics and Automation, 2005. ICRA 2005. Proceedings of the 2005 IEEE International Conference on*, pages 259–264. IEEE, 2005.

[182] Karl Spanner. Survey of the various operating principles of ultrasonic piezomotors. In *Proceedings of the 10th International Conference on New Actuators*, 2006.

[183] Vladimir Stavrov, Galina Stavreva, Emil Tomerov, Vencislav Todorov, and Ivan Buchvarov. In-line thickness control of self-sensing cantilevers for advanced afm applications. In *Electronics Technology (ISSE), 2017 40th International Spring Seminar on*, pages 1–4. IEEE, 2017.

[184] C. Stolle, M. Bartenwerfer, C. Celle, J. Simonato, and S. Fatikow. Nanorobotic strategies for handling and characterization of metal-assisted etched silicon nanowires. *Mechatronics, IEEE/ASME Transactions on*, 18(3):887–894, 2013. ISSN 1083-4435. doi: 10.1109/TMECH.2012.2193591.

[185] Tadao Suganuma. Measurement of surface topography using sem with two secondary electron detectors. *Microscopy*, 34(4):328–337, 1985.

[186] Yu Sun, D Piyabongkarn, A Sezen, BJ Nelson, and R Rajamani. A high-aspect-ratio two-axis electrostatic microactuator with extended travel range. *Sensors and Actuators A: Physical*, 102(1-2):49–60, 2002.

[187] J.M. Tarascon and Michel Armand. Issues and challenges facing rechargeable lithium batteries. 414:359–67, 12 2001.

[188] Claes Thelander and Lars Samuelson. Afm manipulation of carbon nanotubes: realization of ultra-fine nanoelectrodes. *Nanotechnology*, 13(1):108, 2002.

[189] T. Tsuchiya, O. Tabata, J. Sakata, and Y. Taga. Specimen size effect on tensile strength of surface-micromachined polycrystalline silicon thin films. *Journal of Microelectromechanical Systems*, 7(1):106–113, Mar 1998. ISSN 1057-7157. doi: 10.1109/84.661392.

[190] Heinz Unbehauen. *Regelungstechnik I: Klassische Verfahren zur Analyse und Synthese linearer kontinuierlicher Regelsysteme, Fuzzy-Regelsysteme*. Vieweg+Teubner Verlag / GWV Fachverlage GmbH Wiesbaden, Wiesbaden, 15., überarbeitete und erweiterte auflage edition, 2008. ISBN 9783834894915. URL http://dx.doi.org/10.1007/978-3-8348-9491-5.

[191] Ivo Utke, Patrik Hoffmann, and John Melngailis. Gas-assisted focused electron beam and ion beam processing and fabrication. *Journal of Vacuum Science & Technology B: Microelectronics and Nanometer Structures Processing, Measurement, and Phenomena*, 26(4):1197–1276, 2008. doi: 10.1116/1.2955728. URL https://avs.scitation.org/doi/abs/10.1116/1.2955728.

[192] A. Verdaguer, G. M. Sacha, H. Bluhm, and M. Salmeron. Molecular structure of water at interfaces: wetting at the nanometer scale. *Chemical Reviews*, 106 (4):1478–1510, 2006. doi: 10.1021/cr040376l. URL https://doi.org/10.1021/cr040376l. PMID: 16608188.

[193] John S Villarrubia. Modeling scanning electron microscope measurements with charging. In *Frontiers of Characterization and Metrology for Nanoelectronics*, 2013.

[194] Wolfgang Weber. *Industrieroboter: Methoden der Steuerung und Regelung*. Carl Hanser Verlag GmbH Co KG, 2017.

[195] Thomas Wich, Christoph Edeler, Christian Stolle, and Sergej Fatikow. Micro-nano-integration based on automated serial assembly. In *Proceedings of the fifth annual IEEE international conference on Automation science and engineering*, CASE'09, pages 573–578, Piscataway, NJ, USA, 2009. IEEE Press. ISBN 978-1-4244-4578-3. doi: 10.1109/COASE.2009.5234150. URL http://portal.acm.org/citation.cfm?id=1671776.1671875.

[196] Thomas Wich, Christian Stolle, Christoph Edeler, and Sergej Fatikow. Parasitic effects on nanoassembly processes. In *Proceedings of the 2009 IEEE/RSJ international conference on Intelligent robots and systems*, IROS'09, pages 1389–1394, Piscataway, NJ, USA, October 11-15 2009. IEEE Press. ISBN 978-1-4244-3803-7. doi: 10.1109/IROS.2009.5354016. URL http://dl.acm.org/citation.cfm?id=1733343.1733596.

[197] CB Williams and Rob B Yates. Analysis of a micro-electric generator for microsystems. *sensors and actuators A: Physical*, 52(1-3):8–11, 1996.

[198] Tim Wortman and Sergej Fatikow. Carbon nanotube detection by scanning electron microscopy. In *Proc. of the Eleventh IAPR Conference on Machine Vision Applications (MVA)*, 2009.

[199] Hui Xie, Dogan Sinan Haliyo, and Stéphane Régnier. A versatile atomic force microscope for three-dimensional nanomanipulation and nanoassembly. *Nanotechnology*, 20(21):215301, 2009.

[200] Hui Xie, Pierre Lambert, and Stéphane Régnier. Analysis of nanoscale mechanical grasping under ambient conditions. *Journal of Micromechanics and Microengineering*, 21(4):045009, 2011.

[201] Xutao Ye, Yong Zhang, Changhai Ru, Jun Luo, Shaorong Xie, and Yu Sun. Automated pick-place of silicon nanowires. *Automation Science and Engineering, IEEE Transactions on*, 10(3):554–561, 2013. ISSN 1545-5955. doi: 10.1109/TASE.2013.2244082.

[202] P. Yildiz, I.and Bøggild. *Nanobits - exchangable and customisable scanning probe tips*. PhD thesis, 2014.

[203] R Young, C Rue, S Randolph, C Chandler, G Franz, R Schampers, A Klumpp, and L Kwakman. A comparison of xenon plasma FIB technology with conventional gallium LMIS FIB: Imaging, milling, and gas-assisted applications. *Microscopy and Microanalysis*, 17(S2):652–653, jul 2011. doi: 10.1017/s1431927611004132.

[204] Hongjiang Zeng, Tie Li, Malte Bartenwerfer, Sergej Fatikow, and Yuelin Wang. Simultaneous Characterization of Mechanical and Electrical Properties of Nanowire Using MEMS Device. In *Proc. of IEEE Transducers & Eurosensors XXVII*, pages 776–779, Barcelona, Spain, June 2013.

[205] Hongjiang Zeng, Tie Li, Malte Bartenwerfer, Sergej Fatikow, and Yuelin Wang. In situ SEM electromechanical characterization of nanowire using an electrostatic tensile device. *Journal of Physics D: Applied Physics*, 46(30):305501, 2013. doi: 10.1088/0022-3727/46/30/305501.

[206] Dongfeng Zhang, Jean-Marc Breguet, Reymond Clavel, Laetitia Philippe, Ivo Utke, and Johann Michler. In situ tensile testing of individual co nanowires inside a scanning electron microscope. *Nanotechnology*, 20(36):365706, 2009.

[207] Dongfeng Zhang, Jean-Marc Breguet, Reymond Clavel, Vladimir Sivakov, Silke Christiansen, and Johann Michler. In situ electron microscopy mechanical testing of silicon nanowires using electrostatically actuated tensile stages. *Journal of Microelectromechanical Systems*, 19(3):663–674, 2010.

[208] Qifeng Zhang, Evan Uchaker, Stephanie L Candelaria, and Guozhong Cao. Nanomaterials for energy conversion and storage. *Chemical Society Reviews*, 42(7):3127–3171, 2013.

[209] Tianlei Zhang, Gang Zhao, Jiaru Chu, Wenhao Huang, Malte Bartenwerfer, Volkmar Eichhorn, and Sergej Fatikow. Fabrication and characterisation of piezoelectric microcantilever array with carbon nanotube tips assembled by nano-handling. *International Journal of Nanomanufacturing*, 10:265–280, 2014. doi: 10.1504/IJNM.2014.060797.

[210] Yong Zhang, Brandon K Chen, Xinyu Liu, and Yu Sun. Autonomous robotic pick-and-place of microobjects. *IEEE transactions on Robotics*, 26(1):200–207, 2010. doi: 10.1109/tro.2009.2034831.

[211] Xin Zhao, Beatriz Mendoza Sánchez, Peter J Dobson, and Patrick S Grant. The role of nanomaterials in redox-based supercapacitors for next generation energy storage devices. *Nanoscale*, 3(3):839–855, 2011.

[212] Huiyu Zhou, Jiahua Wu, and Jianguo Zhang. *Digital Image Processing: Part I*. Bookboon, 2010.

[213] Yong Zhu and Horacio D Espinosa. An electromechanical material testing system for in situ electron microscopy and applications. *Proceedings of the National Academy of Sciences*, 102(41):14503–14508, 2005.

[214] Yong Zhu, Qingquan Qin, Feng Xu, Fengru Fan, Yong Ding, Tim Zhang, Benjamin J Wiley, and Zhong Lin Wang. Size effects on elasticity, yielding, and fracture of silver nanowires: In situ experiments. *Physical review B*, 85(4): 045443, 2012. doi: 10.1103/physrevb.85.045443.

[215] Ernst Zimmer and Botho Kikut. Device for the automatic gripping and releasing of a tool holder in a manipulator, December 1 1987. US Patent 4,710,093.

[216] Sören Zimmermann. *Dedicated robotic handling and processing at the submicrometer scale: Feasibility studies*. Ingenieurwissenschaften. Verlag Dr. Hut, München and München, 1. auflage edition, 2017. ISBN 9783843931670.

[217] Sören Zimmermann, Tobias Tiemerding, Tie Li, Wenrong Wang, Yuelin Wang, and Sergej Fatikow. Automated mechanical characterization of 2-d materials using sem based visual servoing. *International Journal of Optomechatronics*, 7 (4):283–295, 2013.

[218] Sören Zimmermann, Tobias Tiemerding, and Sergej Fatikow. Automated robotic manipulation of individual colloidal particles using vision-based control. *IEEE/ASME Transactions on Mechatronics*, 20(5):2031–2038, 2015.

[219] Zoltan Zoller and Peter Zentay. Constant kinetic energy robot trajectory planning. *Periodica Polytechnica Mechanical Engineering*, 43(2):213–228, 1999. URL https://pp.bme.hu/me/article/view/1475.

Acknowledgements

The presented work has been carried out at the Division Microrobotics and Control Engineering (AMiR) of the University of Oldenburg, Germany, headed by Prof. Dr.-Ing. Sergej Fatikow.

I express my gratitude to Prof. Fatikow for supervising my Ph.D. thesis, the division's excellent laboratory equipment as well as the confidence in my scientific work. I am grateful for freedom he provided to determine the direction of my research work on my own. Furthermore, I would like to thank the team from the *Shanghai Institute of Microsystem and Information Technology* for setting challenges in nanowire handling and the team of the *DTU Nanotech* for providing microgrippers and NanoBits.

I would like to thank all my colleagues for the excellent collaboration and productive scientific discussions. I thank my beloved wife Joanne for her moral support, her infinite patience and her trust. Lina, Julia, and Mathilda, I would like to thank you for sharing me with my work and patiently enduring my physical and mental absence.

Declaration

I, Malte Bartenwerfer, hereby declare to have written this thesis only based on the sources listed and without the help of others. I have not submitted or prepared the submission of this or any other doctoral thesis at the Carl von Ossietzky University Oldenburg or any other university.

I have honored the German Research Foundation guidelines for safeguarding good scientific practice in the completion of this work.

Hiermit erkläre ich, Malte Bartenwerfer, diese Arbeit ohne fremde Hilfe und nur unter Verwendung der angegebenen Quellen verfasst zu haben. Ich habe bis dato weder an der Carl von Ossietzky Universität Oldenburg noch an einer anderen Universität die Eröffnung eines Promotionsverfahrens beantragt oder anderweitig eine Promotion vorbereitet.

Ich habe die Regeln guter wissenschaftlicher Praxis entsprechend der Richtlinien der Deutschen Forschungsgemeinschaft eingehalten.

Malte Bartenwerfer
30. November 2018